The Use of Photopolymers as Retaining Frits and Monoliths for Electrochromatography in Capillaries or Microfluidic Devices and Some Selected Applications

Dirk Bandilla

A Thesis

in

The Department

of

Chemistry and Biochemistry

Presented in Partial Fulfillment of the Requirements
For the Degree of Doctor of Philosophy at
Concordia University
Montréal, Québec, Canada

February 2004

Your file Votre référence
ISBN: 0-612-90376-1
Our file Notre référence
ISBN: 0-612-90376-1

CONCORDIA UNIVERSITY
SCHOOL OF GRADUATE STUDIES

This is to certify that the thesis prepared

By: **Dirk Bandilla**

Entitled: **The Use of Photopolymers as Retaining Frits and Monoliths for Electrochromatography in Capillaries or Microfluidic Devices and Some Selected Applications**

and submitted in partial fulfillment of the requirements for the degree of

DOCTOR OF PHILOSOPHY (Chemistry)

complies with the regulations of the University and meets the accepted standards with respect to originality and quality.

Signed by the final examining committee:

Dr. M. Frank _____ Chair

Dr. I. Krull _____ External Examiner

Dr. J. Stewart _____ External to Program

Dr. J. Turnbull _____ Examiner

Dr. O.S. Tee _____ Examiner

Dr. C. Skinner _____ Thesis Co-Supervisor

Dr. P. Banks _____ Thesis Co-Supervisor

Approved by _____
Chair of Department or Graduate Program Director

April 5, 2004 _____
Dean of Faculty

Abstract

The Use of Photopolymers as Retaining Frits and Monoliths for Electrochromatography in Capillaries or Microfluidic Devices and Some Selected Applications

Dirk Bandilla
Concordia University, 2004

This work explores the use of two different organic photopolymers for electrochromatography in the capillary format and also demonstrates their incorporation into a microfluidic platform. The first photopolymer studied functioned as a retaining frit for silica-supported, microparticulate stationary phase. After using the photopolymerization procedure in the capillary format the retaining frits were successfully integrated into the microfluidic platform. However, packing the microfluidic device with stationary phase particles could not be accomplished. A second photopolymer possessing C_4-functionalities was therefore investigated as a porous stationary phase. It could be incorporated as a monolith in capillaries and thereby avoided the packing difficulties associated with individual particles and polymer retaining frits. Six polyaromatic hydrocarbons were baseline-separated within two minutes on this monolithic column. The monolith was also successfully created in the microfluidic format as verified by the separation of two fluorescent dyes. Due to the high cost of microfluidic devices the properties of the monolith were studied primarily in the capillary format. Van Deemter plots revealed the potential to use high mobile phase velocities

without sacrificing resolution. Hydrodynamic and electrokinetic flow measurements gave insights into the porosity and tortuosity of the polymer by non-destructive means. Additionally, scanning electron microscopy and atomic force microscopy were employed to elucidate the microscopic structure and evaluate the pore size. The dependence of the electroosmotic flow on percentage and type of organic solvent, pH, ionic strength and concentration of sulfonate moieties in the polymer was measured. Various applications were surveyed with an emphasis on the separation of proteins. Their separation also served to evaluate the manufacturing process in terms of *inter-* and *intra*-capillary reproducibility. By comparing capillary electrochromatography, capillary electrophoresis and micro-LC it was found that chromatography is not the major contributor to the overall CEC separation of proteins. However, the monolithic columns demonstrated very good reproducibility as could be seen by using serum proteins as probes. Separations of small molecules were shown to be greatly based on a chromatographic separation mechanism. These applications included quality assessment in the synthesis of anthracene-2,3-dialdehyde, the separation of oligonucleotides and the separation of non-steroidal anti-inflammatory drugs.

"There is plenty of space at the bottom"

Richard Feynman

This thesis is dedicated to everybody who encouraged me to pursue this work.

Acknowledgements

I would like to express my gratitude towards my research supervisor, Dr. Cameron Skinner, for his never ending support, encouragement and inspiration.

I also wish to thank my co-supervisor, Dr. Peter Banks, as well as my committee members, Drs. Oswald Tee and Joanne Turnbull for all the additional guidance, attention and interest they provided throughout my graduate studies.

Furthermore, I would like to say thanks to the following individuals and institutions:

- Concordia University and the Government of Québec for a Graduate Student International Fee Remission Award.
- The Department of Chemistry and Biochemistry.
- The entire group of Dr. Skinner, i.e., Pieter Roos, Jean-Louis Cabral, Vincent Lau and Zacharias Papachristou for their kindness, helpfulness and an unaccounted number of stimulating and enlightening conversations.
- Dr. Donald Paquette, Dr. Michael Harvey and Mr. Michael Little for the same reasons and a few beers.
- The entire crew of the Technical Service Center at Concordia University.
- The following highly enthusiastic project students who helped me with this project: Rebekah Carson, Erin Templeton, Marie-Eve Beaudoin and Vicky Bablekis.
- M. Raymond Mineau (Université du Québec à Montréal) and Mme. Patricia Moraille (Université de Montréal) for their help with acquiring the SEM and AFM images.
- The employees of Concordia's International Students Office for truly enriching my stay.

Table of Content

List of Figures

List of Tables

List of Equations

List of Abbreviations

ACN	Acetonitrile
ADA	Anthracene-2,3-dialdehyde
AMPS	2-acrylamido-2-methyl-1-propanesulfonic acid
BAC	Butyl acrylate
BDDA	1,3-butanediol diacrylate
BME	Benzoin methyl ether
BODIPY SE	4,4-difluoro-4-bora-3a,4a-diaza-*s*-indacene-3-propionic acid succinimidyl ester
CD	Circular dichroism
CE	Capillary electrophoresis
CEC	Capillary electrochromatography
DMF	*N,N*-dimethylformamide
EOF	Electroosmotic flow
EtOH	Ethanol
GC	Gas Chromatography
GMA	Glycidyl methacrylate
HCl	Hydrochloric acid
HPLC	High-performance (or high-pressure) liquid chromatography
I.D.	Inner diameter
LC	Liquid chromatography
LIF	Laser –induced fluorescence
MeOH	Methanol
μ-HPLC	Micro-high-performance liquid chromatography
MS	Mass spectrometry
MTS	(3-methacryloyloxypropyl)trimethoxysilane
NaOH	Sodium hydroxide
NSA	Non-steroidal anti-inflammatory drugs
O.D.	Outer diameter
PAHs	Polyaromatic Hydrocarbons
%RSD	Percent relative standard deviation
TRIM	Trimethylolpropane trimethacrylate
TRIS	Tris(hydroxymethyl)aminomethane

Chapter 1: Introduction to Electrochromatography

1.1 Overview and historical background

In the quest for ever faster, smaller and more efficient technology in the field of separation science, Capillary Electrochromatography (CEC) has emerged as a promising new development with respect to established technologies, for instance, high-performance liquid chromatography (HPLC). Pioneered in 1974 by Pretorius, Hopkins and Schiefke [1] initially in a 1 mm inner diameter (I.D.) column and its premier implementation in the capillary format in 1981 by Jorgenson and Lukacs [2] its full potential was not realized until 1987 by Knox and Grant.[3, 4] Since the mid-1990s, the technique has experienced a steady growth until the year 2000, when the work for this thesis begun, as illustrated in Figure 1.1:

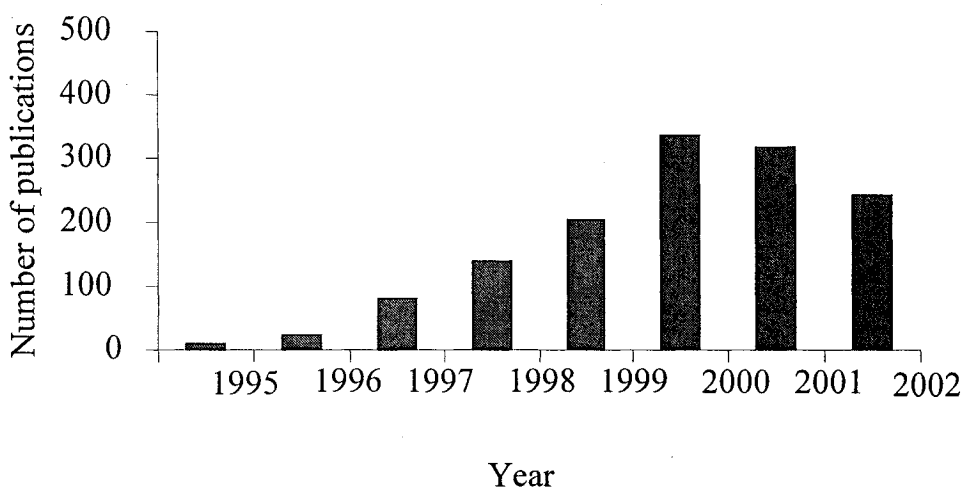

Figure 1.1: Number of publications from 1995 to 2002 enclosing the concept of capillary electrochromatography found in the SciFinder database.

One potential explanation for the flattening of the curve observed since 2001 might be the current transition away from the development of novel stationary phase materials and towards the analysis of real-life samples. Essentially, CEC can be thought of as a hybrid between micro-HPLC (μ-HPLC) and Capillary Electrophoresis (CE) rather than representing a completely novel technique by itself.[5] One of its strengths lies in its underlying dual separation mechanism based on the potential to exploit and eventually juxtaposition both a kinetic separation process (electrophoresis) and a thermodynamic one (chromatography),[6, 7] as accentuated in the following figure:

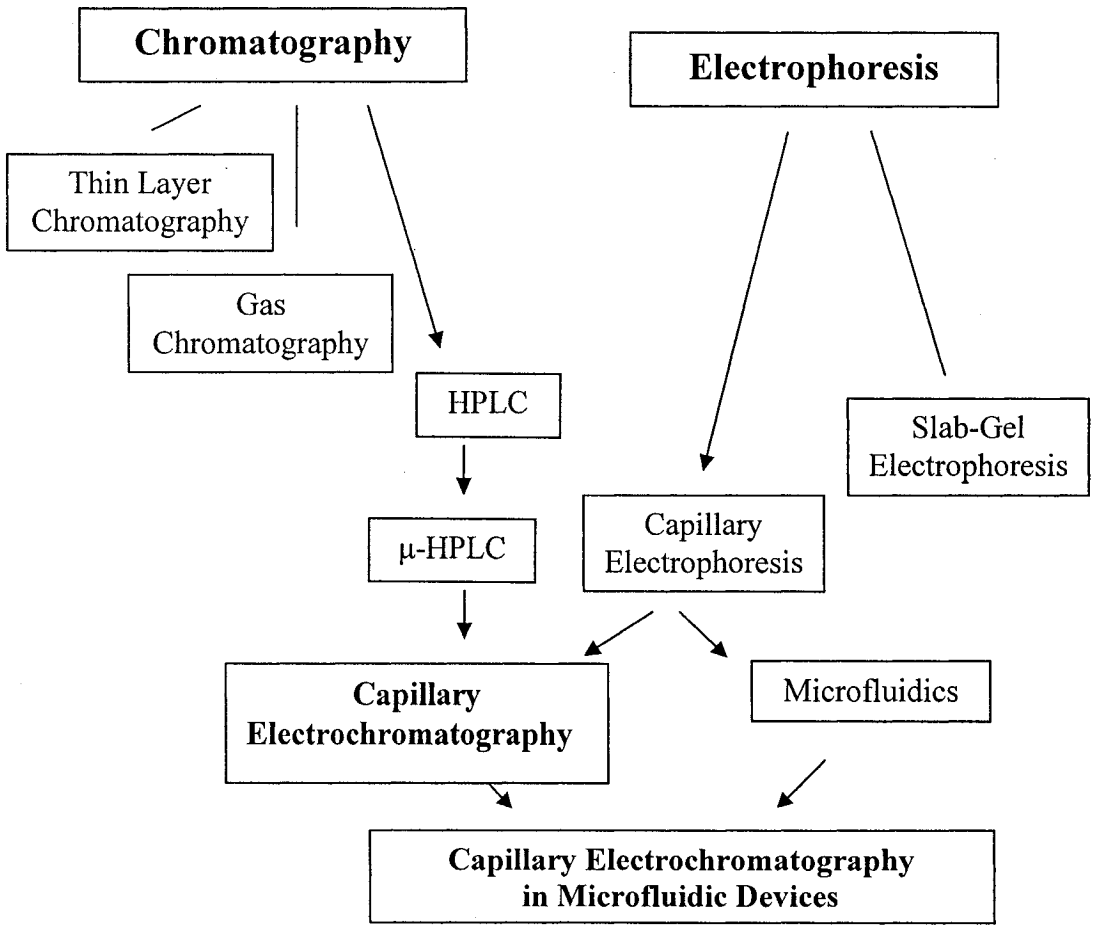

Figure 1.2: Development of several major techniques currently utilized in separation science.

In terms of physical dimensions, HPLC uses columns of 10-30 cm in length with 1-4 mm I.D.[8] Likewise, μ-HPLC (also called microbore-HPLC or simply μ-LC) makes use of capillary columns of roughly the same length with I.D.'s ranging from 0.5-2 mm.[9] CE and CEC both operate with capillaries ranging from 10-100 cm in length and 10-100 μm I.D.[10, 11] Normally, these techniques utilize columns or capillaries of circular geometry unlike microfluidic devices, which contain channels of rectangular geometry. The separation channels in microfluidics rarely exceed 10 cm in length, with channel depths of about 10-20 μm and widths ranging from 20-300 μm.[12]

At this point, it should be briefly noted that for a complete summary on separation techniques one should additionally include centrifugation [13] as well as large I.D. column LC (flash-column LC) and supercritical fluid chromatography. Although it is possible to perform electrochromatography in a large I.D. column format,[14] it is more frequently carried out in the capillary format with an emerging trend towards the microfluidic platform, the latter one often simply referred to as the chip format.[15-21] A chip in this context consists of a small piece of solid material (e.g., glass, silica, plastic) that contains several interconnected channels and reservoirs, plus a cover piece, as opposed to the capillary format where a single piece of flexible capillary of much larger dimensions is employed with the reservoirs being separate entities.[22-28] Nonetheless, both techniques share the same basic principle in that motion is generated through application of a potential difference between inlet- and outlet end. The basic principles to be introduced in the following therefore apply equally to both the chip and the capillary format. In contrast, HPLC and μ-HPLC generate motion by applying a pressure differential between inlet- and outlet end.

The integration of a solid material, commonly referred to as stationary phase, inside the capillary in CEC is the main difference with respect to CE. It should be noted at this point that throughout this thesis "CE" will refer to "plain" CE, i.e., capillary zone electrophoresis, unless specifically indicated otherwise. The presence of the stationary phase allows exploitation of chromatographic separation mechanisms on top of the inherent electrophoretic separation. In order to achieve satisfactory chromatography, the stationary phase needs to have appropriate functional groups.[8] Naturally, the incorporation of a solid material presents a major technical challenge when attempting to modify either a capillary or a chip with the goal of performing CEC. To date, two major techniques are established for the incorporation of stationary phase.[11, 29] For one, it is possible to fill the capillary with individual, spherical, microporous particles (often called microparticulate stationary phase) and lock them in place with porous frits. Analyte and solvent molecules can flow through the frits but particles cannot. A second possibility lies in the use of one single, porous, rod-like piece of solid polymer material, called a monolith. It is anchored to the interior wall of the capillary and thus does not move but, again, permits analyte and solvent molecules to pass through. The only difference between the capillary and the chip format is the inner geometry of the separation channel which is rectangular for a chip and cylindrical in the case of a capillary. The following figure illustrates these two approaches:

A) Frit approach

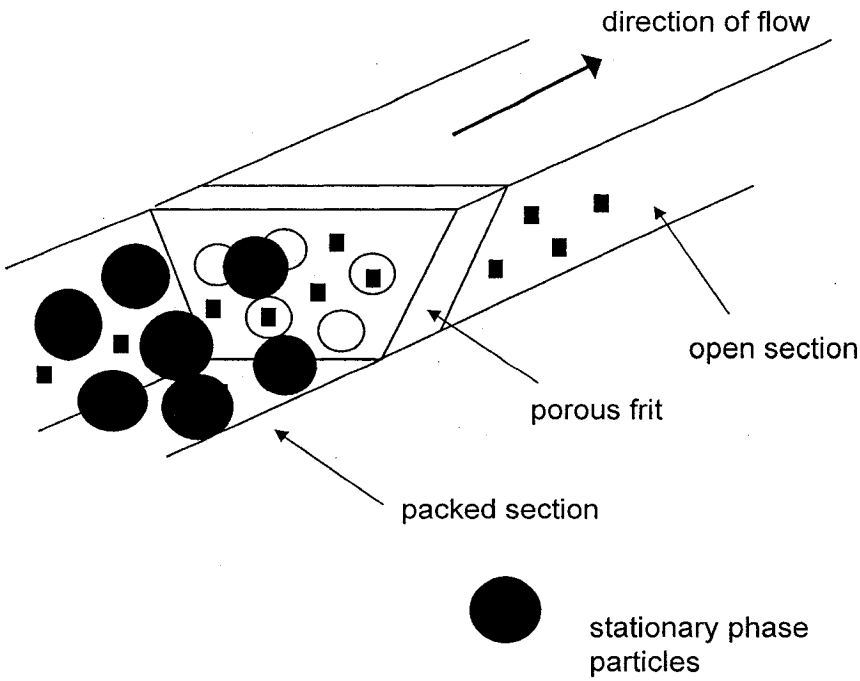

B) Monolith approach

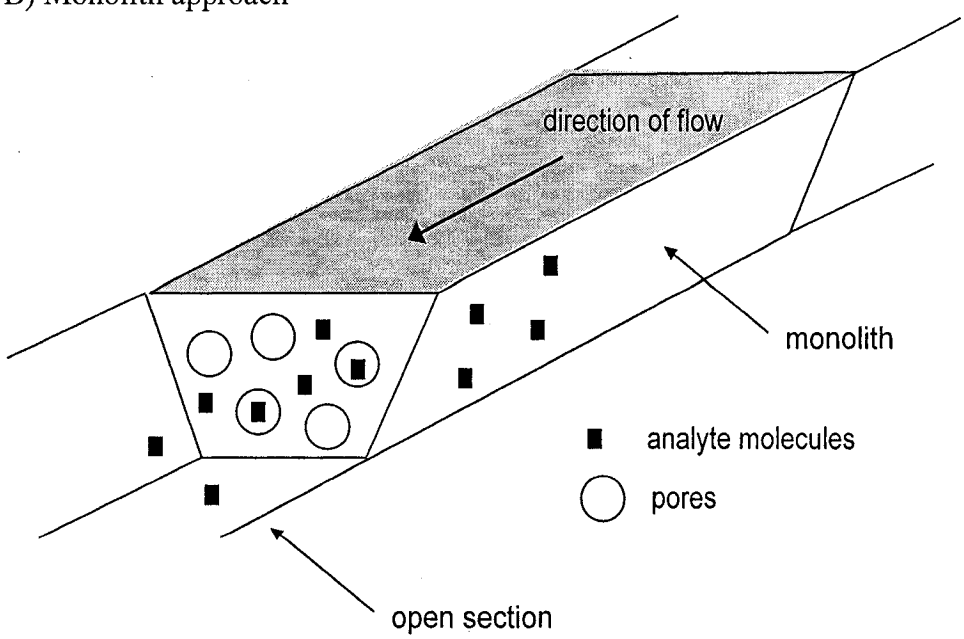

Figure 1.3: Frit approach to lock individual particles in place (a) (only one frit is shown) or monolith approach as stationary phase material (b).

A third technique which avoids any form of discrete stationary phase is binding the stationary phase to the walls of the capillary, usually by means of a chemical reaction.[30-34] This method is called open-tubular CEC; it is used less frequently due to its inherently limited separation efficiency caused by the low surface area to volume ratio.

The capillary format and voltage generated flow go hand in hand with the potential for high speed separations enabling high sample throughput. Additionally, the combination of two distinctively different mechanisms of separation, namely electrophoresis and chromatography, creates the possibility for high efficiency separations. The full strength of CEC will become more evident in the following sections that will treat the briefly introduced aspects (and some additional ones) in greater detail and will pinpoint why this technique holds many advantages with respect to both CE and HPLC. Returning to the first sentence of the introduction "a quest for ever faster, smaller and more efficient technology in the field of separation science" the arguments given so far hopefully demonstrated the technique's potential to meet these goals.

1.2 Generation of motion: the phenomenon of electroosmosis

Imagine a separation device made of quartz, glass or silicon, which contains two reservoirs connected by a capillary, with the reservoirs and the capillary filled with a buffered solution. After applying a voltage between the two reservoirs one will observe that *all ions migrate in the same direction.*[2, 4, 12, 35, 36] This observation contradicts most forms of gel electrophoresis or electrolysis where anions migrate towards the anode and cations towards the cathode.[37] The phenomenon forcing all ions to migrate in the same

direction is called electroosmosis or electroendosmosis and the resulting flow known as electroosmotic flow (EOF). Its origin and direction can be explained by the pH-dependent microscopic processes occurring at the capillary wall.[10, 38]

Regardless of whether the wall is made of quartz, glass or silica, it consists of a silica network with some surface silicon atoms possessing an OH-group (named silanols), which are acidic moieties with a pK_A of around 2.[10] When an aqueous solution with a pH greater than 2 is filled into the capillary a significant number of silanols donate a proton to the solution and become negatively charged. Some of the silanol anions will attract positively charged counter cations from the solution yet due to steric hindrance not all silanol anions will face a counter ion thus giving rise to a potential difference Φ. The most closely bound cations then lose their solvation sphere and become essentially immobilized, i.e., they no longer move under the influence of an electric field. The combined layers of silanol anions and unsolvated cations are commonly referred to as the Stern-layer; an imaginary line connecting the centers of the unsolvated cations is called the inner Helmholtz plane. A diffuse layer of solvated cations follows the layer of unsolvated ones, with an equilibrium between the two. Density and potential of this diffuse layer decrease with increasing distance from the wall up to a certain distance where electroneutrality is reached. A further imaginary line through the first layer of solvated cations is called the outer Helmholtz plane and the overall model developed is commonly referred to as Gouy-Chapman-Stern-Graham model. The potential drop between the outer Helmholtz plane and the distance where electroneutrality is reached is named the Zeta-potential.[10, 38-40] A summary of this model is given in the following figure:

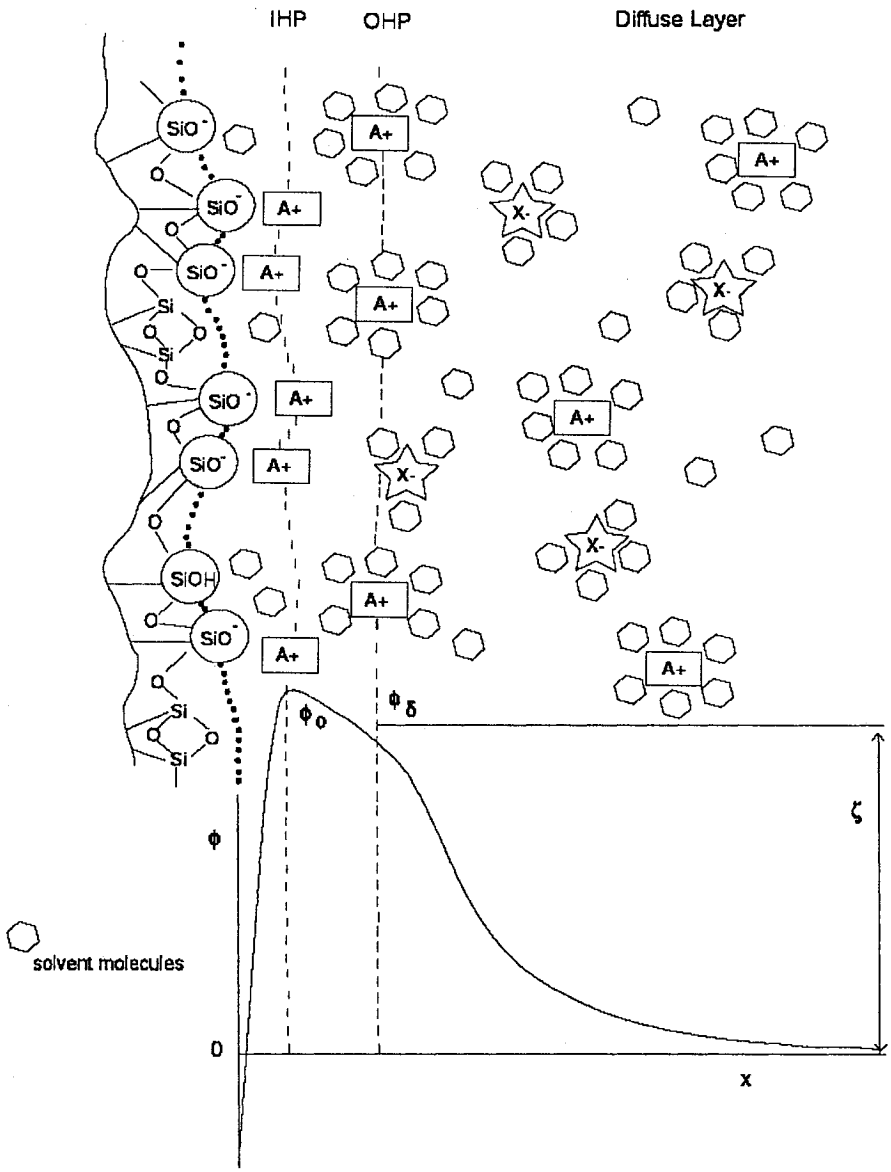

Figure 1.4: Electrokinetic processes and potentials near the surface in a capillary made of silicon, quartz or glass. The squares assigned "A^+" represent cations, the stars named "X^-" anions, "SiO^-" indicates silanol anions. The lower graph describes the dependence of the potential ϕ as a function of distance from the wall, with ϕ_0 standing for the potential at the inner Helmholtz plane (IHP) and ϕ_δ standing for the potential at the outer Helmholtz plane (OHP). ζ represents the Zeta-potential.

Upon application of an electric field the cations experience a force towards the cathode and the anions experience a force towards the anode. As claimed earlier, not all of the negatively charged silanol groups on the wall face a positively charged counter ion

so there will be an excess positive charge in the solution. Consequently, the overall dragging force will be stronger towards the cathode than towards the anode, with the ensuing flow being the EOF. As a result, neutral molecules and even anions are dragged through their hydration spheres towards the cathode. Since EOF is a movement of the bulk solution it affects all analyte molecules (and solvent molecules) to the same extent, i.e., EOF is a driving force but not a separation factor. At a pH below 2 silanol groups become protonated. Investigations by several groups have furthermore established that EOF is not restricted to aqueous solvents but also occurs in many non-aqueous solvents as long as their dielectric constant is sufficiently high.[41-45]

Due to the fact that the EOF is generated at the surfaces a resulting consequence is the piston-like flow profile shown in Figure 1.5.[46, 47] In order to deduce this type of flow profile, which differs greatly from the Poiseuille-like pressure-driven flow profiles (also termed viscous flow) encountered in HPLC and μ-HPLC, and to elucidate some important parameters that influence this flow profile, a more quantitative description of the electrokinetic processes on the capillary wall is needed.

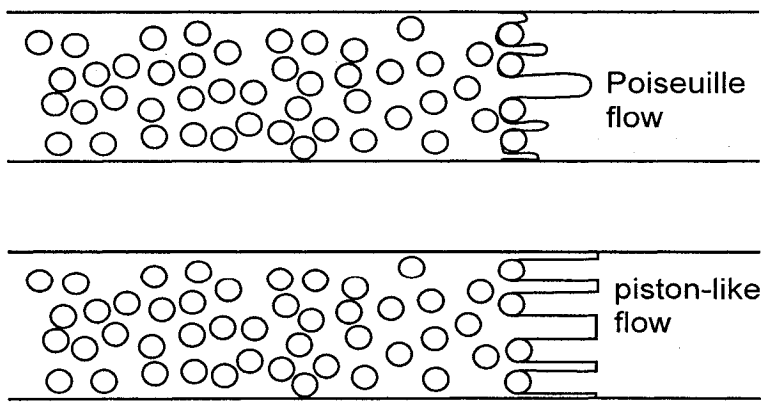

Figure 1.5: Differences in flow profiles between pressure- and electroosmosis-driven systems.

To date, no function is available which describes the potential and charge distributions in the Stern layer. The distribution in the diffuse layer, however, can be expressed as a Boltzmann-Poisson type distribution. When inserting this distribution into a function describing the motion of a liquid in a capillary of cylindrical geometry under the influence of an electric field, Rice and Whitehead obtained the following refinement of the von Smoluchowski equation.[35] It allows for a description of the dependence of the electroosmotic velocity v_{EOF} on the radial distance from the capillary wall:

$$v_{EOF} = \frac{\varepsilon_0 \varepsilon_r \zeta E}{4\pi\eta}\left[1 - \frac{I_0(\kappa r)}{I_0(\kappa \alpha)}\right]$$

Equation 1.1: Dependence of the electroosmotic velocity v_{EOF} (in $m^2*V^{-1}*s^{-1}$) on the radial distance from the channel wall; ε_0 is the permittivity of vacuum, i.e., $8.85*10^{-12}$ $F*m^{-1}$, ε_r is the dielectric constant of water, a dimensionless number of about 80 at 25°C, η is the viscosity of the medium in $kg*m^{-1}*s^{-1}$, E is the electric field strength in $V*m^{-1}$, I_0 is a zero-order modified Bessel function of first kind, κ is the reciprocal of the double-layer thickness (Debye-Hückel parameter) in m^{-1}, α is the radius of the channel in m and r symbolizes the radial distance from the channel center in m.

Upon excluding the electric field strength E from the right side, the remainder, i.e., the proportionality constant between field strength and velocity, is usually referred to as the electroosmotic mobility μ_{EOF}:

$$\mu_{EOF} = \frac{\varepsilon_0 \varepsilon_r \zeta}{4\pi\eta}\left[1 - \frac{I_0(\kappa r)}{I_0(\kappa \alpha)}\right]$$

Equation 1.2: Electroosmotic mobility μ_{EOF} in $m^2*V^{-1}*s^{-1}$. All other symbols have the same meanings as in Equation 1.1.

One important conclusion Rice and Whitehead drew from this equation was that when the radius of the capillary drastically exceeds that of the electric double layer, i.e., $\kappa\alpha >> \kappa r$, the term in brackets approaches unity and thus becomes negligible, leading to a piston-like flow profile. On the other hand, for capillaries with extremely small inner diameters, this condition remains unfulfilled and the resulting flow profile will be Poiseuille-like.

With a piston-like flow profile, and by selecting the appropriately large inner diameters, all analyte molecules can be expected to be carried forward in very narrow bands, thereby enabling the distinction of closely eluting analyte molecules. Compared to pressure-driven techniques like HPLC and μ-HPLC, where the Poiseuille-type flow profiles cause broader bands, higher separation efficiencies should be attainable with the piston-like flow profile in CEC.

One of the most easily adjustable experimental factors on the ζ-potential is the ionic strength, as described in the following equation:[38]

$$\zeta = \frac{\sigma_0}{\varepsilon_0 \varepsilon_r \left(\frac{2000\ F^2}{\varepsilon_0 \varepsilon_r R\ T} \mu \right)^{1/2}}$$

Equation 1.3: ζ-potential in V; σ_0 is the charge density in the Stern layer in $C*m^{-1}$, F the Faraday constant (96495 $C*mol^{-1}$), R the universal gas constant (8.31 $J*K^{-1}*mol^{-1}$), T stands for the temperature in K and μ represents the ionic strength of the solution in $mol*l^{-1}$. The term in parenthesis is the expression for κ from Equation 1.1 and is commonly referred to as Debye-Hückel parameter.

As a result, the electroosmotic velocity decreases with increasing ionic strength. Besides, in order to achieve reproducible EOF the temperature should also remain constant.

All the descriptions made so far were originally deduced for open capillaries without any form of packing, and they were predicted and proven to remain valid for microfluidic devices and packed capillaries as well.[3, 4, 18, 48-53] One should mention at this point that, unlike in CE, EOF in CEC affects only the fraction of analytes not currently interacting with the stationary phase. Moreover, in packed capillaries the description of electrokinetic processes is extended owing to *both* the capillary wall *and* the surface of the stationary phase particles, or the monolith.[54-56] With respect to particles, although the majority of silanol groups of these support particles are either derivatized with some hydrophobic residue, e.g., C_8 or C_{18}, or end-capped, i.e., converted into methyl ether, they still possess a sufficiently high number of free silanol groups to generate EOF (usually between 1 and 3%). These silanols groups are even deemed to be the major contributor to EOF-generation, and not the ones on the wall.[47] The net result is the same as in an non-packed capillary, i.e., all molecules migrate towards the cathode and the flat flow profile is conserved.

When dealing with monoliths one should be aware that often a functional group other than silanol is present. This moiety is usually equally well capable of generating EOF. Examples are sulfonate or amine moieties (the latter one either protonated tertiary or quaternary ammonium groups).[57-61] The direction of the EOF is reversed in the case of the positively charged ammonium ion. [6, 62]

1.3 Separation principles

As pointed out earlier in the introduction, the possibility of exploiting both the electrophoretic and the chromatographic separation mechanism is one of the powerful features of CEC. The two mechanisms shall therefore be explained in greater detail at this point.

A) Electrophoresis

When applying an electric field throughout an aqueous solution, ions tend to migrate towards the electrodes. The velocity of their migration is proportional to the strength of the applied electric field, i.e., voltage per unit distance, but differs for each species of ions:[37]

$$v = \mu \frac{V}{l}$$

Equation 1.4: Electrophoretic velocity v in $m*s^{-1}$; μ indicates the electrophoretic mobility in $m^2*V^{-1}*s^{-1}$ (see Equation 1.5), V stands for the Voltage in V and l symbolizes the distance between the electrodes in m.

The proportionality constant μ accounts for both the acceleration of an ion under the influence of an electric field as well as opposing frictional forces. In an approximation, it is usually described as the ratio of charge to hydrodynamic radius:[10]

$$\mu = \frac{z\ e}{6\ \pi\ \eta\ a}$$

Equation 1.5: Electrophoretic mobility μ in $m^2*V^{-1}*s^{-1}$; z describes the charge number of an ion (dimensionless), e the charge of an electron ($1.60218*10^{-19}$ C), η the viscosity in Pa*s (or $kg*m^{-1}*s^{-1}$) and a stands for the hydrodynamic radius of the ion in m.

For neutral molecules, the numerator in Equation 1.5 becomes zero. Hence, separation of neutral molecules cannot be accomplished with separation techniques exclusively based on electrophoretic mobility.

B) Chromatography

Any type of chromatography is based on the partitioning of an analyte between a stationary and a mobile phase, with different analytes possessing different distribution coefficients.[63] The distribution coefficient is defined as the ratio of the analyte concentration between stationary and mobile phase:

$$K = \frac{C_S}{C_M}$$

Equation 1.6: Distribution coefficient K (dimensionless); C_S is the concentration of analyte in the stationary phase (in appropriate units of concentration) and C_M is the concentration of analyte molecules in the mobile phase (in the same units a C_S).

C) Electrodiffusion

Only recently, Xiang and Horváth postulated the existence of a third separation mechanism which they named electrodiffusion.[64] Provided that an analyte is charged, the fraction of the analyte adsorbed onto the surface of the stationary phase is assumed to

migrate along this surface, with anions always migrating towards the anode and cations always towards the cathode (as in electrolysis). It remains debatable if their prediction really comprises a third separation mechanism or just exhibits a special case of electrophoresis. So far, no quantitative description or experimental confirmations have been reported. Based on the results presented in this thesis, though, and findings by numerous other researchers it can be claimed that electrodiffusion might reduce the electrophoretic mobility but cannot overcome the EOF signifying that, overall, anions and cations still move in the same direction.

Stationary phases and mobile phases in CEC are similar to the ones used in HPLC, and the same variety of separation modes has been explored, i.e., reversed-phase, ion-exchange, size-exclusion, affinity or hydrophobic interaction chromatography.[5, 65, 66] In most cases, a binary solvent system is employed as mobile phase consisting of an organic solvent and an aqueous buffer, with the organic solvent commonly being either acetonitrile (ACN) or methanol (MeOH).[67]

1.4 Band broadening factors

The plug-like flow profile generated by electroosmosis results in very small and sharp sample zones in both capillaries and chips. Upon detection, however, these zones will not be the same length as the injected zone but appear as more-or-less bell-shaped peaks, i.e., they have experienced some form of band broadening during their journey through the packing. Band broadening ultimately sets the limit on the separation power of a particular technique: the broader the bands, the more difficult it becomes to distinguish

between closely eluting analytes. The recent emergence of monoliths as an alternative to microparticulate stationary phase currently dominates the thorough analysis of band broadening based on theoretical considerations.[68, 69] This section will briefly revisit some of the general phenomena causing band broadening as they were originally derived for Gas Chromatography (GC), HPLC and later CEC. CE is of minor importance in this context because in theory only one source of band broadening is significant, i.e., longitudinal diffusion.[70] In the following, the focus will lie on those factors that show different characteristics between HPLC and CEC, with the intention of emphasizing the strength of CEC.

A quantitative model that enables the description of band broadening for many separation techniques is the so-called *additive different contribution model for packed beds* developed by Horváth and Lin [71, 72] and adapted for CEC by Dittmann and Rozing.[73, 74] The underlying fundamental expression to quantify band broadening is the plate height (H). It is defined as the ratio of the variance of a peak to the column length (L):

$$H = \frac{\sigma^2}{L}$$

Equation 1.7: Plate height H in mm; σ^2 is the variance of a peak in mm^2 and L is the column length in mm.

The less a sample zone disperses during its journey through the packing, the lower will be its variance and therefore its plate height. Notably, the expression "plate height" (despite its unit) has no physical meaning but is merely historical and a convenient measure to compare the efficiencies of different separation techniques or modes of operation. If a peak has a small variance then a technique is theoretically capable of differentiating

between many closely eluting analytes. In the additive different contribution model the factors affecting the total variance are presumed to contribute separately from one another. It therefore states the total variance of a peak to be the sum of the individual variances of the independently contributing band broadening factors:

$$\sigma_{total}^{\ 2} = \sum_{i=1}^{n} \sigma^2{}_i$$

Equation 1.8: Total variance of a peak σ_{total}^2 in mm^2; σ_i symbolizes the individual causes of band broadening in mm.

Consequently, the total plate height is the sum of the individual plate heights, i.e., the individual causes for band broadening:

$$H_{total} = \sum_{i=0}^{n} H_i$$

Equation 1.9: Total plate height H_{total} in mm.

The underlying principle why all these factors cause band broadening lies not in their nature itself but rather in their non-instantaneous behavior: they simply require a certain amount of time to occur and only affect a limited number of analyte molecules at a time. During that period, however, the unaffected majority of analyte molecules continues moving towards the detector and thus broadens the sample zone.

Five terms are commonly suggested to account for band broadening in packed beds:

A) Eddy diffusion.

B) Longitudinal diffusion in the mobile phase.

C) Resistance to mass transfer in the mobile phase.

D) Resistance to mass transfer in the stationary phase.

E) Resistance to mass transfer in the stagnant mobile phase.

A) Eddy diffusion (also called multiple-path broadening)

Every molecule flowing through a packing travels a different path. Due to non-uniformities in the packing these paths are not equal. Hence, in the end not all molecules will have traveled the same average length and will therefore arrive at the detector at different times. The non-uniformity of the inter-particle distances further aggravates this process with pressure-driven flow because the velocities in the channels between the particles vary. In electroosmosis-driven flow on the other hand, the velocities are constant throughout all channels (as shown in Chapter 1.2, p.6). The pathlengths are still not equal but the differences are reduced. The use of pressure-driven flow is further restricted to capillaries packed with 3 μm particles or larger since finer packing material causes an increase in capillary resistance to an extent where the pumps are unable to maintain the desired flow rate.[75] Electroosmosis-driven flow is unaffected by these problems, therefore it conveniently enables the use of smaller particles (usually 1.5 μm) which results in higher uniformity of the packing thus minimizing Eddy diffusion even further.[4, 76]

Both uniformity and particle diameter are incorporated in the quantitative expression for Eddy diffusion:[73]

$$H_{Eddy} = 2\,\lambda\; d_p$$

Equation 1.10: Eddy diffusion H_{Eddy} in mm; d_p stands for the particle diameter in mm and λ for a dimensionless packing factor estimated to be about 1.5 for HPLC and 0.1 for CEC, respectively.[73]

It should be noted that the particle diameter (d_p) also affects the packing factor (λ): when d_p becomes too small the particles tend to agglomerate thereby reducing the uniformity of the packing and also leading to overlap of the electroosmotic double-layer. The smallest employable particle size was calculated to be 40 nm (for an ionic strength of 0.1 M). At this value, significant overlap of the electric double layer is anticipated which renders generation of EOF impossible.[48, 49]

B) Longitudinal diffusion in the mobile phase

During their journey through the capillary, sample molecules will randomly diffuse forward and backward (longitudinal) with regard to the center of the sample zone due to longitudinal concentration gradients, as described by Fick's Second Law of Diffusion.[37, 63] One solution for the law's underlying partial differential equation is the so-called Einstein-equation. For packed beds, longitudinal diffusion is reduced by the packing material, leading to the inclusion of an "obstruction" factor and resulting in the following expression:[73]

$$H_{LD} = \frac{2\gamma D_M}{u_0}$$

Equation 1.11: Longitudinal diffusion H_{LD} in mm; γ stands for a dimensionless obstruction factor, D_M refers to the diffusion coefficient of solute in the mobile phase (usually around 10^{-3} mm^2*s^{-1}) and u_0 represents the average velocity of the mobile phase in $mm*s^{-1}$.

C) Resistance to mass transfer in the mobile phase

The third contribution to band broadening stems from lateral diffusion. From Figure 1.5, which showed the two different flow profiles, the existence of concentration gradients can be deduced not only in front of and behind the center of the sample zone (longitudinal) but also sideways (lateral) from it. As a consequence of these lateral concentration gradients analyte molecules will experience lateral diffusion. In analogy to Eddy diffusion, the existence of flow velocity differences in pressure-driven flow profiles enhances band broadening. In CEC, lateral concentration gradients do also exist but to a lesser extent due to the plug-like flow profile. A quantitative description for this process is given in the following equation:[73]

$$H_{RtMTMP} = \frac{\omega\ d_p^2}{D_M} u_0$$

Equation 1.12: Resistance to mass transfer in the mobile phase H_{RtMTMP} in mm; ω represents a dimensionless packing factor similar to λ in the Eddy term and all other symbols have the same meaning as in Equation 1.11.

The remaining two factors are independent of the flow profile, i.e., the degree of band broadening is essentially the same for HPLC and CEC:

D) Resistance to mass transfer in the stationary phase

The finite amount of time required for the adsorption of a molecule onto the stationary phase is another cause for band broadening and can be approximated as:[73]

$$H_{RtMTSP} = 2\frac{k_i^{'}}{(1+k_i^{'})^2} t_D u_0$$

Equation 1.13: Resistance to mass transfer in the stationary phase H_{RtMTSP} in mm; $k^{'}_i$ is the (usually) dimensionless capacity factor and t_D is the average adsorption / desorption time in s. All other symbols have the same meaning as in Equation 1.11.

E) Resistance to mass transfer in the stagnant mobile phase

The last contribution to band broadening takes into account the porosity of the particles making up the stationary phase. It does not apply when non-porous stationary phase particles are employed (1.5 μm particles, for instance, are usually non-porous [77]). Most stationary phase particles contain many small pores (both flow-through, also called intra-particle channels, and dead-end pores). They comprise a substantial amount of the chromatographic surface area required for interaction with analyte molecules. This implies that apart from flow *around* the particles (termed interstitial flow) there must also be substantial flow *through* the pores of the particles (called intra-particle flow). With pressure-driven flow, most interstitial flow is dominated by convection. Relative to that, mobile phase in the pores does not move but is stagnant due to the small inner diameters which result in a resistance too high to be overcome by conventional pumps used for HPLC and μ-HPLC. Consequently, sample molecules must first diffuse through this

stagnant mobile phase before they can interact with the stationary phase within those pores. The overall process is described in the following equation:[73]

$$H_{RtMTStMP} = \frac{\frac{(1-f+k_i')^2}{30(1-f)(1+k_i')^2} d_P^2}{\gamma' D_M} u_0$$

Equation 1.14: Resistance to mass transfer in the stagnant mobile phase $R_{tMTStMP}$ in mm; f stands for the (dimensionless) fraction of mobile phase in the pores and γ stands for a dimensionless tortuousity factor that accounts for the tortuous paths in the pores. All other symbols have the same meaning as in Equation 1.11.

With the prerequisite of pore sizes being large enough so that no overlap of the electroosmotic double layer occurs, CEC has again been shown to be advantageous. Now the flow in both flow-through and dead-end pores is not governed by diffusion but by electroosmosis, the latter being a convective flow substantially faster than diffusion.[48, 49, 68, 69, 78, 79]

Based on the additive contribution model one can now conveniently express the total plate height H_{total} resulting from all five causes of band broadening:

$$H_{total} = H_{Eddy} + H_{LD} + H_{RtMTMP} + H_{RtMTSP} + H_{RtMTStMP}$$

Equation 1.15: Total plate height H_{total} II (in mm).

Equation 1.15 serves as the theoretical base to explain experimentally determined plate heights for different mobile phase velocities. It can be simplified by recalling that the three resistance to mass transfer terms contain the velocity in the numerator,

longitudinal diffusion is inversely proportional to the velocity, and the Eddy term is velocity-independent. In analogy to van Deemter plots in Gas Chromatography, one can therefore restate Equation 1.15 to obtain a more useful equation for highlighting the role of the mobile phase velocities:

$$H_{total} = A + \frac{B}{u_0} + Cu_0$$

Equation 1.16: Total plate height III ("van Deemter Equation") H_{total} in mm; u_o represents the average mobile phase velocity in $mm*s^{-1}$, A stands for the Eddy diffusion term (Equation 1.10), B implies longitudinal diffusion (Equation 1.11 without velocity term) and C contains all three resistance to mass transfer terms (Equations 1.12, 1.13 and 1.14, all without velocity term).

For experimentally derived plate heights, Equation 1.16 serves as a foundation for finding the velocity that yields the minimum plate height and thus maximum efficiency. It can also serve to compare efficiencies for different techniques or packings. In this respect, both theoretical calculations and experimental results reported by several authors have shown that CEC using microparticulate stationary phase is normally superior to HPLC by a factor of 2. This is primarily ascribed to differences in Eddy diffusion, in lateral diffusion and in resistance to mass transfer in the stagnant mobile phase. [4, 53, 73]

After determining the flow rates that lead to the lowest achievable plate height, the overall separation efficiency is commonly expressed as the number of theoretical plates N defined as the ratio between capillary length and plate height:

$$N = \frac{L}{H}$$

Equation 1.17: Number of theoretical plates N (dimensionless); L stands for the capillary length from inlet to detector in cm or m and H indicates the plate height in the same unit as L.

On top of all these five major causes of band broadening additional factors must be considered as well. Since their contribution is usually less important than the previous causes and a suitable quantitative description often lacking, only brief reference will be given here. A prevalent problem stems from potential mismatches in conductivities between sample and mobile phase, named electrodispersion, and is easily recognized by characteristically triangular peak shapes.[38] Its occurrence can be avoided by adjusting ionic strengths and thus conductivities between mobile phase and sample, e.g., by desalting the latter one. Other additional factors consist of reasons commonly referred to as extra-column band broadening. They include band broadening caused by the injection process, capillary irregularities at the injection end, the frits, connection pieces (for instance, when coupling a chip through a capillary to a mass spectrometer), the detection process and data processing.[80, 81] Frits somewhat present an exception as they sometimes significantly contribute to band broadening.[82]

1.5 Individual particles versus monoliths

Most of the early work in CEC employed the frit approach introduced in Chapter 1.1: the introduction of retaining frits at the in- and outlet was necessary in order to confine microparticulate stationary phase inside the capillary. Otherwise the particles would move out of the capillary since they also possess electrophoretic mobility

stemming from silanol or other functional groups at their surface. A variety of methods to manufacture such frits have been reported in the literature.[11] One common approach is filling the capillary at the inlet with bare silica slurry, followed by sintering the capillary at this position with a heated wire. This process fuses the capillary and silica-slurry together, yielding a porous frit.[4, 65, 73, 83-87] Thereupon, the capillary is filled with stationary phase slurry, either hydrodynamically or electrokinetically. Filling by centrifugation has been reported as well.[88-90] The sintering process is then repeated at the outlet. Overall, the process requires high operator skills since it is deemed to be challenging and tedious for both manufacture of the frits and the filling process. Besides, it often results in poor chromatographic reproducibility. The limited flexibility and fragility of the capillary at the locations of the frits frequently leads to accidental breakage.[91] Heterogeneities inside the frits can enhance band broadening and contribute to bubble formation at the interfaces as potential nucleation sites.[82, 92] Moreover, sintering is not a practical option for chips because the high thermal conductivity would result in very large frits and the elevated temperatures would likely damage the chip. The necessity for several pieces of equipment (e.g., connectors, reservoirs, pumps) causes the approach to be more expensive compared to the monolith approach which does not require any of them. Preliminary studies using CEC in our laboratory fully confirmed these concerns when preparing frits.[93] Such difficulties might also help to explain the ten year gap between the first full realization of the potential of CEC by Knox and Grant in 1987 [3] and the more wide-spread acceptance of CEC as a separation technique in the mid 1990's.[9]

Still, there is one aspect of using frits and, in turn, microparticulate stationary phase that should not be overlooked: in theory it should be possible to unload the stationary phase particles as well. At first sight, this does not appear as a realistic option since at least one frit would have to be removed, which is something simply not possible with sintered frits due to the way they are manufactured. Yet if frits were made from a different material, for instance, a polymer that could be dissolved when desired, an alternative would have been found. A polymer frit would also present an approach useful for the chip format since no damage to the chips during manufacture of the frits is to be expected. A monomer solution yielding a porous polymer upon photopolymerization has been described in the literature by Zare and co-workers.[94] Reproduction of their method in the capillary format with some technical modifications, followed by its implementation in the chip format will be described in the first part of Chapter 3 of this thesis.

Quite a different approach in introducing a stationary phase material would be the monolithic approach. Its aim is to incorporate only one, extremely large particle (in the cm range) instead of many, small, individual particles (in the μm range). Anchoring this large particle to the capillary wall through a chemical reaction would alleviate the need for retaining frits and would greatly decrease manufacturing time. There is normally no such particle of the exactly right dimensions of the capillary geometry available (which furthermore would somehow have to be pressed into the capillary). Consequently, an *in situ* reaction starting with liquid precursors to form the desired single particle offers an alternative. The liquid precursors could simply be loaded into the capillary via gravity flow or through a syringe without further equipment needed. Because polymer frits have already been shown to be a possibility, their manufacturing would only have to be

modified in a way that they yield a polymer long enough to serve as one single particle. This particle should then ideally possess a functional group yielding the desired chromatographic properties, for instance, C_{18}-moieties for reversed-phase CEC. It could be part of the initial polymerization mixture, or be added on later. Such long pieces of polymers displaying large single particles are termed monoliths, monolithic stationary phases, monolithic columns or continuous beds.

The literature already mentions a wide range of suitable precursors that have been successfully exploited to yield monolithic stationary phases for HPLC and CEC.[6, 57, 95-106] Their initial development was sparked by distinctively different reasons than providing frits. Originally developed to provide greater pH-stability for HPLC compared to silica-supported particles,[107] the new goal was to diminish band broadening caused by the stagnant mobile phase, as conceptualized by Hjertén in 1992.[108] When dealing with microparticulate stationary phase in HPLC, most of the intra-particle liquid is stagnant. Therefore, any transport of analyte inside the particles (where the bigger part of the chromatographic area is located) is governed by slow diffusion. As outlined earlier, considerable band broadening is the result. For a monolith, the absence of interstitial channels should decrease band broadening because there are now presumably only intra-particle channels. Still, the channels have to be broad enough so that the pumps can deliver sufficient convective flow, and the occurrence of dead-end pores with essentially no convective flow but only diffusion will nonetheless put some restraints on the separation efficiency. These restraints do not necessarily apply for CEC, though. Here, EOF is the dominant driving force everywhere and narrow channels do not exhibit a problem as long as there is no significant double layer overlap. Narrow channels actually

simply add more surface area and thus increase capacity implying another profound advantage. The same applies for dead-end pores where EOF still should manage to provide sufficient convective flow. Not surprisingly, several authors consequently observed better resolution when comparing CEC to HPLC separations that both used the same monolith.[17, 109]

Another driving factor for developing monolithic stationary phases was the potential to generate tailored, or custom-made, stationary phases in terms of surface area, functional groups and porosity simply by adjusting the composition of the monomer mixture (provided that a thorough understanding of all parameters affecting the polymerization is known).

Regarding the nature of monoliths, they can be made of synthetic organic materials (rigid organic polymer-based monoliths) or from inorganic materials based on sol-gel technology, the use of natural polymers has been reported as well.[9, 79, 109] Monoliths from synthetic organic material can be further subdivided into acrylate- and methacrylate-based polymers, polystyrene-based or acrylamide-based polymers.[9, 29, 66] A typical monomer mixture consists of monomer, cross-linker, a binary or ternary mixture of porogenic solvents, an initiator and usually a co-monomer. The cross-linker is the backbone of the monolith and the monomer contains the functional-group to yield chromatographic properties, e.g., a C_8- or C_{18}-groups for reversed-phase CEC. Polymerization occurs through a step-wise chain reaction and can be thermo- or photo-initiated, with the photo-initiated procedures sometimes being significantly faster. The role of the co-monomer is to provide a functional group capable of EOF-generation.

Lastly, before the photopolymerization is investigated in greater detail, one last aspect of monoliths *and* polymer frits should be mentioned briefly. Since they both allow only dissolved sample or solvent to pass through they also function as physical filters to retain particulate matter from the sample, an aspect that apparently so far has not found much attention in the literature but will be of importance for the unfiltered biofluid separations to be discussed in Chapter 6.

1.6 Photopolymerization for frits and monoliths

Viklund et al. attempted a thorough characterization of the polymerization process for the preparation of their monolith. They observed initial nuclei-formation by the monomer and cross-linker that both grew in size but also almost immediately started interconnecting with one another. The porogenic solvents themselves did not participate in the reaction but competed with unreacted monomer for the solvation of the nuclei, i.e., restricting the growth of the nuclei. Hence, the binary mixture always consists of a solvent providing high solubility for unreacted monomer and a second one providing low solubility. Pore size of the monolith was found to be highly dependent on the ratio of these two solvents.[110]

Briefly revisiting porous polymer frits at this point, it becomes evident that they are not anything else other than extremely short monoliths that lack the functional groups necessary to achieve chromatography. Figure 1.6 shows the structures of glycidyl methacrylate (GMA), trimethylolpropane trimethacrylate (TRIM) and benzoin methyl ether (BME), i.e., the monomer, cross-linker and photoinitiator used in this work for the generation of the porous polymer frits:

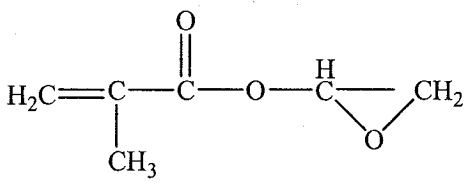

GMA

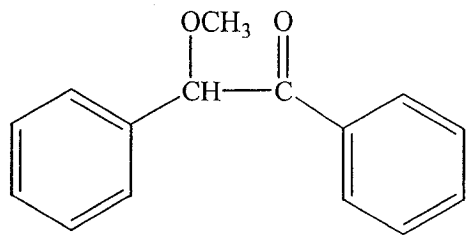

BME

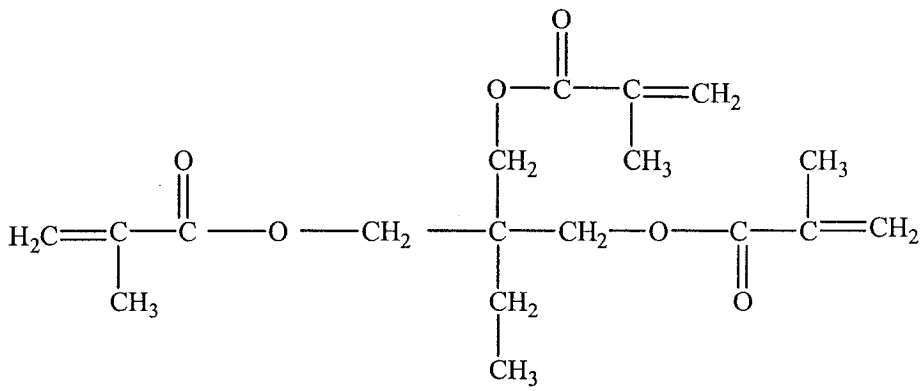

TRIM

Figure 1.6: Monomer (GMA), cross-linker (TRIM) and photoinitiator (BME) involved in the preparation of porous polymer frits.

Photoinitiated polymerizations in capillaries occur significantly faster than thermally initiated reactions, e.g., compare the work by Ngola et al. and Zhang et al. [111] and [112] (30 minutes versus several hours). In order to afford control of size and location of a frit, a second benefit of photopolymerization is that light can be focused more easily than heat.

BME was selected as a photoinitiator based on its absorbance maximum at 365 nm, a wavelength that allows photopolymerization in UV-transparent capillaries, i.e., Teflon-coated capillaries.[110, 113-116] Polyimide-coated capillaries (which are more widely

used) permit photopolymerization, too, but only after removal of the protective coating.[117] The polymerization can furthermore be accomplished in glass chips as long as they enable sufficient transmission at this wavelength.[118]

Photoinitiators are usually built around the benzoyl chromophor due to its excellent photochemical reactivity and strong absorption in the UV-range. Figure 1.7 illustrates the formation of the two radicals upon absorption of a photon, a process known as α-cleavage or the Norrish I photoscission process:

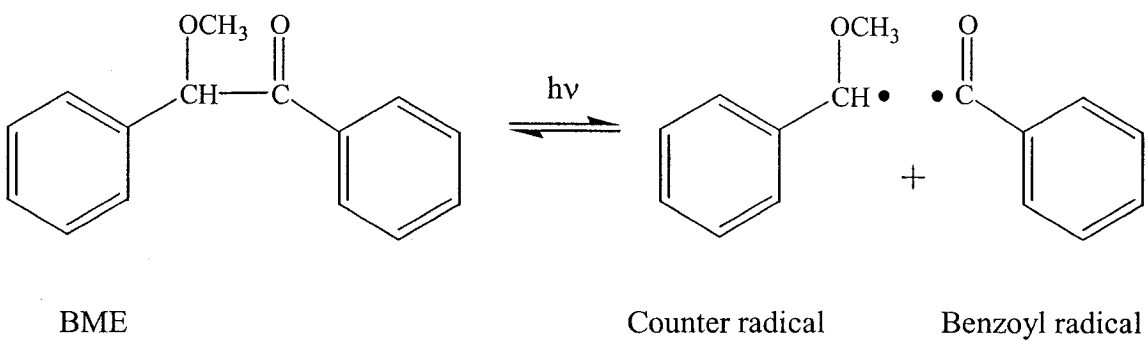

Figure 1.7: Alpha-cleavage of BME.

The benzoyl radical has been recognized to be the primary initiating radical for the polymerization reaction, with its counter radical taking part to a lesser extent.[119] Since Oxygen is known to deactivate BME after BME has undergone intersystem crossing from the singlet to the triplet state, the occurrence of Oxygen in the polymerization mixture should be avoided by degassing the reaction mixture.[114]

The polymerization mixture to obtain the CEC monolith also exploits BME as a photoinitiator. In this case, the monomer is butyl acrylate (BAC), co-monomer is 2-

acrylamido-2-methyl-1-propanesulfonic acid (AMPS) and the cross-linker is 1,3-butanediol diacrylate (BDDA), as depicted in Figure 1.8:

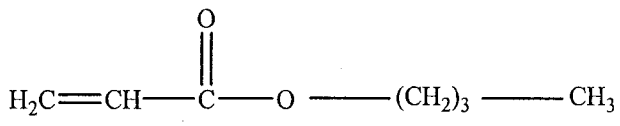

BAC

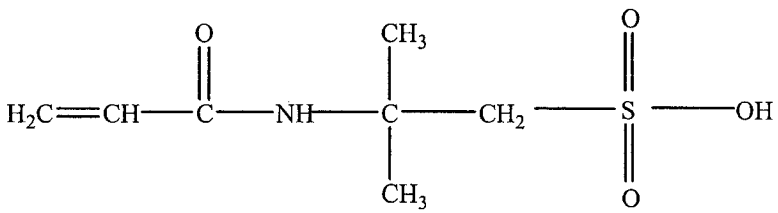

AMPS

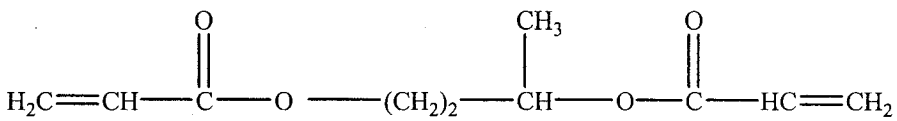

BDDA

Figure 1.8: Monomer (BAC), co-monomer (AMPS) and cross-linker (BDDA) involved in the preparation of the monolith.

1.7 Capillaries versus chips

Traditionally, CEC is conducted in the capillary format with the same type of capillaries employed as in CE, i.e., made of fused-silica, a material that permits EOF-generation on its wall when in contact with certain liquids (see Chapter 1.2, p.6). Since

fused-silica is rather fragile, coating of the capillaries enhances flexibility and prevents accidental breakage. The standard coating is polyimide, a substance with low transmittance in the UV-region. Hence, a detection window must be formed by burning off a small length (around 1-5 mm) of the polyimide with a lighter or etching it away with hot, concentrated sulfuric acid, followed by rinsing off the charred remainder with methanol. As long as only a small piece of polyimide is burnt off, the flexibility of the capillary is not significantly compromised, especially when the window is positioned inside the detector which adds stability. The situation changes for the photopolymerization of monoliths because now a rather long strip of polyimide (several cm) has to be removed for successful irradiation of the polymerization mixture and flexibility of the capillary is greatly reduced. For this reason, parts of the Results section of this thesis investigate the use of Teflon-coated UV-transparent capillaries. Their coating provides sufficient transmission in the UV-region for photopolymerization and also eliminates the need for creating a detection window.

Both types of capillaries are identical with regards to their dimensions, which range from 10-100 cm in length with 10-200 μm I.D and 180-360 μm O.D., respectively. [10, 11] Typical injection volumes are in the low nanoliter range and the applied field strengths range from 100 V/cm to 1 KV/cm. The following picture illustrates a typical setup for CEC (which is essentially the same as any CE setup apart from the packing):

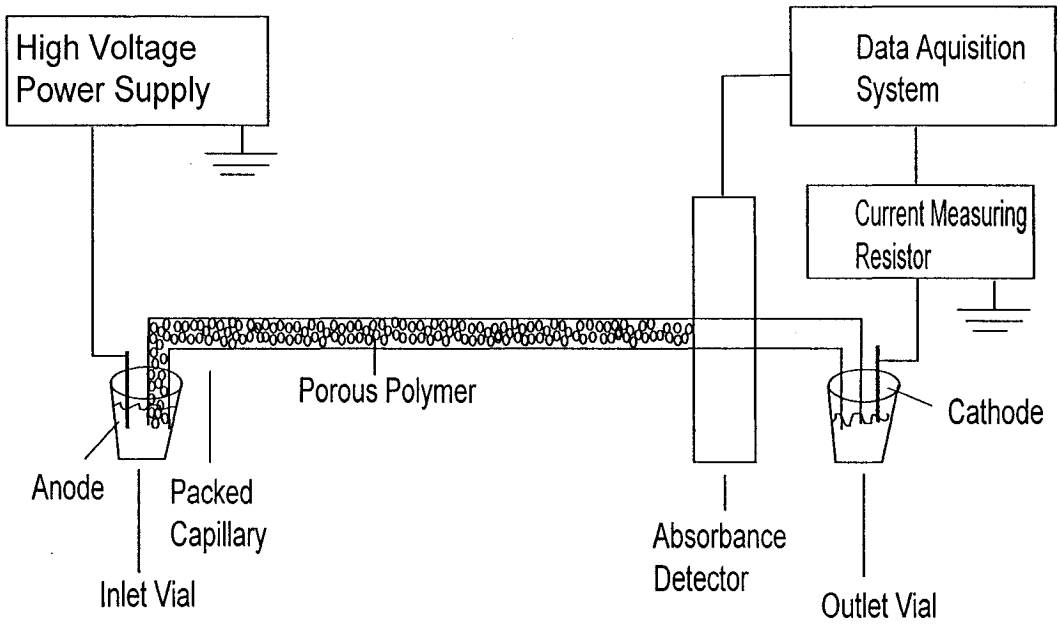

Figure 1.9: Typical configuration of a CEC-system.

Analysis times from around 2 min [82] up to 100 min [54] have been reported. Apart from variables like pH, solvent composition and so forth, the applied electric field strength is among the factors one should optimize in order to combine resolution and high speed. In analogy to CE, the maximum is determined by the heat transfer properties of the packed capillary and the field strength causing dielectric breakdown of the fused-silica.[120, 121] If the heat generated inside the capillary can no longer be dissipated efficiently the mobile phase will ultimately heat up, produce temperature gradients that degrade the separation and, in the extreme, bubble generation causes the current to break down. Before this point is reached, though, the degree of band broadening will change from run to run due to the temperature dependence of the diffusion coefficient. Given that some of the factors describing band broadening have the diffusion coefficient in the numerator and others in the denominator, it is difficult to anticipate if band broadening

actually increases or decreases but reproducibility will definitively be compromised.[3] On the positive side, a certain amount of heat can speed up separations by diminishing interactions between analyte and stationary phase.[54, 112] However, this heat is usually contributed to the system from the outside, for instance, by thermostating the capillary. A large surface to volume ratio partially governs effective dissipation. The extent of temperature gradients (both inside the capillary and with the surroundings) plus the thermal resistances of all materials involved (i.e., mobile phase, fused- silica and coating) also influence the dissipation. Heat generation inside a capillary is directly proportional to the conductivity (and thus the ionic strength) and the applied electric field.[122, 123] A complex relation to the structure of the packing material exists as well.[3, 124] Bubble generation naturally occurs faster with organic solvents due to their lower boiling points. It should be noted that once a bubble is generated (be it by inefficient heat dissipation or any other mechanism), subsequent removal becomes difficult and almost always requires connection of the capillary to a high-pressure pump thus essentially requiring an extra HPLC instrument to be available.[125] If the applied field strength exceeds a certain threshold, dielectric breakdown of the capillary occurs where the current is not transported through the mobile phase inside the capillary but through the capillary material itself. For fused-silica, this value has been calculated to be around 1 KV/cm.[126]

Heat transfer properties were one of the arguments that spawned the development of microfluidic devices: their surface to volume ratio is notably higher so heat can be dissipated more effectively. Besides, since a chip is thick and inflexible, it does not need a protective coating surrounding the channels, a distinct advantage over capillaries since coatings tend to be thermal insulators.[10] Higher field strengths in microfluidics enable

completion of analyses within a few seconds without worrying about heat generation and dissipation (the exception are silicon-based chips due to the semiconductive properties of silicon which prohibit high field strengths [27]).

Development of microfluidics is based on many different strategies and offers many potential advantages over more conventional separation vehicles. Generally, one can think of them as being embedded in the larger field of nanotechnology. Richard Feynman first presented this tantalizing subject in 1959 in his now famous talk at Caltech. It revolutionized the microelectronic industry in subsequent years and for nearly 15 years now has cast its spell on the analytical community.[15, 30, 36, 127] Yet it is less the dimensions but rather the fluid volumes manipulated on chips that are truly "nano", for instance, injection volumes of about 0.1 nL.[128] In a broader context, chips are often referred to as "lab-on-a-chip" or "micro-total-analysis-systems" supporting the notion that, in theory, the single entity of a chip can incorporate all functional elements necessary to perform an analysis, i.e., mixing chambers, separation channel, detector, communication electronics and so on.[26]

Along this theme, one chip can contain a large number of each of these elements, e.g., several separation channels switched in series or in parallel. The channels switched in series allow for polydimensional analysis, e.g., a separation based on electrophoresis followed by a separation based on chromatography. Alternatively, channels in parallel permit the simultaneous analysis of many different samples at once. This strategy enables researchers to cope when very high numbers of separations are necessary, e.g., for high-throughput screening in drug research, and also facilitates automation.[129] The large amount of data obtained in a brief period of time allows for a thorough statistical

treatment, an issue of major importance when dealing with validation issues, or the application of chemometric tools. The possible incorporation of a high number of branching-channels contributes an additional dimension to the design and can, for example, greatly facilitate aspects like gradient elution or post-column labeling. Such features can be included in the capillary format, too, but the mere connection of two capillaries often imposes major technical problems (and costs). The production process for microfluidics (for instance, photolithography for glass and quartz chips) allows many channels and chambers to be incorporated in one, single chip without any significant increase in the production costs.

Provided that effective ways of mass productions are developed in the future, the tiny size of chips makes them ideal for use in hand-held instruments. Such devices can deploy the lab at the sample site and considerably decrease time and costs associated with sample transport, instead of vice-versa. Potential applications are manifold, e.g., point-of-care clinical measurements at home or extraterrestrial applications, just to mention a few.[12, 26, 27] An aspect that chips share with capillaries in CE, CEC and μ-HPLC but not with traditional wider-bore columns (like in HPLC) is that only minute amounts of both sample and mobile phase are required. This becomes crucial when the analyte is precious and sample size limited, for example, in single cell analysis.[130] Likewise, very small amounts of waste are generated. During one day of operation microliter amounts of waste are generated with chips or capillary-based methods as compared to several liters of solvent produced by a conventional HPLC instrument. Environmental friendliness and cost effectiveness are important considerations to foster acceptance of new methodologies. Mass production of chips might further allow disposability of chips

which renders rinsing and reconditioning steps redundant, albeit compromising the aforementioned environmental friendliness. In comparison, rinsing and reconditioning in CE can easily cost more time than the actual analysis.[131]

The majority of miniaturized separation instruments reported, until recently, were instruments utilizing a purely electrophoretic separation principle (although the very first instrument designed was actually a miniaturized gas chromatograph [132]). To date, the number of publications in the literature is still limited where the microfluidic device employs a chromatographic rather than an electrophoretic separation mechanism.[15, 16, 18, 20, 21, 30, 32, 111, 133-137]

As it is not uncommon for novel techniques, one has to overcome several difficulties before the scientific community generally accepts the new technique. Apart from novel aspects of fluid dynamics and the need to prove that monoliths can be implemented reproducibly, one major problem inherent to microfluidics is the short optical pathlengths of the channels, which limit the mainstay of UV-VIS absorbance detection.[70, 137] Depending on the material, detection in the UV region is furthermore severely compromised due to the limited transmittance of glass and many plastics, with quartz presenting the pricey exception. The author of this thesis worked with glass chips (the exact design to be illustrated in Chapter 3) and used laser-induced fluorescence (LIF) as the detection method of choice in the VIS region. Regrettably, only a minority of analytes possesses natural fluorescence in this range. Hence, most analytes have to be labeled with a fluorescent tag prior to detection, with the consequences for the chromatographic properties so far being unpredictable. However, under the assumption that saturation has not been reached, one benefit ascribed to this mode of detection is the

linear dependence of the signal on the radiant power incident on the sample, unlike in UV-VIS detection, as shown in the following equation:[138]

$$F = kc\Phi$$

Equation 1.18: Dependence between emitted fluorescence F (arbitrary units) and radiant intensity Φ incident on the sample; k is a proportionality constant (contains the pathlength of the detection cell, the quantum efficiency of the analyte and its absorptivity) and c stands for the analyte concentration.

The high radiant powers of lasers used as light sources for the excitation of analyte molecules can consequently offset the small optical pathlengths encountered when using capillaries or microfluidic devices even though the chip is less than ideal for UV/VIS absorbance detection and glass strongly absorbs below 350 nm. Nevertheless, the transmittance of the chip employed in this work (Corning 0211 Borosilicate) is 90% at 365 nm, i.e., still large enough for photolytic cleavage of the photoinitiator BME in order to start the polymerization reaction.[138]

The main part of the result section of this thesis will describe characterizations and applications with photopolymers in capillaries since Concordia University does not have production facilities and only a very limited number of glass chips could be acquired. Nonetheless, Chapter 3 will deliver a proof of principle and demonstrate the incorporation of these photopolymers as both frits and monolithic stationary phases and a simple separation.

1.8 Summarizing the potential of electrochromatography

A brief table summarizes and highlights the most important aspects that make CEC a promising alternative with regards to more established separation technologies like HPLC, μ-HPLC and CE. One important aspect pointed out by several authors involving yet another intrinsic strength of CEC is the unique wealth of information that can be gained when coupling it to mass spectrometry (MS) via electrospray ionization (either in the capillary or in the chip format). Unlike many other detection methods, MS allows for both structural and quantitative information.[139, 140] Although low volumetric flow rates in CEC (nL/min) compared to μ-HPLC (μL/min) often require sheath flow and electrical contact at both ends of the capillary must be maintained (which complicates the electrospray source) the high separation efficiencies afforded in the liquid phase when compared to HPLC or μ-HPLC even justify these laborious efforts necessary to couple CEC to MS. With respect to CE, CEC uses buffers and mobile phases that are often more compatible with MS due to low ionic strengths, low surface tensions and high volatility. This thesis does not include any studies involving MS but they will hopefully be part of future work by the author's successor(s). For the sake of clarity, the following table does not distinguish between CEC in the capillary or in the chip format and furthermore assumes CEC, μ-HPLC and HPLC are all carried out using monoliths.

Table 1.1: Comparison between CEC, μ-HPLC, HPLC and CE

	CEC	μ-HPLC	HPLC	CE
Separation of neutral analytes? [2]	Yes	Yes	Yes	No[1]
Separation of charged analytes? [3]	Yes	No	No	Yes
Separation of charged analytes in stationary phase? [4]	Eventually (postulated)	No	No	N/A
Solvent consumption	Few microliter per day	Several microliter per day	Several liter per day	Few microliter per day
Sample volume	Nanoliter	Nanoliter	Microliter	Nanoliter
Sensitivity (absorbance detection)	Low (pathlength about 100 μm)	Medium (pathlength about 500 μm)	High (pathlength about 1 cm)	Low (pathlength about 100 μm)

Table 1.1 continued

	CEC	μ-HPLC	HPLC	CE
Heat dissipation	Good due to low ionic strengths of solvents	N/A	N/A	Less efficient due to higher ionic strengths
Potential for photopolymerization	Yes	Yes	No [5]	N/A
Type of mass transport [6]	Convection	Convection and diffusion	Convection and diffusion	Convection
Flow profile [6]	Piston-like	Poiseuille-like	Poiseuille-like	Piston-like
Possibility to act as a physical filter	Yes	Yes	Yes	No
Frequency of bubble formation [7]	Occasional	Rare	Rare	Very rare

1) An exception is micellar electrokinetic chromatography but this mode of operation is in most cases incompatible with MS due to the surfactants involved. Its separation efficiency is also limited.

2) Based on a chromatographic mechanism, i.e., hydrophobic interactions with a stationary phase.

3) Based on an electrophoretic mechanism, i.e., charge to size ratio.

4) Based on the postulated mechanism of electrodiffusion.

5) HPLC columns are commonly made of steel or plastic, neither material is suitable for photopolymerization. Monolithic columns in HPLC can only be made using thermal polymerization.[8]

6) The resulting advantages for band broadening have been discussed in section 1.4.

7) With subsequent breakdown of the current.

1.9 Contribution to original knowledge

A brief overview on the experimental work conducted for this thesis with emphasis on the contribution to original knowledge shall be given at this point with emphasis on the novelties of this research.

The following chapter will provide technical details regarding the instrumentation and list all materials and reagents. Starting with Chapter 3, the result section will first describe the incorporation of porous polymer frits in capillaries and the subsequent filling with microparticulate stationary phase. A separation of neutral analytes, in this case polyaromatic hydrocarbons (PAHs), will demonstrate that CEC indeed has been realized. Although the work is based on a procedure published by Zare and co-workers [94] it does

contain an important technical modification in the use of the "pig" to create the inlet frit. Besides, the novel incorporation of these frits into a chip will also be demonstrated and does present a novelty. Since subsequent electrokinetic loading of the chip with microparticulate stationary phase could not be achieved, the remainder of Chapter 3 explores a monolith as an alternative based on a procedure published by Ngola et al.[111] yet modified to permit photopolymerization. A rapid separation of polyaromatic hydrocarbons is shown. Separating two fluorescent dyes on-chip illustrates that monolithic CEC can also be carried out in the chip format and that chromatography indeed occurs. Chapter 4 then treats methods to characterize the monolith as well as UV-transparent capillaries. Although these methods have been applied to different monoliths by other authors they have not yet been applied to the monolith described in this thesis. Numerous chromatographic properties are evaluated, for example, van Deemter plots for various PAHs. Flow rate measurements via μ-HPLC determine column permeability and tortuosity. Optical characterization of both the packing and the capillaries employs Atomic Force Microscopy (AFM) and Scanning Electron Microscopy (SEM). This is the first employment of AFM to characterize monoliths in CEC. Chapter 4 also reports the characterization of the EOF as a function of several variables, e.g., ionic strength and pH, just to mention a few. For the first time, wave-guiding properties of UV-transparent capillaries are reported and several capillary cutting techniques compared. Lastly, it looks into the problem of bubble generation and into new methods to recover capillaries from bubbles.

Chapter 5 introduces protein separations in greater detail, again a novelty with this monolith. Maximum loadability, detailed comparisons to other separation techniques,

dependence on percentage organic solvent are just a few of the factors investigated. Surprisingly, it cannot be proven that chromatography is the underlying mechanism for the separation of the proteins selected for this research. Nonetheless, the use of monoliths is a valuable alternative towards other techniques since they appear to greatly diminish irreversible protein adsorption onto their surface, as can be seen from the separation of serum proteins in Chapter 6. This chapter further explores novel applications for the monolith, e.g., the separation of non-steroidal anti-inflammatory pharmaceuticals, oligonucleotides, or quality control monitoring of synthesis products for a fluorescent dye. In all cases, chromatography definitively does drive the separation. Chapter 6 also presents preliminary results for the separation of bovine milk proteins and human amniotic fluid constituents (the fluid that surrounds the fetus). A summary and outlook will be given in Chapter 7.

Chapter 2: Experimental

This chapter summarizes the instrumentation and experimental setups that were used *without* further modification in order to conduct this research. It does not describe instrumental modifications or arrangements made for individual experiments. Rather, these are listed, and explained, in the Results sections of the relevant chapters. Additionally, this chapter lists all suppliers of instrumentation, materials and reagents used for this research. It also provides an overview of all solutions and suspensions.

All aqueous solutions were prepared using HPLC-grade water (18 MΩ, Millipore, Billerica, MA, USA). Unless indicated otherwise, all materials and reagents were stored according to vendors' recommendations. Sample solutions were generally prepared just prior to injection by diluting stock solutions with the respective mobile phase to yield the desired concentrations. Mobile phase was prepared on a daily basis by mixing the desired volumetric amounts of organic solvent and aqueous buffer. The pH of a mobile phase exclusively refers to the aqueous buffer portion. Brown 1.5 ml polypropylene flat top microcentrifuge tubes (Fisher Scientific, Neapan, Canada) served as mobile phase and sample reservoirs. They were exchanged each run in order to minimize buffer depletion through electrolysis.[141]

2.1 Instrumentation for experiments in the capillary format

Experiments were conducted using a laboratory-built CEC instrument with the experimental setup already shown in Figure 1.9 (p.34). UV-transparent (Teflon-coated)

and polyimide-coated capillaries were purchased from Polymicro Technologies (Phoenix, AZ, USA). In both cases, they had 360 μm O.D. and 100 μm I.D. Capillary cutters were bought from Chromatographic Specialties (Brockville, Canada). The Shortix™ column cutter was acquired from Scientific Glass Technology (Middelburg, The Netherlands). Platinum wire (0.5 mm diameter) for the electrodes was purchased from Goodfellow (Cambridge, UK). Potentials were applied to the inlet vial using a Spellman Model CZE 1000R high-voltage power supply (Happauge, NY, USA). The capillary current was measured via a current to voltage converting resistor at 20 Hz using a PCI-1200 (12 bit resolution) data acquisition board (National Instruments, Austin, TX, USA). Injection and separation voltages were controlled through an analog output port of the board using a program written in LabView 5.1 graphical programming language (National Instruments). Detection was provided using either a Unicam 4225 UV detector (Mississauga, Canada) operated at 214 nm or 254 nm with a sensitivity of 0.01 absorbance units full scale and a rise time of 0.1 s or an ISCO CV^4 Variable Wavelength Capillary Electrophoresis Detector (Lincoln, NE, USA) operated with the same sensitivity but a rise time of 0.4 s. Absorbance signals were collected at 20 Hz and digitized using the previously described board. Data was presented in graphical form by reading the files into IGOR Pro Version 3.15 (WaveMetrics, Lake Oswego, OR, USA) and analyzed using GRAMS/32 Version 4.01 (Thermo Galactic, Salem, NH, USA). Photopolymerization for both frits and monoliths was carried out with a General Electric H85A3 high-pressure Mercury vapor lamp (General Electric, Toronto, Canada). Spectral output was 4.1 mW/cm^2, with the lamp placed 50 cm above the capillary. The spectral

output was measured using an Indicator Model 154BT power meter (Laser Instrumentation, Chertsey, UK).

2.2 Apparatus for column packing

CEC columns were packed using a Waters 600E System Controller HPLC pump (Waters, Milford, MA, USA) and a 600 Multisolvent Delivery System (Waters). Silica SealTight Tubing Sleeves F-242X (1/16'' O.D., 0.15'' I.D.) and PEEK F-300 Two-Piece Fingertight Fittings with replaceable F-142 PEEK Ferrules were purchased from Upchurch Scientific (Oak Harbor, WA, USA).

2.3 Instrumentation for experiments in the chip format

The chip employed in this study (see Figure 3.3, p.47) was made of Corning 0211 Borosilicate glass (Precision Glass and Optics, Santa Anna, CA, USA) with an area of 4''x 4'' and a thickness of 600 μm. It was purchased from Alberta Microelectronic (Edmonton, Canada) and originally designed by R. Oleschuk in Edmonton using L-Edit software for photomask design (Tanner, Pasadena, CA, USA). Marine Silicone, used to glue the reservoirs to the chip, was obtained from General Electric (Toronto, Canada). For the same purpose, "Lepage 12 Five Minute Epoxy" glue and "Mastercraft" epoxy were acquired from Canadian Tire (Toronto, Canada). In order to control all the electrophoretic voltages necessary for packing the chip with microparticulate stationary phase and for all liquid handling a power supply and relay system was employed that had

been designed and manufactured by L. Carson and C. Skinner (University of Alberta, Edmonton and Concordia University, Montreal, Canada). It allowed for simultaneous control of 5 electrodes via a +10 KV output, -10 KV output and three bipolar +/- 4 KV outputs. High voltage relays (SO5LTA235, Kilovac, Santa Barbara, CA, USA) enabled toggling of the high voltages between sample injection and mobile phase dispensing. Electrical contact between the high voltage leads and reservoirs was made through Platinum electrodes (0.5 mm diameter, Goodfellow, Cambridge, UK). A confocal microscope for analyte detection on the chip was designed by C. Skinner and manufactured by the machine shop of Concordia University. The design is given in Appendix I (p.183). A 5 mW air-cooled Argon-ion laser (Uniphase, San Jose, CA, USA) with an output wavelength of 488 nm was used as an excitation source. The fluorescence signal was monitored by a photomultiplier tube model P28 (Hamamatsu, Bridgewater, N.J., USA) operated at 500 V. The current was recorded at 10 Hz via a current to voltage converting resistor using a PCI-1200 (12 bit resolution) data acquisition board (National Instruments). Computer control of the power supply and data acquisition was accomplished by a program written by C. Skinner using National Instruments' LabView 5.1 programming language (National Instruments) through the I/O port of the data acquisition board. Data was presented in graphical form by reading the files into Excel (Microsoft, Seattle, WA, USA). Digital images of porous polymer frits in chips were taken using a DVC-1310 Monochrome Digital Camera (DVC Company, Austin, TX, USA) and analyzed using Vision Builder 6 (National Instruments).

2.4 Instrumentation for μ-HPLC studies

The μ-HPLC system (Figure 4.3 p.91) consisted of a Waters 600E System Controller HPLC pump (Millipore, Bedford, MA, USA), a 600 Multisolvent Delivery System (Millipore) and a 486 Tunable Absorbance Detector (Millipore). The injection volume was 20 μL. Split-flow was realized with a zero dead-volume tee union purchased from Valco (Houston, TX, USA). A 15 cm x 0.46 cm Spherisorb-Octyl 5 μm column (Chromatography Sciences Company, Montreal, Canada) served as the flow resistor for the split flow. The Unicam 4225 UV detector with 0.01 absorbance units full scale and a 0.3 s rise time was employed for detection through the capillary. Connection between the tee union and the capillary was achieved using the same fittings and tubing described under 2.2.

2.5 Scanning Electron Microscopy

All capillary images were collected at 7 KV using a Hitachi (S-2300) Scanning Electron Microscope coupled to a Kevex image analysis system. (Hitachi, Brisbane, CA, USA). The capillaries were coated with vacuum deposited gold to improve conductivity by a Polaron PS3 Mini Sputter Coating Unit (Polaron, Newhaven, UK). Prior to analysis, the sample to be investigated was prepared inside a capillary as described in Chapter 3 and the pushed out hydrodynamically by connecting the capillary to an HPLC pump.

2.6 Atomic Force Microscopy

Images were acquired with a Digital Instruments AFM Nanoscope III Dimension 3100 (Veeco, Woodbury, NY, USA). Measurements were performed in tapping mode with a Rotated Tapping Mode Etched Silicon Probe Model RTESP7 (resonance frequency 188.5 KHz, Veeco). Sample preparation occurred identically as described for scanning Electron Microscopy.

2.7 Circular Dichroism Spectroscopy

Circular dichroism (CD) spectra were recorded with a Jasco J-710 Spectropolarimeter (Jasco, Easton, MD, USA) in the wavelength range of 200-260 nm and a resolution of 0.2 nm. Speed of collection was 100 nm/min, response time 0.25 s, band width 1 nm and sensitivity 50 mdeg.

2.8 Materials and reagents

A) Reagents and materials for porous frits and monolith:

Glycidyl methacrylate (GMA), technical grade trimethylolpropane trimethacrylate (TRIM), A.C.S. grade isooctane, HPLC grade toluene, butyl acrylate (BAC), 1,3-butanediol diacrylate (BDDA), (3-methacryloyloxypropyl)trimethoxysilane (MTS), 2-acrylamido-2-methyl-1-propanesulfonic acid 99% (AMPS), Amberlite IRA-900 ion-exchange resin and A.C.S. grade absolute ethanol (EtOH) were all acquired from Sigma-

Aldrich (Oakville, Canada). Benzoin methyl ether 98% (BME) was purchased from Fluka (Sigma-Aldrich, Oakville, Canada), HPLC-grade acetonitrile (ACN) and HPLC grade methanol (MeOH) from Fisher Scientific (Neapan, Canada). A.C.S. grade sodium hydroxide (NaOH) was purchased from ICN Biomedicals (Aurora, OH, USA), A.C.S. grade glacial acetic acid from J.T. Baker (Phillipsburg, NJ, USA). Nucleosil 100-3 C_{18} microparticulate stationary phase was kindly donated by Macherey-Nagel (Düren, Germany).

B) Analytes for chip studies:

4,4-difluoro-4-bora-3a,4a-diaza-*s*-indacene-3-propionic acid succinimidyl ester (BODIPY SE) and fluorescein were purchased from Molecular Probes (Eugene, OR, USA). Stock solutions were made weekly by dissolving the desired amount in 1 mL DMF and kept in the dark.

C) Polyaromatic hydrocarbons:

Naphthalene, acenaphthene, anthracene, pyrene, fluoranthene, pyrene, chrysene, benzo[k]fluoranthene and benzo[a]pyrene were all obtained from Sigma-Aldrich (Oakville, Canada). Stock solutions of PAHs were prepared in 1 mL DMF on a monthly base.

D) Proteins:

Myoglobin (horse heart), transferrin (human), α-lactalbumin (bovine milk), β-lactoglobulin A (bovine milk) and α-chymotrypsin (bovine pancreas) were obtained from

Sigma-Aldrich. Protein stock solutions were made freshly on a daily basis in 1 mL 5 mM pH 7.4 phosphate buffer.

E) Oligonucleotides:

PermHisTag (62 bases), D246E (45 bases) and Oligo-CL (22 bases) were purchased from BioCorp (Montreal, Canada). For comparison, PermHisTag was also bought from Integrated DNA Technologies (Coralville, IA, USA). They were diluted with the respective mobile phase immediately before use.

F) Non-steroidal anti-inflammatory drugs:

Ibuprofen, ketoprofen and naproxene were acquired from Sigma-Aldrich. Stock solutions were made on a weekly base by dissolving the desired amount in 1 mL ACN.

G) Biofluids:

Human serum was bought from Sigma-Aldrich. Stock solutions were prepared on a daily base by diluting the serum with the respective mobile phase. Human amniotic fluid was a gift from Dr. K. Koski, McGill University (Montreal, Canada) and kept frozen at -85°C until assayed. It was injected undiluted. Quebon 2% Milk (Longueuil, Canada) was used for the milk analysis. It was diluted in the respective mobile phase prior to use. None of the fluids were filtered before use.

H) Other reagents:

Thiourea and caffeine were acquired from Sigma-Aldrich. Thiourea stock solutions were made weekly by dissolving the desired amount in 1 mL of water, the same

applies for caffeine. Anthracene-2,3-dialdehyde (ADA) was purchased from Molecular Probes. Stock solutions were prepared on a daily base by dissolving the desired amount in 1 mL DMF and kept in the dark.

I) Buffers:

Sigma Ultra grade sodium tetraborate decahydrate, monobasic sodium phosphate, dibasic sodium phosphate and Tris(hydroxymethyl)aminomethane (TRIS) were all acquired from Sigma-Aldrich. A.C.S. glacial acetic acid was acquired from J.T. Baker (Phillipsburg, NJ, USA).

All buffers were prepared by the same principle that either the free acid or base was dissolved in approximately 80% of the final volume of water. The pH was then adjusted by dropwise addition of HCl or NaOH, respectively. Thereupon, the resulting solution was further diluted with water to yield the desired final volume. For instance, phosphate buffer 5 mM pH 6.8 was made as follows: 150 mg monobasic sodium phosphate was dissolved in approximately 200 mL HPLC grade water and the pH adjusted by dropwise addition of 1 M NaOH solution. The solution was then further diluted to 250 mL with HPLC grade water in a volumetric flask. Borate buffer 5 mM was prepared by dissolving 477 mg sodium tetraborate decahydrate in 800 mL HPLC grade water and the desired pH also adjusted by dropwise addition of 1M NaOH solution. The solution was then further diluted to 1 L with HPLC grade water. All solutions were filtered with a Millex (Millipore, Bedford, MA, USA) 0.45 μm non-sterile syringe driven filter unit prior to use. Phosphate buffers were kept frozen at -20° C in order to minimize bacterial growth.

Chapter 3: Electrochromatography in Capillaries and Microfluidic Devices: Microparticulate Stationary Phase versus Monoliths

Inspired by the work of the first CHEM 419 student in our laboratory, M. Max Bogaert,[93] and at the same time discouraged by the technical difficulties and limitations of sintered frits he encountered in capillaries, the initial attempt of this thesis' author was to facilitate the incorporation of frits into capillaries through the use of porous polymers based on the methodology published by Svec and co-workers.[94, 110] The first part of this chapter will describe the author's work on how to pack a capillary with microparticulate stationary phase and at the same time incorporating porous polymer retaining frits (using the reagents shown in Figure 1.6, p.30). The process will be described in some detail in order to illustrate the technical challenges experienced when using conventional, polyimide-coated capillaries. The intended length of the packed bed in the capillary was approximately 15 cm. Due to the shorter distances on a chip (approximately 5 cm), it was anticipated that the time-consuming packing process would be significantly faster. Moreover, since a side-channel is provided, the chip format would allow for simultaneous generation of the frits, whereas in a capillary the outlet frit has to be made prior to filling the capillary with stationary phase, and the inlet frit can only be made after the filling.

Since overall the use of polymer frits did not prove to be satisfactory, the second part of this chapter will describe the manufacture of monoliths in both capillaries and chips (using the reagents presented in Figure 1.8, p.32).

3.1 Incorporation of porous polymer frits into capillaries and their subsequent filling with microparticulate stationary phase

In order to fill the capillary with stationary phase, a modified version of the high-pressure filling method in which the capillary is connected to an HPLC pump was adapted.[81, 93] Coupling between the capillary and the HPLC pump was accomplished as follows: first, the capillary was inserted into a 380 μm I.D. tubing sleeve. The sleeve was then inserted into standard HPLC fingertight fitting with ferrule connected to a 1/16'' union with the union's dead volume serving as a reservoir for the suspension of the microparticulate stationary phase. Afterwards, the union was connected to standard HPLC heavy wall tubing leading to the HPLC pump. The capillaries were polyimide-coated ones with a total length of approximately 50 cm, although UV-transparent ones could be used as well but they were not yet marketed at that time. The following figure illustrates the layout of a packed capillary with polymer frits:

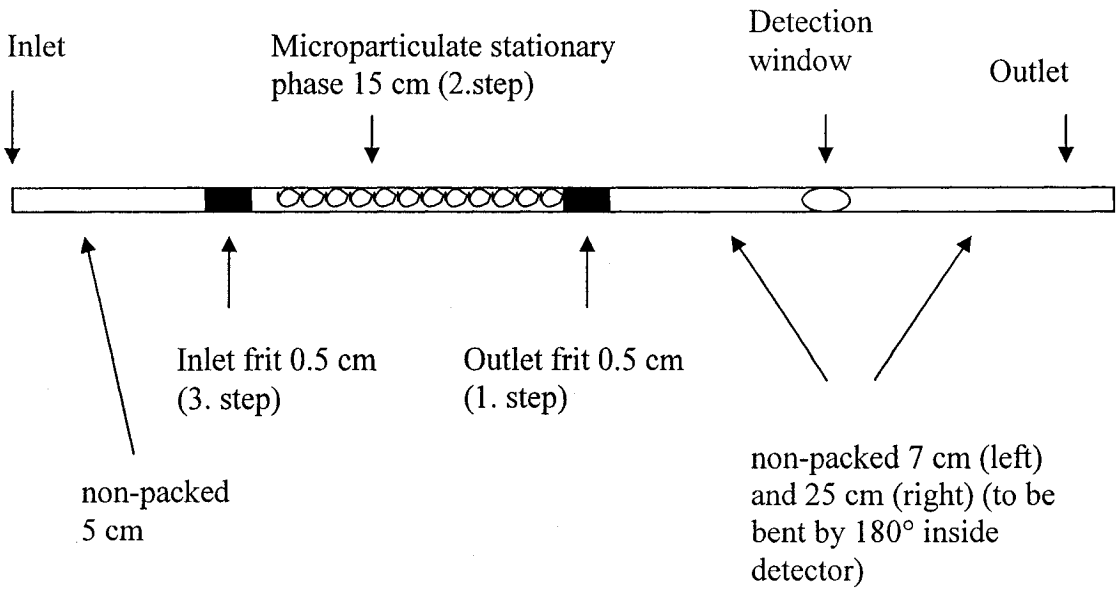

Figure 3.1: Layout of a packed capillary using porous polymer frits and microparticulate stationary phase. The capillary material is fused-silica coated with polyimide. Distances are approximations for a capillary of 50 cm total length.

A) Preconditioning of the capillary

Prior to making the actual column, 1.5 mL monomer (GMA) and 1.5 mL crosslinker (TRIM) solutions were prepared by adding approximately 150 mg of Amberlite ion-exchange resin to each solution, with overnight stirring of the solutions in the dark to remove inhibitors. The morning after, the solutions were centrifuged in order to remove the ion-exchange resin.

Preliminary experiments had indicated that the polymer frits inside the capillary moved under the influence of an electric field when using an aqueous mobile phase. A possible explanation could be contraction and subsequent "slipping away" of the polymer

frit in the aqueous phase as compared to the organic solvent system used during frit manufacture. One possible method to stabilize the polymer frit could be to roughen the inner surface of the capillaries to improve binding, e.g., by using an etching reagent during the preconditioning protocol such as 1 M NaOH. Apart from the stabilization effect, a preconditioning protocol also rinses and cleans by removing impurities from the capillary and thus leads to more reproducible retention times.[142] For the polymerization procedure in this thesis, a final drying step with Helium concluded the sequence. This step aimed to expel any water from the capillary before introducing the monomer mixture. Hence, the preconditioning steps were: purging with MeOH for 1 min, water for 1 min, 1 M NaOH for 1 min, water for 1 min and Helium for 2 min, with all steps carried out at 40 psi.

B) Preparation of the outlet frit

Prior to the actual polymerization, the polyimide coating of the capillary had to be removed at two positions to create two windows: the first one for photopolymerization of the outlet frit (approximately 20 cm away from the designated inlet end of the capillary) and the second window for detection (see Figure 3.1, p.57). Both windows were about 1 cm in length. In theory, detection should be performed immediately behind the outlet frit to restrict additional band broadening in the non-packed section of the capillary. However, in reality the two windows were separated by approximately 7 cm. This distance between the two windows was mandatory since the capillary had to be bent by roughly 180° in order to fit into the detection cell. If this section were to be packed it would become too fragile and susceptible to accidental breakage. The polyimide of the

capillary was removed by holding the capillary over the flame of a lighter for a short time and then rinsing off the burnt coating with MeOH.

Since a pore size of 2.5 μm appeared to be appropriate for retention of the 3 μm packing material the following mixture was prepared (according to Table 1 [110]): in a 1.5 mL brown Eppendorf tube 15 mg BME was mixed with 505 μL isooctane, 173 μL toluene, 142 μL TRIM and 335 μL GMA. To ensure complete dissolution of the BME the mixture was vortexed and ultrasonicated. A 5 min purge with Helium followed in order to expel any Oxygen. Thereafter, the polymerization mixture was hydrodynamically filled into the capillary. Parafilm sealed the ends of the capillary and aluminum foil covered everything apart from the window for the frit. The edges of the window were furthermore painted with liquid paper which efficiently blocked radiation and allowed defining the edges of the polymerization window more accurately compared to merely burning off the coating. Designated length of the frit was 0.5 cm in order to minimize any potential band broadening caused by the frit. Irradiation for 30 min was performed under a Mercury vapor lamp. Afterwards, the capillary was removed and the liquid paper washed off with acetone. The capillary was then connected to the HPLC pump and any unreacted monomer purged out with MeOH.

C) Packing of the capillary

After removal of unreacted monomers the capillary was disconnected. The HPLC tubing was turned upside down so that the outlet end of the union pointed upwards. The pump was switched on and the union gradually filled with ACN. When the union was completely filled, the pump was turned off and 100 μL liquid were manually removed

from the union and replaced by microparticulate stationary phase suspension (approximately 10 mg / 300 μL ACN) that had been vortexed for approximately 30 s. Reconnecting and bending the HPLC tubing by 180° allowed the capillary to point towards the ground. The pump was turned on again at a flow rate of approximately 0.04 mL/min. Within a few minutes a column of stationary phase material started to build up inside the capillary. With elevated column height the backpressure increased in order to maintain the flow rate. Typically, backpressure values reached the instrumental maximum of 3000 psi within 5-10 min.

When the packing ceased to build up any further, the flow was stopped and the capillary disconnected. The union was refilled with stationary phase suspension and the packing process repeated until the packed column had reached the desired height of around 15 cm (approximately five fillings were needed to reach this height).

D) Preparation of the inlet frit

A window for the inlet frit could only be made after completing the packing since prediction of the exact length of the packed bed was limited to a range of ± 2 cm. The conventional way of burning the window with a lighter is not applicable for filled or packed capillaries anymore because the liquid inside the capillary immediately starts boiling, with the resulting pressure wave purging out both packing and frits. A milder approach is the use of hot, concentrated sulfuric acid (160°C) to etch away the polyimide coating. Refilling the capillary with monomer mixture also requires an ingenious solution: hydrodynamic filling becomes obsolete because of the excessive backpressure generated from the packing material. Since the preparation of the inlet frit requires only

minute quantities of monomer mixture it would be harmful to the pump (and also fairly expensive) to fill one of the solvent reservoirs of the HPLC instrument with monomer mixture. Instead, the capillary was disconnected and the union replaced by an empty standard HPLC column that had been modified by placing a small piston-like metal plug into it, simply referred to as a "pig". Any liquid (ACN was used here) delivered by the pump pressure-drove the "pig" towards the outlet of the HPLC column. Two O-rings mounted around the "pig" supported its motion and prevented the liquids on each side from mixing with one another. Preliminary experiments had shown that any mixing between monomer mixture and ACN or MeOH inhibited polymerization at ACN or MeOH contents larger than 10% (V/V). When the "pig" had almost reached the outlet end, approximately 100 μL of monomer mixture was placed on top of it. The capillary inlet was connected to the outlet of the HPLC column and subsequently filled with monomer mixture. After the capillary was filled with monomer mixture, the photopolymerization continued in exactly the same manner as previously described for the outlet frit.

E) Conditioning of the packed capillary

Before using a packed capillary for separation, conditioning of the capillary by purging with the intended mobile phase is necessary to generate both a constant EOF and to align the C_{18}-chains. [143] At first, the column was pressure-conditioned via the HPLC pump for approximately 30 min followed by electrokinetic conditioning using the CEC apparatus described in Figure 1.9 (p.43) until both a constant current and constant absorbance were observed.

The following electrochromatogram depicts the separation of seven PAHs on this type of packed capillary:

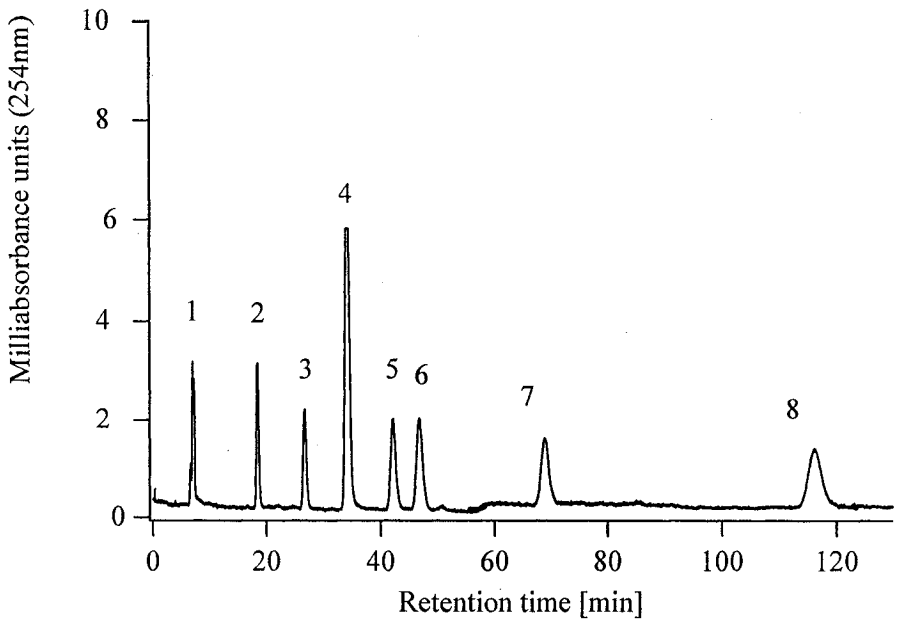

Figure 3.2: Separation of seven PAHs by CEC employing porous polymer frits, with 3 μm C_{18}-coated silica particles serving as microparticulate stationary phase. The distance between inlet and inlet frit was 5 cm, the length of the packed bed was 15 cm and the distance between outlet frit and detector 7 cm. Total length was 50 cm. Sample injection was carried out for 10 s at 15 KV and a separation voltage of 15 KV applied. The mobile phase consisted of 60% ACN / 40% 10 mM pH 9.4 borate buffer (V/V) and the ISCO CV^4 detector was employed. Order of elution and number of theoretical plates per meter (N/m, see Equation 1.17, p.24) were: DMF (1) (EOF-marker); Naphthalene (2) 62,000 N/m; Acenaphthene (3) 68,000 N/m; Anthracene (4) 93,000 N/m; Fluoranthene (5) 69,000 N/m; Pyrene (6) 60,000 N/m; Chrysene (7) 77,000 N/m; Benzo[a]pyrene (8) 74,000 N/m.

3.2 Usefulness of this approach to CEC and other observations

In the beginning, inspiration to pursue the idea of packed CEC with polymer frits stemmed from an article published by Svec and co-workers.[94] The use of the "pig" displays a new technical aspect (Svec did not report on how to create the outlet frit), the reason being that the "pig" demonstrates a unique way of pressure-filling the monomer mixture into the capillary without causing damage to the HPLC instrument. Attempting gravity filling or manual pressure-filling (through a syringe) are not realistic because the resistance from the packing renders these approaches impractical.

Contrarily to Svec who separated three organic benzene compounds, Figure 3.2 showed the separation of seven PAHs. Owing to their homologous properties and the absence of charged groups, PAHs are exploited quite frequently by researchers to test new CEC- or HPLC packings.[46, 57, 74, 76, 77] Besides, PAHs are an interesting sample due to their long term accumulation in the soil and the resulting health risks.

The number of theoretical plates reached in this experiment compares favorably with most HPLC separations but could possibly be enhanced by decreasing the distance between outlet frit and point of detection. Unfortunately, using the ISCO detector demands severe bending of the capillary for insertion into the detector. Several capillaries broke during installation if the detection window was right behind the outlet frit. These window / frit locations account for the most fragile sections of the capillary because of the lacking protective polyimide coating. For this reason, the detection window was created approximately 7 cm after the outlet frit so that only the non-packed section had to be bent. This section does not contribute to the separation because PAHs are neutral (it can only contribute to the separation of charged analytes through electrophoresis) yet

possibly enhances band broadening through longitudinal diffusion and extra-column band broadening. It should be noted that during the time of this particular set of experiments the UNICAM detector or UV-transparent capillaries used in later experiments were not yet accessible.

A major obstacle with packed capillaries and sintered frits previously encountered by Bogaert was their limited lifetime of often only a few runs, and the time-consuming packing process of generally several hours.[93] By contrast, the method described here allows for relatively rapid packing, i.e., a length of 15 cm of stationary phase can be reached within about 20 min (including the time required for refilling the reservoir with stationary phase suspension). The packing itself occurs in a sedimentation-like fashion, i.e., the particles do not agglomerate before or during the actual filling. This enables them to find the best orientation to one another. One consequently achieves a dense packing thus minimizing band broadening. During the packing process no devices that agitate the capillary were employed. Such devices, e.g., vortexers or ultrasonic baths are frequently used by other researchers in order to prevent clogging of the stationary phase at the contact point between reservoir and capillary.[81] On the other hand, continuous shaking might add sufficient energy to the stationary phase particles to enable entanglement of the C_{18}-chains with one another and thus might itself become a cause for clogging.

Limited column lifetimes of only a few runs were also not observed with the capillaries described here. Instead, lifetimes of up to three days were achieved. When a capillary failed it was normally caused by breakage due to its high fragility at the frits. One reason for the prolonged separation lifetime could lie in the absence of gas bubbles. Such bubbles are commonly believed to be caused by changes in the EOF between the

packed segment and the sintered silica frits. Consequently, different velocities of the mobile phase at the interfaces between frits and stationary phase can lead to high shear forces and subsequent bubble formation.[4, 85, 91, 92] When using a polymer frit, base-catalyzed cleavage of the epoxy groups of the polymer is expected to yield diol-groups when using alkaline mobile phases.[144] A diol group should be capable of generating an electric double layer similar to the ones at the surface of the capillary and the surface of the particles. Potentially, the magnitude of EOF generated by diol groups in the polymer frits rather resembles that of the stationary phase particles and so diminishes velocity differences at the interfaces and subsequent gas-bubble formation.

Several additional findings were made during the course of this project, partially resulting from the work of a CHEM450 student, Mrs. Rebekah Carson who was co-supervised by the author.[117] In order to keep the discussion within reasonable limits they are summarized in the following:

- Polymerization can be carried out using fluorescent room lights (standard household fluorescence lamps) in approximately 6 hours.
- Polymerization is strictly restricted to the exposed area; the polymer does not creep into unexposed regions.
- Frits can withstand a pressure of about 1500 psi but experience a slow movement with EOF (around 3 mm/day).
- A variety of acids, or bases, do not dissolve the polymer, even at elevated temperatures. Recycling of polymerized capillaries (or microfluidic devices) is therefore not possible.

- O-rings in the "pig" have to be exchanged after manufacture of three capillaries since the monomer mixture slowly erodes them.
- Crude separations are possible when attempting to use this polymer as a monolithic stationary phase for CEC or as a sheet for Thin Layer Chromatography.
- Introduction of C_{12}- or C_{18}-functionalities by adding lauryl acrylate, lauryl methacrylate or stearyl methacrylate to the polymerization mixture also yields a polymer. However, liquid cannot be pumped through, indicating little or no porosity.

No further experiments were conducted with this type of capillary because implementation in the chip format demanded priority due to its more original aspects.

3.3 Incorporation of porous frits into the microfluidic format

Figure 3.3 shows a sketch of the layout of the chip used by the author:

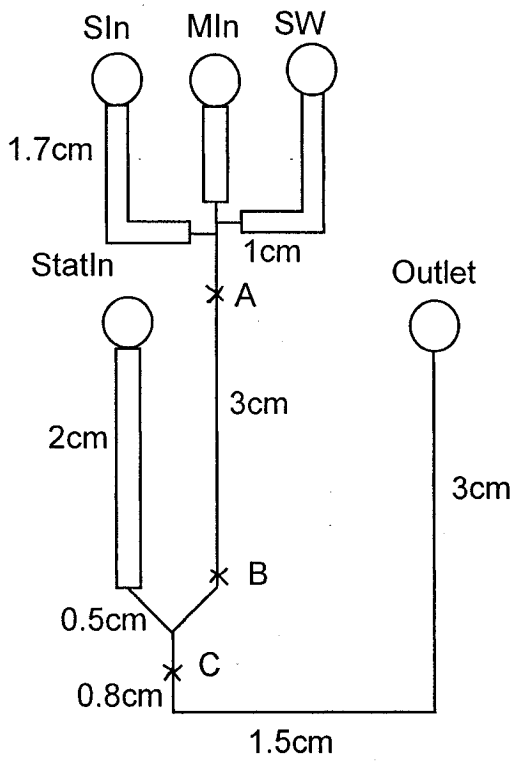

Figure 3.3: Sketch of the glass chip used to perform CEC. 'SIn' stands for 'sample inlet', 'MIn' for 'mobile phase inlet', 'SW' for 'sample waste' and 'StatIn' indicates 'stationary phase inlet', respectively. 'A' and 'C' are locations for the porous polymer frits. The distance between 'A' and 'B' marks the section where the monolith is incorporated (to be discussed in Chapter 3.5). Throughout the chip, the widths of the wider channels are 300 μm while the narrower channels are 50 μm wide. Channel depths are 15 μm everywhere. Access holes marked by the circles represent reservoirs or mixing chambers and have a diameter of 2 mm.

A) Manufacture of the frits

As was seen earlier, in the capillary format the stationary phase had to be loaded before making the outlet frit. Contrarily, the generation of the frits at positions 'A' and 'C' can be done simultaneously since, at least in theory, the side channel enables filling with the microparticulate stationary phase. Significantly shorter manufacturing times, compared to the capillary format, should thus be expected.

Fabrication of the frits inside the chip was readily achievable. Reservoirs had to be glued onto the access holes using epoxy-glue. These reservoirs consisted of the upper halves of ordinary micropipette tips. Two different epoxy-glues and one silicone-glue showed resistance against the polymerization mixture sufficient for the duration of polymerization (about 1 hour). However, upon exposure to ACN (serving as solvent for the stationary phase suspension), leakage occurred through the silicon-glue. Therefore only epoxy-glue was used.

By filling just *one* reservoir with the monomer mixture all channels could be filled hydrodynamically when applying a small vacuum using a water-jet pump. The remaining volume in this reservoir was first removed and then a fixed volume (20 μL) of monomer mixture pipetted into *all* reservoirs to avoid any hydrodynamic flow during the photopolymerization. The reservoirs were sealed with Parafilm to prevent evaporation. Using aluminum foil as a mask did not prove adequate in the chip format but rather resulted in polymerization outside the desired locations for the frits. It was simply impossible to apply a sufficiently smooth layer of the foil and any roughness could easily lead to reflection of light into the masked regions resulting in polymerization far away from the intended locations. Hence, to block any unwanted radiation, small black boxes

made of cardboard were placed over the reservoirs and black electrical tape attached over all channels except for the projected locations of the frits. The thickness of the chip was approximately twice as large as the outer diameter of a capillary (600 μm versus 360 μm) so an irradiation time of 60 min (instead of 30 min for capillaries) was deemed appropriate. After irradiation and inspection under a microscope, all reservoirs except for the outlet one were filled with MeOH to purge out any unreacted monomer. The outlet reservoir was emptied completely to allow hydrodynamic flow only in its direction. Applying a small vacuum generated by a water-jet pump assisted this step. Figure 3.4 shows a digital image of the two frits successfully incorporated into the chip:

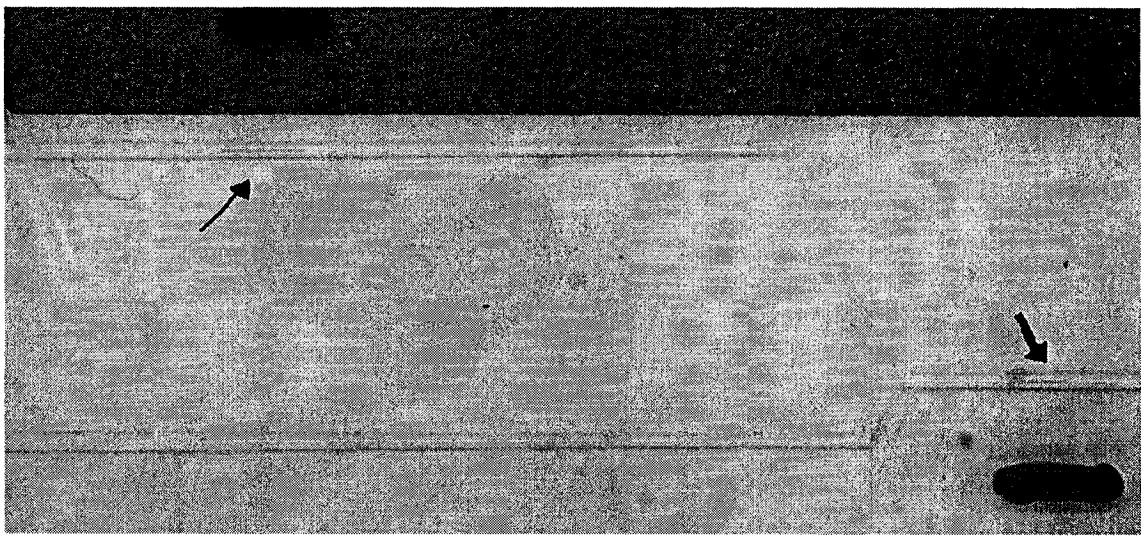

Figure 3.4: Incorporation of porous polymer frits in a microfluidic device. The arrows point at the two frits inside the channel (marked as positions 'A' and 'C' in Figure 3.3).

B) Filling the chip with stationary phase particles

Conventional pressure-filling with an HPLC pump becomes unfeasible in a chip since it cannot withstand high pressures and, secondly, coupling to the pump becomes very challenging from a plumber's point of view. Preliminary studies had also indicated that after incorporation of the frits applying a vacuum did not generate sufficient hydrodynamic flow to move the particles. This leaves electrokinetic packing as the last resort, a method rarely ever used either in the chip- or in the capillary format.[18, 88] Several initial experiments did not yield any substantial packing. Due to the limited number of chips available for this study, an inexpensive "poor man's chip" was conceived of in order to examine the electrokinetic packing process in more detail. This "chip" simply consisted of two reservoirs connected by a piece of capillary containing one frit, as illustrated in the following figure:

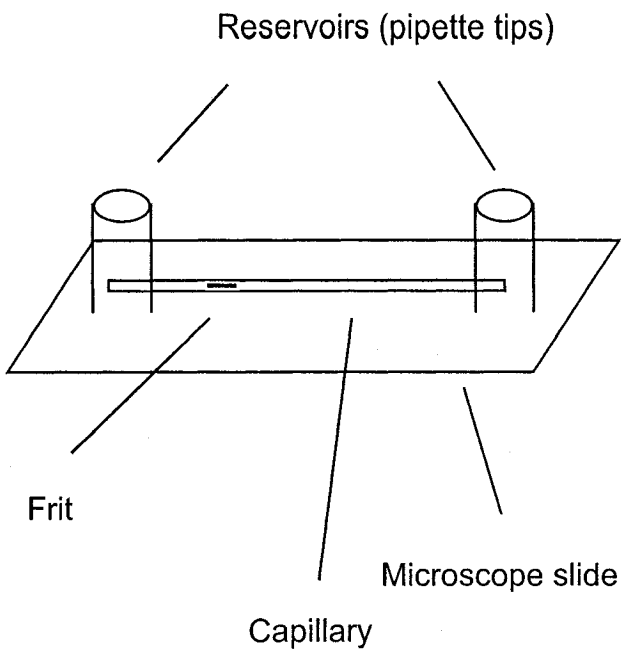

Figure 3.5: "Poor man's chip" to simulate electrokinetic packing in a microfluidic device.

The particle suspension was prepared in ACN since other solvents (MeOH, aqueous buffers and mixtures thereof) had been shown to lead to sedimentation or agglomeration of the particles more rapidly than ACN. The particle suspension was vortexed briefly before filling it into the inlet, with the duration of vortexing being found to be uncorrelated to the speed of sedimentation.

Upon application of an electric field, a rather unexpected particle movement was observed: below a threshold value for the electric field strength of approximately 500 V/cm, the particles moved with the EOF whereas the direction changed upon exceeding this value. Furthermore, rapid packing was seen to lead to a packed length of approximately 3 cm within a few minutes. Thereafter, the incoming particle stream orientated itself into a single-file pearl necklace-like line in the middle of the capillary

thus slowing down the packing speed considerably. Polarization effects could be responsible for the pearl necklace-like orientation.[40] The packing was terminated at this point since agglomerates of particles would break off from the packing and migrate back to the inlet. For compression of the packing, purging with a 5 mM pH 8.1 Tris buffer led to an increase in packing density and to a reduction in packing length from 3 to 1 cm.

These findings correlate with results from Oleschuk et al. who could not accomplish a packing length of more than five mm yet did not elaborate on the possible reasons.[18] Summarized, the observations can be stated as follows:

- For unknown reasons, the electrophoretic mobility of the particles employed depends on the applied field strength; their orientation is furthermore governed by polarization effects.
- The maximum achievable length of the packed bed is 3 cm before and 1 cm after compression.
- Agglomerates of particles always move against the EOF.

It should be added that the observations were made by watching the packing process under an optical microscope. Many more attempts were undertaken to obtain longer packed beds, e.g., by testing different solvents, stirring the reservoirs to prevent agglomeration and using voltage gradients, but none of these attempts proved to be successful.

A further complication was that upon implementing the electrokinetic packing in the chip format, the small achievable length of the packing was frequently accompanied

by rigorous bubble formation. Their removal from the chip was unfeasible since high pressure could not be readily applied. Overall, these problems rendered this packing approach not very promising forcing the author of this thesis to seek alternatives.

3.4 Incorporation of a monolith in the capillary format

Searching for alternatives to accomplish CEC in the chip format led the author to a publication by Ngola et al. [111] that described the incorporation of a monolith into both the capillary- and the chip format. Although the authors obtained relatively long analysis times for the separation of three neutral organic compounds in the chip format (around 40 min), the particular monolith was nonetheless found intriguing. Upon polymerization unreacted monomer could simply be purged out electrokinetically thus avoiding the necessity for high pressure (and consequently the mandatory HPLC pump). Towards miniaturization, this implies an important step since the fewer functional elements are needed for packing the more easily the latter goal is achieved. Another appealing factor was the monomer's butyl moiety (see Figure 1.8, p.32) which the author of this thesis found to be promising with respect to protein separations.[116, 145] Lastly, Ngola et al. mentioned a preconditioning procedure that covalently linked the monolith to the capillary wall and so inhibited any movement of the monolith.

For this thesis, the procedure described was modified to enable photopolymerization, instead of thermo-initiation (Ngola et al. used 2,2'-azobisisobutyronitrile, instead of BME). Regarding the studies described in this chapter, the capillaries employed were polyimide-coated with the coating removed over the entire length of the monolith, making the capillaries exceptionally fragile. On the positive side,

though, the drastically simplified and accelerated manufacture protocol permitted easy fabrication of several capillaries within one working day. Monolith preparation in the capillary format will be described next, followed by its incorporation in the chip format.

A) Pretreatment of the capillary

In order to approximate lengths typically found in chips, approximately 5 cm of the polyimide coating of a 20 cm long capillary were burnt off. The capillary was then initially filled with a solution consisting of 20% MTS, 30% glacial acetic acid and 50% water (V/V), and left overnight with the capillary ends sealed. Solutions of 1.5 mL monomer (BAC) and 1.5 mL crosslinker (BDDA) were prepared by adding approximately 150 mg of Amberlite ion-exchange resin to each solution. Thereupon, the solutions were stirred overnight in the dark to remove inhibitors. Centrifugation of the solutions the next day removed the ion-exchange resin.

B) Manufacture of the monolith

A casting solution was prepared consisting of 20% EtOH, 60% ACN and 20% 5 mM pH 6.8 phosphate buffer (V/V). In 1 mL of this solution, 3.0 mg AMPS and 15.0 mg BME were dissolved followed by the addition of 150 μL BDDA, 340 μL of BAC and 1.5 μL of MTS. After ultrasonication for 30 s, the capillary was first rinsed with this solution for 2 min. Next, the capillary ends were sealed and the entire capillary put under the Mercury vapor lamp for 25 min. Preliminary studies indicated a minimum irradiation time of 20 min. Since only the distance from the inlet to the point of detection was to be polymerized the remaining parts (detector to outlet) were masked with black electrical

tape. After irradiation, the tape was removed and the polymer inspected for cracks or bubbles. Usually, small bubbles were found at the inlet and outlet ends and these parts consequently cut off. Unreacted monomer was removed by applying a voltage of 10 KV for 30 min with the outlet end as the cathode using a mobile phase of 80% ACN / 20% 5 mM pH 10.0 borate buffer (V/V). Lastly, the capillary was preconditioned for 2 h, again at 10 KV with the desired mobile phase, usually 50% ACN / 50% 5 mM pH 10.0 borate buffer (V/V). The two hours were essentially the time needed to reach absorbance baseline stability. Current measurements revealed the resistance in the polymerized section to be approximately 1.9 times higher than in the non-polymerized one (see Appendix III, p.188). The only limitation to capillary lifetime determined so far was accidental breakage of the capillary.

The following figure shows a typical recording of the current during the first preconditioning step:

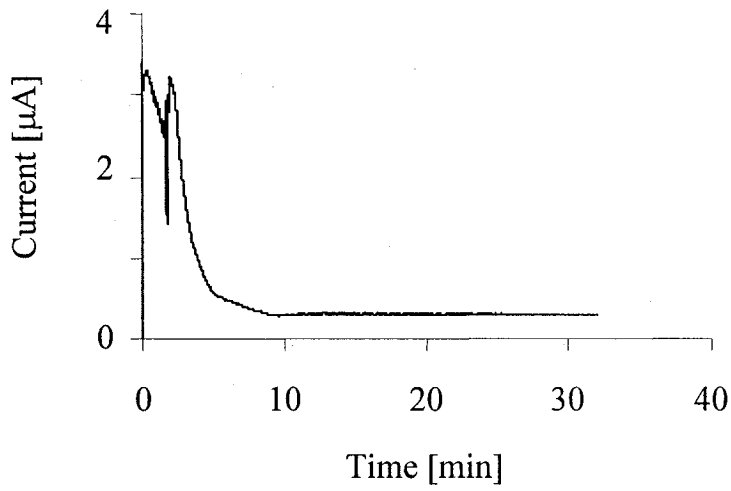

Figure 3.6: Typical recording of the current for the first preconditioning step in CEC employing a monolith.

The initial current decays within the course of approximately 5 min until it reaches its final value in the low microampere range. Current in this order of magnitude was reported to be typical for mobile phases possessing low ionic strength and high organic solvent content.[146] Malfunctioning capillaries can be readily detected at this point since their initial current decays much more rapidly until it becomes essentially undetectable.

The second preconditioning step employs the designated mobile phase for the separation. If the aqueous content or the ionic strength (or both) increase, the observed current should therefore augment and vice versa. PAHs were again used as probes to test the monolith. The separation of six PAHs in less than 3 min using this monolith is illustrated in the following picture:

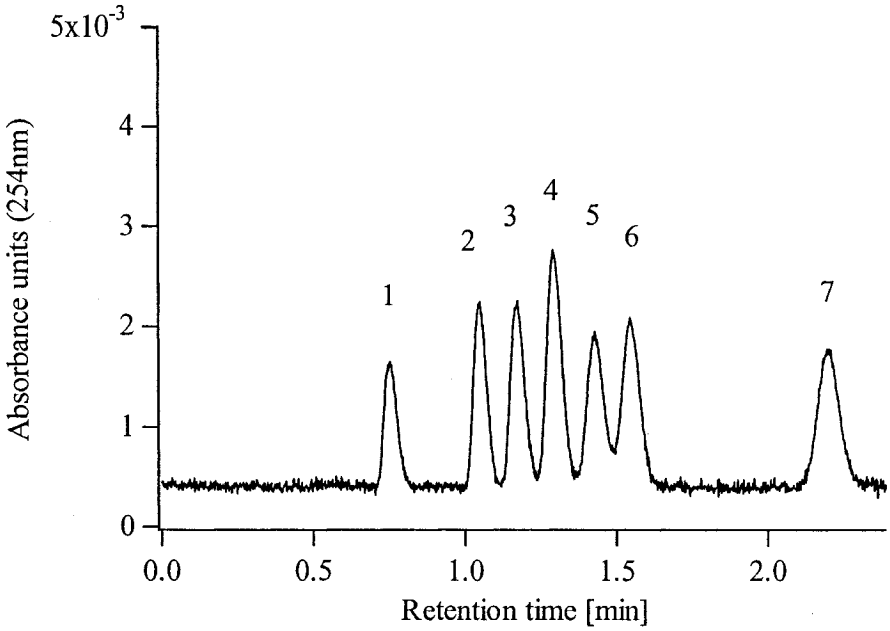

Figure 3.7: Separation of six PAHs by CEC using a monolithic stationary phase. The length of the monolith was 4.8 cm, the length from the inlet to the monolith 5.5 cm, total length was 18 cm. The separation voltage was 10 KV and sample injection carried out at 5 KV for 3 s. The mobile phase consisted of 80% ACN / 20% 5 mM pH 8.1 Tris (V/V). The Unicam detector was employed. Order of elution and number of theoretical plates per meter (N/m, see Equation 1.17, p.24) were: Thiourea (1) (EOF-marker); Naphthalene (2) 45,000 N/m; Acenaphthene (3) 61,000 N/m; Anthracene (4) 74,000 N/m; Fluoranthene (5) 59,000 N/m; Pyrene (6) 67,000 N/m; Benzo[a]pyrene (8) 78,000 N/m.

This particular separation was selected since it demonstrates the possibility of very rapid separations even in the capillary format. The length of the monolith (5 cm) approximates the length to be found in the chip format. No attempts were undertaken to optimize this separation since it sufficiently demonstrated the ability of the monolith to separate uncharged analytes solely based on a chromatographic separation principle. A non-polymerized section of 5 cm had to be included ahead of the monolith, otherwise, the capillary would not have been long enough to fit into the detector. The open section probably again contributed to band broadening. Since polyimide-coated capillaries were still employed, removal of a relatively large amount of the coating was necessary and

fragility was admittedly extremely high even though the Unicam detector did not require any bending of the capillary. The fragility problem ultimately forced the author to seek out alternatives leading to the exploitation of UV-transparent capillaries for all experiments described in the following chapters.

3.5 Incorporation of the monolith in the chip format

Preparation of the chip and subsequent photopolymerization were achieved identically to the procedure described for the incorporation of frits (though using the different monomer mixture). The only difference was that this time unreacted monomer could be removed electrokinetically by applying a potential of 5 KV between mobile phase inlet and outlet for approximately 30 min followed by preconditioning for 2 h with the desired mobile phase for the intended separation. The relatively long preconditioning time required the reservoirs to be refilled frequently due to their inherently small volumes that facilitated evaporation.

As mentioned earlier, the glass chip demands absorbance detection above 360 nm. Alternatively, Laser-Induced Fluorescence (LIF) detection can be readily employed. Two fluorescent dyes that emit in the visible range were therefore chosen as model analytes, namely BODIPY succinimidyl ester (BODIPY SE) and fluorescein. Their molecular structures indicate BODIPY SE remaining neutral at any pH while fluorescein is negatively charged at a pH > 6.4:[147]

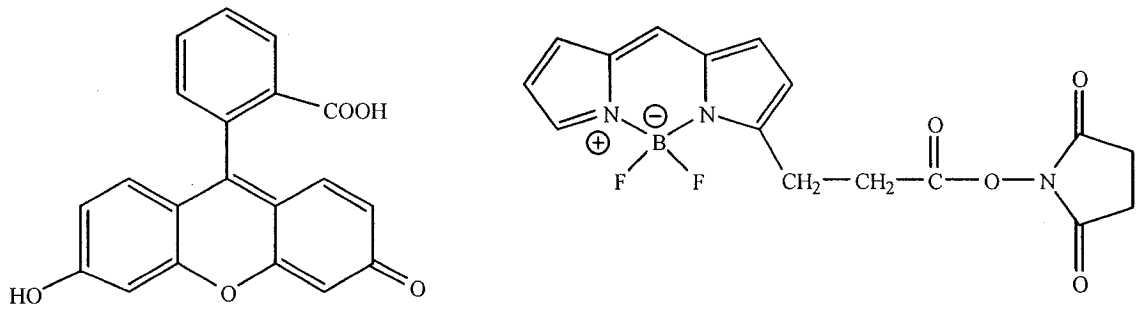

Fluorescein BODIPY Succinimidyl ester

Figure 3.8: Molecular structure of fluorescein and BODIPY SE.

The separation of BODIPY SE and fluorescein is depicted in the following figure:

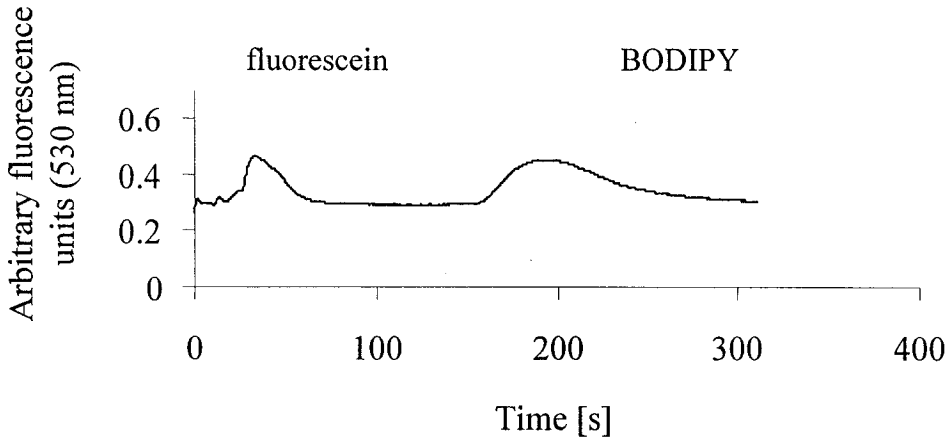

Figure 3.9: Separation of two fluorescent dyes in a microfluidic device using a monolithic stationary phase. The length of the monolith was 3 cm with the point of detection being right behind the monolith (see Figure 3.3, p.67). The applied separation voltages were +500 V at the mobile phase inlet, -125 V at the sample inlet, -50 V at the sample waste and -5000 V at the outlet. Injection was carried out by applying +1250 V at the sample inlet, +500 V at the mobile phase inlet and – 50 V at the sample waste for 30 s. A confocal microscope illustrated in Appendix I (p.184) was used for detection. The mobile phase consisted of 60% Methanol / 40% 10 mM pH 9.3 Borate (V/V). Order of elution and number of theoretical plates were: Fluorescein (1) (700 N/m); BODIPY SE (2) (2100 N/m).

If merely electrophoresis took place, at pH > 6.4 BODIPY SE should be eluting with the EOF *before* fluorescein since the latter one is negatively charged and therefore possesses a negative electrophoretic mobility (see Equation 1.5, p.14). The reversed order of elution, though, proves the presence of chromatography since only the latter one could cause a neutral analyte to elute *after* a negatively charged one.

Although the numbers of theoretical plates demand improvement, e.g., by finding the optimum sample injection parameters, both the successful incorporation of the monolith into the chip format and the occurrence of a chromatographic separation mechanism were verified by this separation. Numerous additional technical challenges had to be overcome during this particular set of experiments. However, they primarily resulted from the power supply and the confocal microscope applied for detection and shall not be elaborated here (instead, they are described in the report from CHEM419 student Mrs. Vicky Bablekis [148]).

All the results presented so far served to outline the path that eventually would lead to the use of a monolith as stationary phase in chip-based CEC. Successful incorporation of the monolith into the chip format was demonstrated. Yet due to the limited availability of microfluidics, chip-based CEC was not pursued any further during the time allocated to this thesis. Instead, it was deemed more reasonable to thoroughly investigate and characterize the behavior of this particular monolith in the capillary format before any future continuation in the chip format.

Chapter 4: Characterization of the Monolith in the Capillary Format

Starting with an investigation of the chromatographic properties of the monolith through further separations involving PAHs, a physico-chemical characterization will be used to estimate porosity, tortuosity and permeability of the packing. To verify and "visualize" these factors, Atomic Force Microscopy (AFM) and Scanning Electron Microscopy (SEM) will be exploited to shed light on the surface topography, morphology and the distinct types of pores present in this monolith. The chapter continues with an investigation on how the EOF depends on experimental variables. On a side note, all separations described from now on were carried out using Teflon-coated UV-transparent capillaries. Due to their enhanced flexibility the monolith could always stretch from the capillary inlet to the point of detection, i.e., there was neither an open segment in-between capillary inlet and beginning of monolith nor in-between the end of the monolith and the point of detection. Various "peculiarities" of UV-transparent capillaries will be treated. Lastly, different methods will be compared to expel the occasional gas-bubbles from the capillary.

4.1 Characterization of chromatographic properties through the use of polyaromatic hydrocarbons as probes

One of the most promising aspects of monoliths lies in their earlier mentioned ability to permit high mobile phase flow velocities while simultaneously maintaining low

plate heights. The next two plots illustrate the relation between flow velocity and plate height (van Deemter plots) for two PAHs:

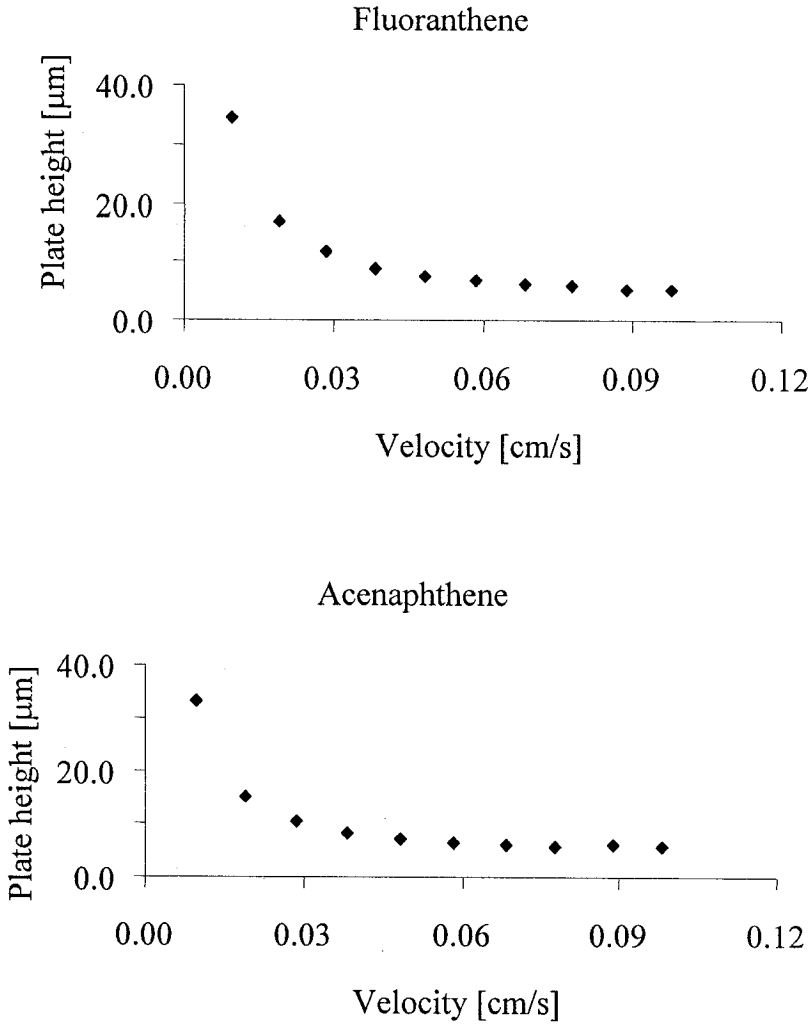

Figure 4.1: Plots of plate height versus mobile phase velocity for two PAHs (van Deemter plots). The mobile phase consisted of 80% ACN / 20% 5 mM pH 10.0 borate buffer (V/V). Sample injection was carried out for 5 s / 2 KV and the applied separation voltage ranged from 1 KV to 10 KV. The velocities were determined from the ratio of capillary length from inlet to detector (18.5 cm) and the elution time of the unretained marker DMF. The total length of the capillary was 38 cm. The peak width at half height was used to determine the plate height according to Equation 1.7 (p.16).

PAHs are again considered well-suited probes in this context since it has already been proven in the previous chapter that they indeed interact with the monolith. Due to the absence of any charges this interaction must be a pure chromatographic one based on partitioning (see Chapter 1.3, p.13) and therefore the overall separation is not obscured by any electrophoretic migration. The two graphs demonstrate the plate heights becoming nearly independent from the velocity of the mobile phase once the flow has reached a magnitude of $\geq$ 0.03 cm/s. Recalling Equation 1.15 (p.22) that outlined the contributions from the individual sources of band broadening to the overall plate height the magnitude of all three mass transfer terms was seen to be directly proportional to the mobile phase velocity. Therefore, Figure 4.1 proposes the velocity dependence of the mass transfer terms to be greatly diminished. A possible rationalization might be an eventual lack of stagnant mobile phase either because the respective pores (dead-end pores) are absent and only flow-through pores exist or dead-end pores do exist but the EOF generates sufficient convective flow inside them to prevent chromatographic interactions from becoming diffusion limited.[68, 69] This suggest that the fifth cause of band broadening, i.e., resistance to mass transfer in a stagnant mobile phase (see Equation 1.14, p.22), barely contributes to the overall plate height. A conclusion that can be safely drawn from this experiment is that high flow velocities can be applied without compromising plate heights. Consequently, exploitation of the monolith enables high separation efficiencies combined with short analysis times. The maximum flow velocity depends on the maximum applicable electric field strength which so far is restricted by arcing of the electrodes at field strengths exceeding 350 V/cm. Therefore, no predictions can be made if the flow-independent plate heights will be still observed at even higher velocities.

To strengthen the notion that the polymer has the aptitude to separate analytes through a chromatographic separation mechanism based on partitioning, the following figure illustrates the relationship between the percentage organic solvent in the mobile phase (i.e., ACN in borate buffer) and the capacity factor:

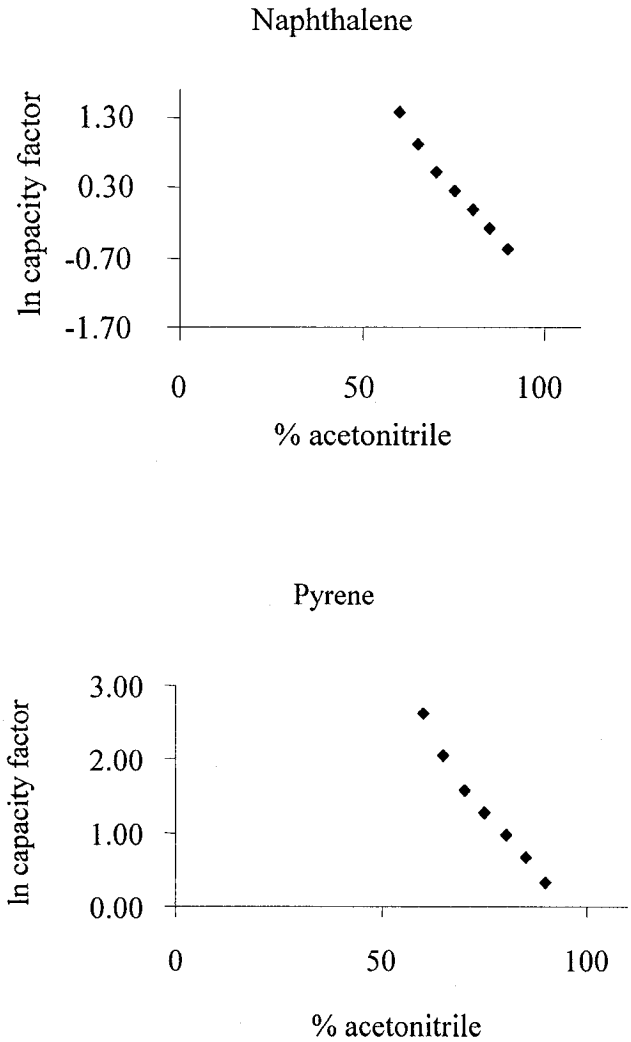

Figure 4.2: Plots of ln capacity factor for two PAHs versus percentage ACN in mobile phase, with 5 mM pH 10.0 borate buffer accounting for the remaining percent (V/V). Separation voltage was 10 KV and sample injection performed for 5 s at 5 KV. DMF served as unretained marker to determine the EOF and calculate the capacity factors. All other conditions and parameters were kept identical to the ones described in Figure 4.1.

The capacity factor k' was calculated in analogy to LC:[145, 149]

$$k' = \frac{t_r - t_0}{t_0}$$

Equation 4.1: Capacity factor k' (dimensionless); t_r denotes the retention time of the analyte in s or min and t_0 refers to the elution time of an unretained marker (DMF in this case) in the same dimension.

In essence, the capacity factor describes the time the analyte spends in the stationary phase compared to the time it spends in the mobile phase. Hence, it provides similar information as the partition coefficient (see Equation 1.6, p.14), i.e., it quantifies the degree of partitioning between analyte and stationary phase. However, unlike the partition coefficient, it can be calculated directly from the electrochromatogram and does not require the exact volumes of monolith and mobile phase in the capillary to be known. The higher the amount of organic solvent the more effectively can the mobile phase compete with the monolith for retaining the analyte. A negative slope is therefore expected when plotting the natural logarithm of the capacity factor versus the percentage organic solvent.[145] For all four tested PAHs (only two are shown here) linear, negative slopes were obtained. Complementing the earlier proven fact that the monolith is capable of separating neutral analytes, this study verifies that the separation is brought about by a mechanism based on partitioning, i.e., reversed-phase CEC takes place.

4.2 Physico-chemical characterization of the monolith

Chapter 1 of this thesis outlined the potential of monoliths for the reduction of band broadening. Three experimentally accessible structural parameters of the monolith gain interest in this context: porosity, tortuosity and the specific permeability coefficient.[51, 150, 151] In chromatography, the total porosity is defined as the ratio of the volume of the non-solid portion of the monolith to the total volume. It can be further subdivided into *inter*-particle and *intra*-particle porosity:[150, 152]

$$\varepsilon_{total} = \varepsilon_{inter} + \varepsilon_{intra}$$

Equation 4.2: Total porosity ε_{total}; ε_{inter} refers to the inter-particle porosity and ε_{intra} to the intra-particle porosity (all values are dimensionless).

Given that a monolithic column is characterized here, ε_{inter} refers to flow-through pores in the macropore range (i.e., diameter > 50 nm) whereas ε_{intra} relates to the sum of dead-end pores in the mesopore range (i.e., 1.5-50 nm) and, provided they exist, also to dead-end pores in the micropore range (< 1.5 nm). Literature values enclose total porosities for monoliths in HPLC as well as for CEC.[152] However, in CEC the only values reported so far for both inter- and intra-particle porosities were measured for packed capillaries but not for monoliths.[51, 151]

The tortuous flow path in the monolith or packed bed is expressed as the tortuosity τ. Small values of tortuosity correlate to low packing factors and result in little Eddy diffusion (see Equation 1.10, p.19). Tortuosity can also be interpreted as a measure

for homogeneity, a factor deemed important in the reduction of bubble formation and over-heating.[124] In CEC, both total porosity and tortuosity can be obtained through conductivity measurements.[51, 151]

Lastly, the specific permeability coefficient B^0 quantifies the ability of a porous material to transport a fluid at a given pressure differential. It can be thought of as the hydrodynamic analog to electrical conductance.[62] A high permeability is desired for enhanced mass transfer. It is routinely determined for HPLC columns and also serves as an intermediate step to calculate the total porosity and from there the inter- and intra-particle porosity.[150] To date, the literature mentions only values for a few monoliths used in CEC.[62]

Due to the limited number of published data for other monoliths, the values presented here should be thought of as reference values, with the general idea of establishing a framework for monolith characterization in the future when (hopefully) a potential successor of this work will attempt to optimize the monolith through chemical modifications.

A vital aspect of these three structural parameters is that their determination does not require any sophisticated instrumentation. Besides, the monolith is characterized in its "natural environment", i.e., inside the capillary and using the desired mobile phase. Examples for alternative characterization methods include Nitrogen adsorption/desorption and Mercury-intrusion porosimetry to measure surface area, pore size and pore size distributions. Apart from the need for sophisticated instrumentation these methods require preparation of large quantities of bulk polymer outside its "natural environment", followed by extraction, drying and crushing to yield a powder. It is

difficult to anticipate how these steps change the properties of the monolith, e.g., through shrinkage in the dried state compared to potential swelling when surrounded by mobile phase.[66] Also, the powder consistency introduces a third type of porosity (the one describing the volume in-between powder particles) which often cannot be distinguished from the inter-particle porosity.[152] Along this theme, previous pore size measurements using Nitrogen adsorption/desorption carried out in our laboratory for the earlier described polymer for frit manufacture yielded values differing by three orders of magnitude from published ones, a problem that was confirmed in a personal communication with F. Svec.[117]

A) Determination of total porosity and tortuosity in CEC-mode

The total porosity ε_{total} is calculated according to the procedure published by Rathore et al.[51] based on Archie's Law. It relates ε_{total} to the conductivity ratio between the section containing the monolith and the open section of the capillary:

$$\frac{\sigma_{packed}}{\sigma_{open}} = \varepsilon_{total}^{m}$$

Equation 4.3: Archie's Law; ε_{total} represents the total porosity of the monolith (dimensionless), σ_{packed} the conductivity in the monolithic section in $A*V^{-1}*m^{-1}$, σ_{open} refers to the conductivity in the open section in $A*V^{-1}*m^{-1}$ and m is an empirical constant that is usually approximated as 1.5 for media with porosities higher than 0.2.[51]

In order to determine the conductivity ratio the currents have to be measured in the presence and in the absence of monolith, i.e., two capillaries are needed.

The tortuosity factor τ is obtained from the elution time of an unretained marker, e.g., thiourea or DMF:

$$\tau = \frac{\mu_{EOF,p} t_0 V_p}{L_p^2}$$

Equation 4.4: Tortuosity factor τ (dimensionless); $\mu_{EOF,p}$ denotes the electroosmotic mobility in $m^{-2}*V^{-1}*s^{-1}$, t_0 refers to the elution time of an unretained marker in s, V_p to the voltage drop in the packed section in V and L_p stands for the length of the monolith in m.

A preliminary comparison between five capillaries showed the currents to be reproducible within 1.5% RSD. The following table shows the total porosities and tortuosity factors for these five capillaries:

Table 4.1: Total porosity and tortuosity factors for five capillaries. Capillary dimensions were 33 cm total length and 18.5 cm length of the monolith. A voltage of 10 KV was applied. The mobile phase consisted of 50% ACN / 50% 5 mM pH 10.0 borate buffer (V/V). Thiourea was used as an unretained marker.

Capillary	Total porosity ε_{total}	Tortuosity factor τ
1	0.53	1.67
2	0.54	1.64
3	0.50	1.76
4	0.48	1.81
5	0.50	1.76
Mean	0.51	1.73
STDEV	0.02	0.07
%RSD	4.80	4.18

At first sight, using always the same value for the empirical constant m in Equation 4.3 might not seem intuitively justified. Yet the overall porosity is fairly robust even when varying this constant.[62] One drawback Rathore et al. mention in their publication is the dependence of the total porosity on the morphological shape when determined from the conductivity ratio. This in turn might render comparisons between particles and monoliths very difficult and also aggravates comparisons between different types of monoliths. However, the most pressing issue with this type of measurement is that the measured currents to determine the conductivity ratio are in the low μA range. Although the currents appear to be fairly reproducible, the author of this thesis frequently observed cross-talk between the current recorder and the detector. The values might therefore not necessarily present absolute ones but rather relative ones, thus restricting the application of this methodology to the author's laboratory (a comparison to other values found for porosities by different authors using different monoliths will be part of the following section).

The mean of the tortuosity factor is 1.73. Only one reference value could be found in the literature which was 0.7 but was determined for a packed capillary.[151] Nevertheless, the tortuosity factor appears to be rather high leading to a potentially high degree of Eddy diffusion.

B) Determination of the specific permeability coefficient

A setup enabling μ-HPLC studies is a prerequisite for determining the specific permeability coefficient B^0. The next figure sketches this setup:

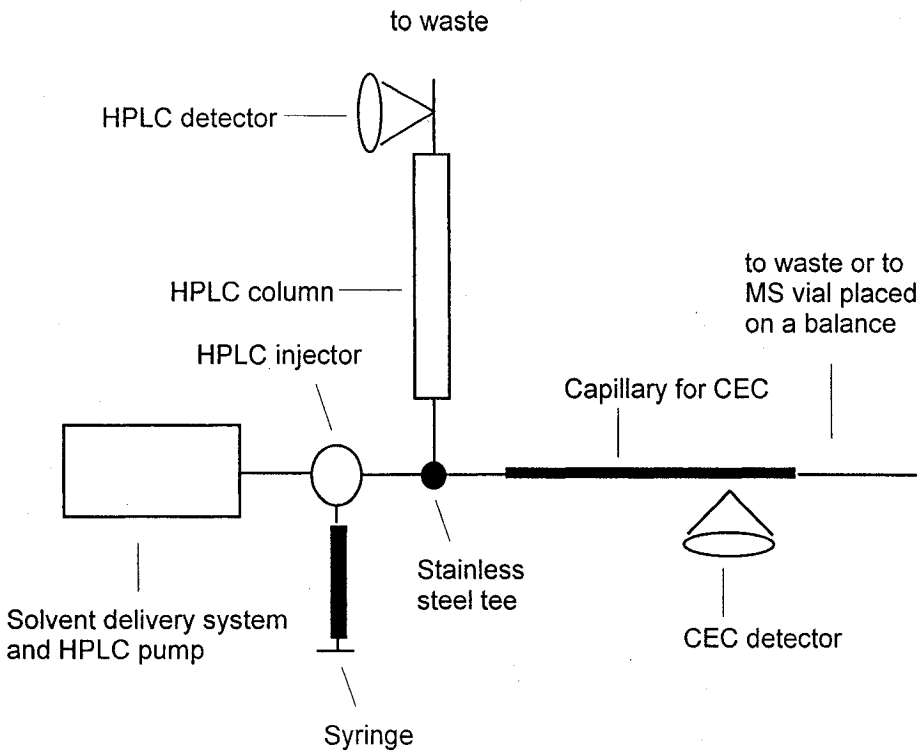

Figure 4.3: Split-flow apparatus for μ-HPLC studies. The purpose of incorporating the HPLC column is to allow the HPLC pump to operate at a practical flow rate (about 1 mL/min) and pressure (about 1000 psi). This pressure is also used to supply solvent via the tee to the monolithic capillary at the very low flow rate of approximately 1 μL/min.

Determination of the specific permeability coefficient B^0 is attained by rearranging Darcy's Law:[62, 106, 150]

$$B^0 = \frac{FL\eta}{\pi r^2 \Delta p}$$

Equation 4.5: Specific permeability coefficient B^0 in cm^2; F stands for the measured flow rate in cm^3*s^{-1}, L is the length of the polymer in cm, η denotes the viscosity of the mobile phase in $N*s*cm^{-2}$, r symbolizes the radius of the capillary in cm and Δp indicates the pressure difference in $N*cm^{-2}$.

Setting up the μ-HPLC apparatus permits easy determination of the measured flow rate by simply weighing the eluent from the capillary at different time intervals. The instrumental flow rate differs from the measured flow rate since the former one accounts for both the flow through the HPLC-column *and* the capillary whereas the latter one accounts *only* for the flow through the capillary. Knowing the density of the eluent, one obtains the measured flow rate from the slope of a plot of eluent mass versus time:

$$F = \frac{M}{\rho t}$$

Equation 4.6: Measured flow rate F in cm^3*s^{-1}; M denotes the mass of the eluent in mg, ρ the density of the eluent in $mg*cm^{-3}$ and t the time in s.

The next plot illustrates a typical plot of mass versus time:

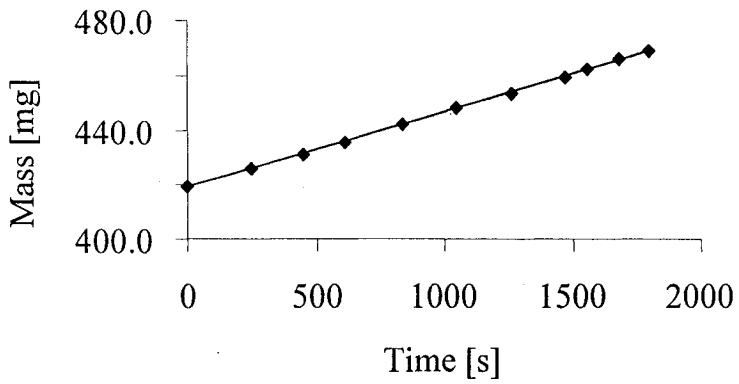

Figure 4.4: Plot of mass versus time to determine the measured flow rate. An instrumental flow rate of 1.0 mL/min was applied. The capillary length was 19.3 cm to detector and 37.2 cm total, mobile phase consisted of 50% ACN / 50% 5 mM pH 10.0 borate buffer (V/V).

Since a large number of experiments described in this thesis operate with a mobile phase consisting of 50% ACN / 50% 5 mM pH 10.0 borate buffer (V/V) the same mobile phase was used throughout this set of experiments. Its viscosity was approximated as $8.5*10^{-4}$ $N*s^{-1}*m^{-2}$, a value determined for a 50/50 mixture of ACN and pure water by Wright et al.[43] The density had always been recorded just prior to the actual experiment and was typically found to be around 890 $mg*cm^{-3}$. The measured flow rate was 1.5 mg/min which indicates that the tee union splits the flow between HPLC column and capillary in a ratio of approximately 700:1.

Once the specific permeability coefficient has been determined the following equation yields the total porosity:[150]

$$\varepsilon_{total} = \frac{B^0 \Delta p}{u_0 \eta L}$$

Equation 4.7: Total porosity ε_{total} (dimensionless); u_0 stands for the elution velocity of an unretained marker in $cm*s^{-1}$ and all other symbols have the same meaning as in Equation 4.5.

Assuming the definite presence of both dead-end and flow-through pores, their distinction in terms of inter- and intra-particle porosity becomes only feasible if one can employ two unretained markers. One has to be small enough to fit into the dead-end pores whereas the other one has to be large enough to be excluded from all dead-end pores:[150]

$$\varepsilon_{inter} = \frac{u_0 \varepsilon_{total}}{u_1}$$

Equation 4.8: Inter-particle porosity ε_{total}; u_1 stands for the elution velocity of an unretained marker that is too large to fit into any dead-end pores (in $cm*s^{-1}$) and all other symbols have the same meaning as in Equation 4.7.

One prerequisite for this reasoning is that only two types of pores exist in the first place, i.e., one type of dead-end and one type of flow-through pores. Furthermore, both types should possess a sufficiently narrow pore size-distribution to prevent any overlap between them. Just to give an example, a possible complication could occur if one type of dead-end pores (in the mesopore range, for instance) would allow the large unretained marker to fit in and another type of dead-end pores (in the micropore range, for instance) would not. The value for the intra-particle porosity would be too small in this case. Conventional analytes to characterize pore sizes are polystyrenes. However, their use is restricted to drastic operating conditions, e.g., the mobile phase consisting of 100% tetrahydrofuran.[152, 153] A potential alternative might lie in the use of biopolymers since they allow the exploitation of conventional mobile phases. Just to give an example, transferrin should be highly negatively charged at pH 10. Assuming electrostatic repulsion between transferrin's negatively charged residues and the monolith's sulfonate moieties, transferrin might not interact strongly with the stationary phase and, in addition, might be too large to fit into any dead-end pores. Thiourea, on the other hand, is routinely used as an EOF marker and should be small enough to fit into all pores without interacting with the stationary phase. The partial separation of transferrin and thiourea in μ-HPLC mode is shown in the following figure:

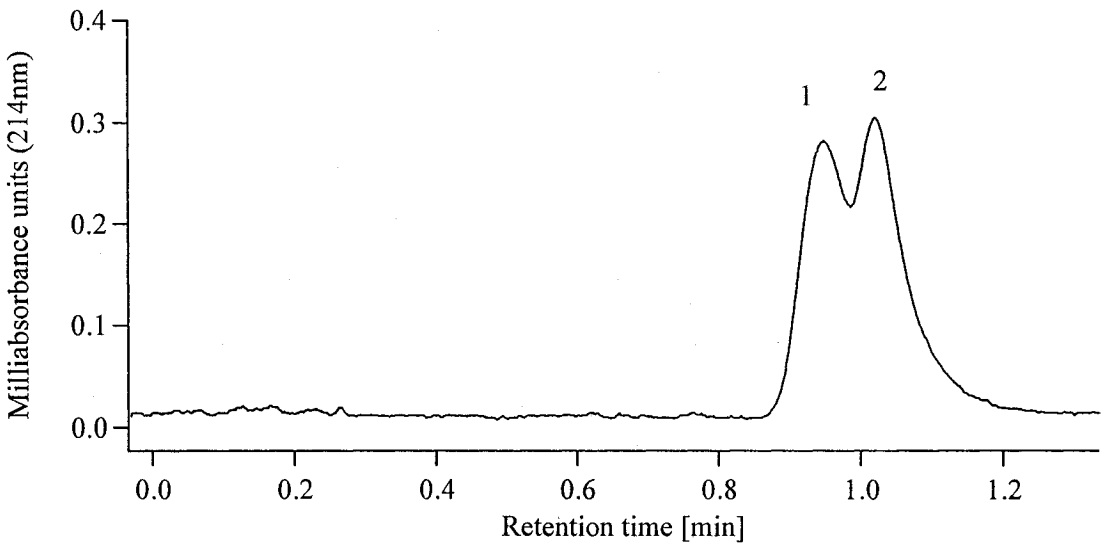

Figure 4.5: Separation of transferrin (1) and thiourea (2) in μ-HPLC. Spiking experiments confirmed the identity of the peaks. An instrumental flow rate of 0.6 mL/min was applied. The injection volume was 20 μL and all other parameters kept identical to the ones listed in Figure 4.4.

Indeed, transferrin elutes before thiourea. A more detailed study was carried out for one capillary with the respective retention times used to calculate inter- and intra-particle porosities. First, repeated measurements were performed at one flow rate (0.8 ml/min) in order to estimate the reproducibility within this one capillary. The flow rate was then varied. Since a change in flow rate results in a change in applied pressure the specific permeability coefficient should remain unaffected (see Equation 4.5, p.91). The results are summarized in the following table:

Table 4.2: Specific permeability coefficient, total porosity, intra- and inter-particle porosity in dependence of the flow rate. Capillary dimensions were 37.2 cm total length and 19.3 cm length of the monolith. The mobile phase consisted of 50% ACN / 50% 5 mM pH 10.0 borate buffer (V/V). The relative standard deviations (%RSD) refer only to the five consecutive measurements at 0.8 mL/min.

Pump flow rate (mL/min)	Specific permeability coefficient B^0 (10^{-10} cm^2)	Total porosity ε_{total}	Intra-particle porosity ε_{intra}	Inter-particle porosity ε_{inter}
0.8	7.54	0.37	0.02	0.35
0.8	8.47	0.42	0.03	0.39
0.8	8.59	0.42	0.03	0.39
0.8	8.33	0.41	0.03	0.38
0.8	9.59	0.44	0.03	0.41
%RSD	7.7	6.3	16.0	22.3
0.6	9.33	0.44	0.03	0.41
1.0	8.63	0.41	0.03	0.38

The results underline that the experiments can be carried out with a reasonable reproducibility, and the determined factors show no dependence on the flow rate thereby proving the applicability of Equation 4.5. The permeability coefficients are approximately twice as high as values found for some other monoliths employed in HPLC indicating a high permeability of the monolith.[106] Total porosities are slightly lower than the ones determined earlier from the conductivity ratio (0.41 versus 0.51, respectively), a mismatch noted by other authors as well.[62] They lie in the range typically found for microparticulate stationary phase in CEC and HPLC [51, 150, 151] but also for some monoliths.[62, 106] In other cases, though, reported values for the total porosities of monoliths for CEC are higher (around 0.7).[51] Regarding inter- and intra-particle porosities, values accounting for 80-90% of the total porosity for the former one and 10-20% for the latter one have been reported for monoliths employed in HPLC [152] which corresponds to the findings presented here.

To close this section it has to be conceded that additional studies are required to compare permeability coefficients between different capillaries. Such a comparative study will shed light on the reproducibility of the manufacture process (an alternative method of testing this reproducibility by using model analytes will be described in Chapter 5). The use of transferrin furthermore only displays a first approximation in order to determine intra-particle porosities. Its size is not exactly known because, for instance, it may be denatured in the mobile phase, and any possible chromatographic interaction with the monolith cannot really be excluded at this point. The determination of total porosity and tortuosity from the conductivity ratio is hampered by the very low currents

that have to be measured and that both one capillary with and one without a monolith are needed. Nevertheless, to the best of the author's knowledge it is so far the only way to estimate the tortuosity.

4.3 Imaging by scanning electron microscopy and atomic force microscopy

The previous section suggested the occurrence of two different types of pores: flow-through and dead-end pores with the former ones presumably in the macropore range and the latter ones in the mesopore range plus eventually in the micropore range. Methods to visualize these two types of pores and thus qualitatively confirming the results from the previous section are presented in the following.

Scanning Electron Microscopy (SEM) is a technique that can deliver an image of the monolith and so permits evaluation of the morphology of the polymer. For this reason, SEM is used by virtually every researcher developing monoliths. The next figure displays an image of the monolith inside the capillary and an enlarged view on the exposed surface of the monolith:

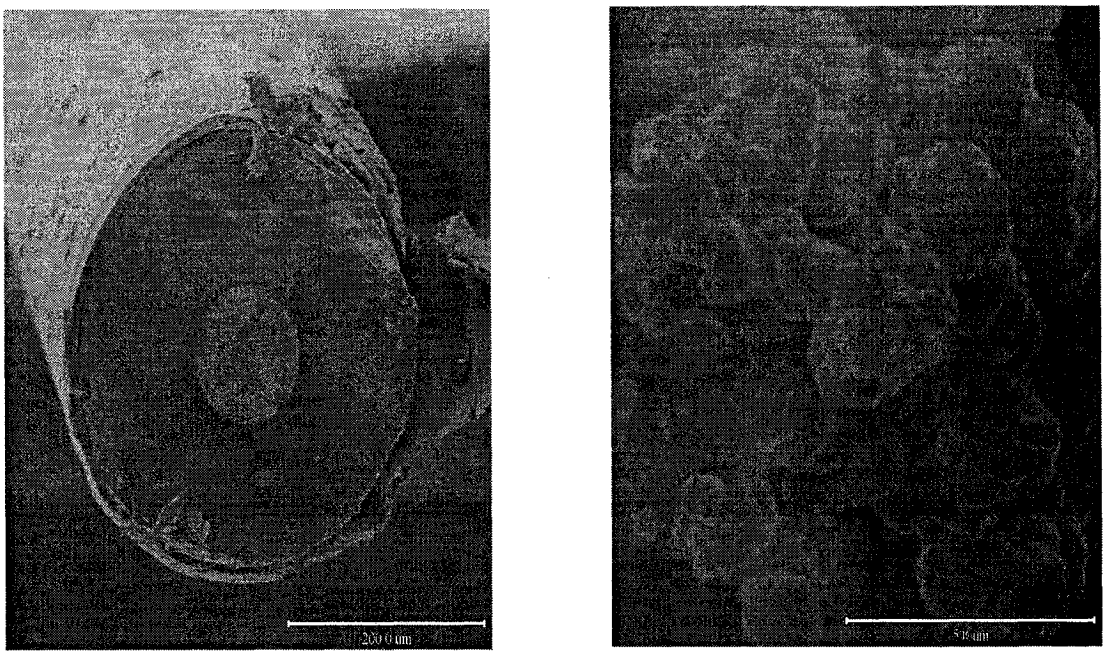

Figure 4.6: SEM images of the monolith inside a UV-transparent capillary (left side) and enlarged image (right side).

The enlarged image supplies information on the morphology of the monolith. It shows a prevalence of larger agglomerates of approximately 3 μm diameter. These agglomerates are composed of smaller, fused globular entities of roughly 1 μm in diameter. Information on the types of pores is not readily available from these images due to insufficient resolution in the depth dimension. Besides, sample preparation is fairly elaborate since a conducting surface is needed. Moreover, the images were acquired in the absence of mobile phase, i.e., the polymer might have been subjected to shrinkage. When enlarging the image showing the monolith inside the capillary and comparing it to images from other monoliths published in the literature that are attributed a high porosity, e.g.,[106, 110] the previous section's results on total porosity and tortuosity are qualitatively confirmed, i.e., the monolith does seem to have a rather low total porosity and possesses a relatively dense network.

Atomic Force Microscopy (AFM) is an alternative imaging technique from the family of scanning probe microscopes that does not require a conducting surface.[154] In order to facilitate imaging, the monolith has to be pushed out of the capillary, which in turn makes sample preparation approximately the same as in SEM. Due to better resolution in the depth dimension AFM should provide more information on the surface topology, surface roughness and pore structure than SEM.[155] To date, there is only one report in the CEC literature employing AFM where it is used to image different steps during the synthesis of a monolith.[105] As yet, no publication elucidates the pore structure of monoliths. Making use of AFM is more widespread in CE or open-tubular CEC to visualize modifications of the capillary wall.[155-157] In the present work, both contact and tapping modes were evaluated but contact mode did not deliver any useful images.

The following tapping mode image displays an area of 5 x 5 μm^2 from the bird's eye perspective:

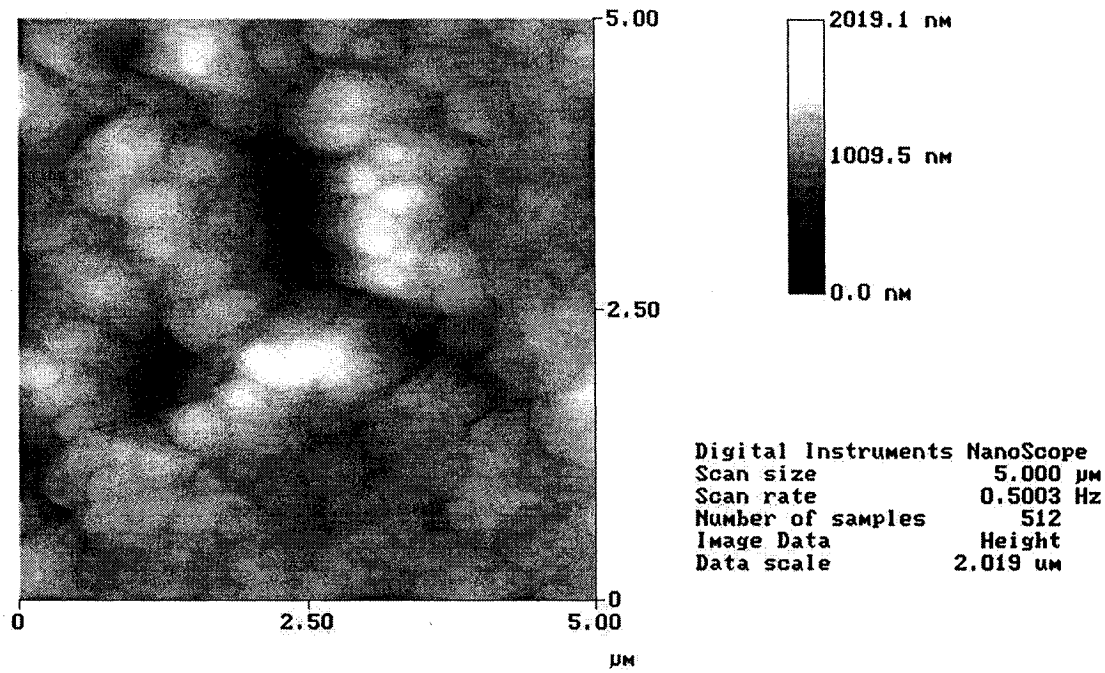

Figure 4.7: AFM image of the monolith (5 x 5 μm^2) from the bird's eye perspective.

Unlike SEM, information on the morphology of the polymer actually becomes less accessible in AFM but therefore pore structure and topology of channels become visible. First, the macropores can be observed as larger (dark) channels with a diameter of approximately 500 nm and varying geometry. Secondly, mesopores with smaller, groove-like structures on the order of few nanometers can be seen. These mesopores are more readily seen in the perspective view in the next picture:

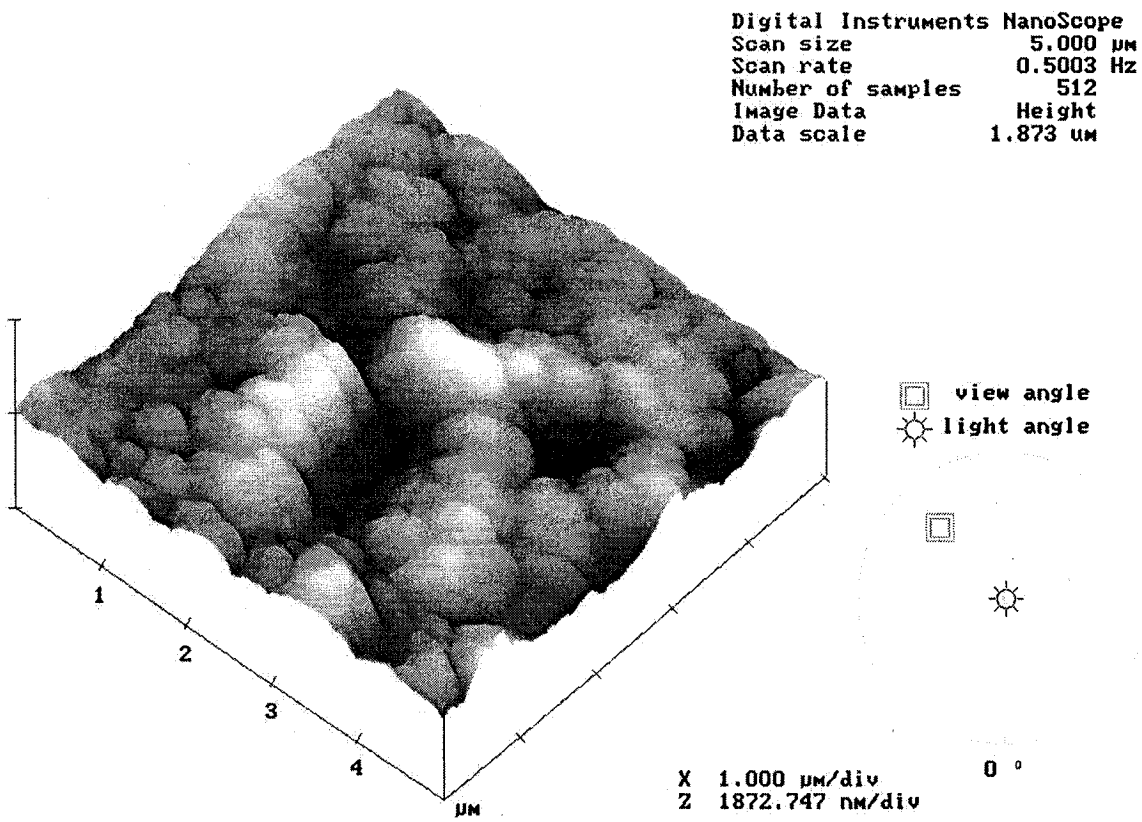

Figure 4.8: AFM image of the monolith (5 x 5 μm^2) from an angular perspective.

This perspective essentially confirms the occurrence of two different types of pores as predicted in Chapter 4.2. Several additional images were taken from different slices of this monolith and also from other monolithic capillaries (not shown here) confirming that the structures displayed here are truly representative for the monolith.

Unfortunately, it is not yet possible to evaluate if the mesopores are flow-through pores or whether they are actually dead-end ones. After all, the earlier reported intra-particle porosities could also exclusively stem from micropores only. AFM measurements to probe the depths of the mesopores yielded a depth of approximately 100

nm when scanning an area of 1 x 1 μm^2, but it remains questionable whether the tip of the cantilever really reached the bottom of the pore.

To summarize the results from the SEM and AFM studies it can be said that a globular structure of the monolith is visualized by SEM yet no real information is available on the pore structure other than that the overall porosity is fairly low. AFM imaging can contribute this missing piece of information and confirms the notion that two distinct types of pores exist, one in the macropore range and one in the mesopore range without elucidating the nature of the latter ones as being either dead-end or flow-through (the macropores must be flow-through ones otherwise no bulk flow could possibly be observed). So far, micropores cannot be visualized with either SEM or AFM.

4.4 Investigations on the electroosmotic flow

Equations 1.2 and 1.3 (p.10 and p.11, respectively) described the dependence of the EOF on a variety of variables. Some of them will be investigated in greater detail in the following such as the amount of AMPS in the polymerization mixture, the type and amount of organic solvent in the mobile phase, the pH and, lastly, the ionic strength.

In essence, two different functional groups contribute to the EOF: silanol groups on the capillary wall and sulfonate moieties stemming from AMPS on the surface of the monolith. Since the monolith only occupies the section of the capillary from the inlet to the detector, silanol groups can be considered to be the main contributor to the EOF in the remaining, open part. In the section occupied by the monolith, in theory silanol groups on the capillary wall not covalently linked to the monolith and sulfonate moieties

can generate EOF. One might therefore pose the following questions. First, in the absence of sulfonate groups (easily accomplished by not including AMPS in the monomer mixture) will there still be significant EOF? If yes, the existence of a significant amount of remaining silanol groups on the wall would be proven. The second question is: can the EOF be enhanced by increasing the amount of AMPS in the monomer mixture? The following graph tries to provide an answer by measuring the electroosmotic mobilities μ_{EOF} in several capillaries with different amounts of AMPS in the polymerization mixture:

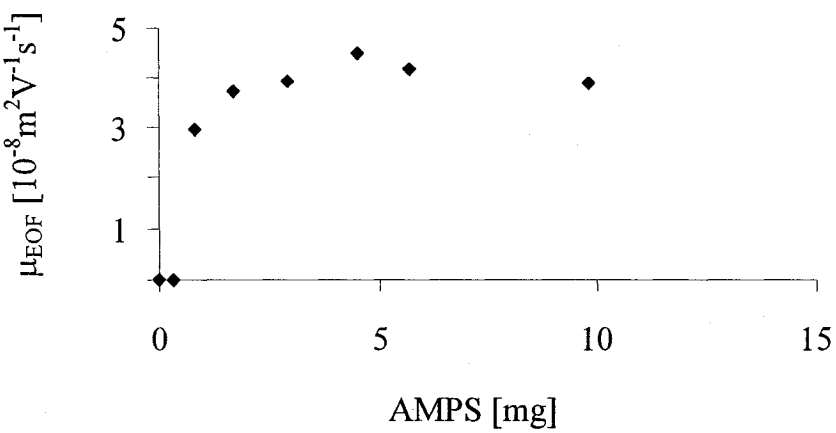

Figure 4.9: Plot of electroosmotic mobility (μ_{EOF}) versus amount of 2-acrylamido-2-methyl-1-propanesulfonic acid (AMPS) in the monomer mixture. All capillaries were of approximately the same length, i.e., 20.0 cm inlet to detector (containing the monolith) and 31.0 cm total length. Mobile phase consisted of 50% ACN / 50% 5 mM pH 10.0 borate buffer (V/V). A voltage of 10 KV was applied. Each point on the graph represents the average from 5 runs. Standard deviations were below 1% in all cases (error bars are therefore not shown).

The following equation served as the basis to calculate the electrophoretic mobilities:[10]

$$\mu_{EOF} = \frac{L_{packed} L_{total}}{V t_{thiourea}}$$

Equation 4.9: Electrophoretic mobility μ_{EOF} in $m^2*V^{-1}*s^{-1}$; L_{packed} stands for the length of the packed segment of the capillary in m, L_{total} for the total length of the capillary in m, V denotes the applied voltage in V and $t_{thiourea}$ is the elution time for thiourea in s.

The curve indicates a saturation-like behavior: a certain amount (0.6 mg) of AMPS is necessary in order to obtain any flow. Without or with very little AMPS no EOF can be established signifying the absence of a sufficiently high number of silanol groups on the wall to maintain EOF. At values exceeding 2 mg the EOF cannot be enhanced any further. Equation 1.3 (p.11) showed that if silanol groups are the main contributor the ζ-potential depends linearly on the charge density. Assuming that this relation applies equally to sulfonate groups it appears that a maximum value for the charge density exists. One possible explanation could be steric hindrance: excess sulfonate moieties might not be incorporated during the polymerization process and are subsequently purged out during the preconditioning step. An alternative reasoning could be changes in the porosity by increasing the number of mesopores (and thus the overall surface) in order to accommodate all the sulfonate groups and to prevent steric hindrance. This would not necessarily alter the charge density and thus not lead to a higher EOF. Even if it amplified the EOF such an increase might be balanced out by a higher tortuosity resulting in no overall change in the elution time of the unretained marker.

Other researchers employing AMPS using different polymerization mixtures did not observe a plateau region but a constant increase.[158] Their measurements involved only four different concentrations of AMPS, though.

Also affecting the EOF is the type and amount of organic solvent in the mobile phase. CEC routinely employs binary solvent systems, similar or identical to the ones used in HPLC or non-aqueous CE. They consist of an organic solvent and a low ionic strength aqueous buffer of the desired pH. In this context, MeOH and ACN can be assumed to be the most frequently used organic solvents.[44] Among the many reasons for their popularity, low viscosities and high dielectric constants are noteworthy since they both influence the electroosmotic mobility (Equation 1.2, p.10). The EOF should increase with decreasing viscosity and increasing dielectric constant.[43] The following figure shows the relation between the measured electroosmotic mobility and the percentage organic solvent in the mobile phase for both ACN and MeOH:

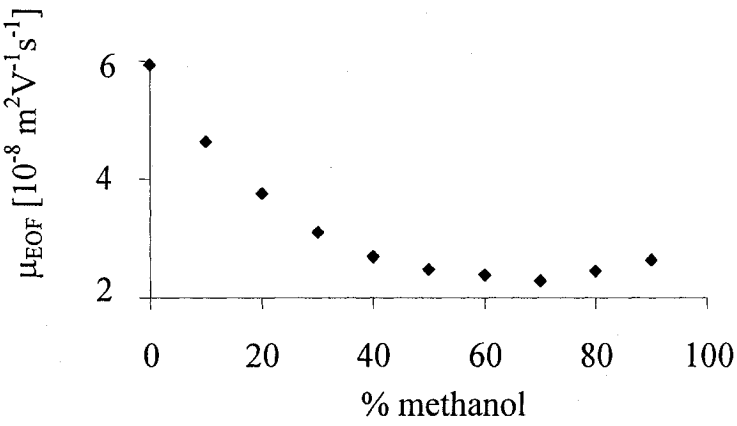

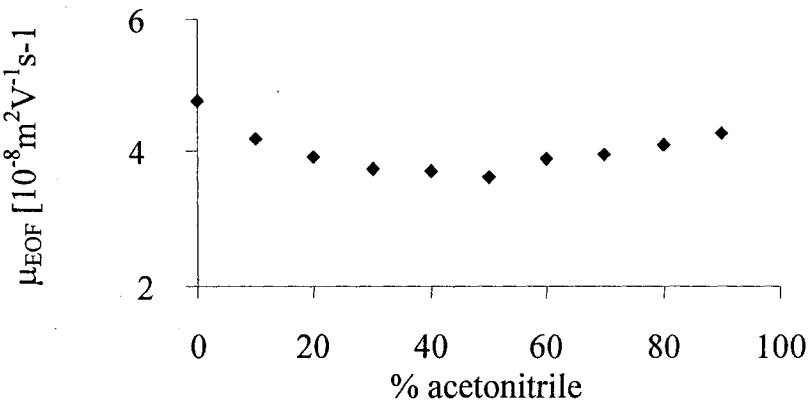

Figure 4.10: Plots of electroosmotic mobility (μ_{EOF}) versus type and percentage of organic solvent (ACN and MeOH) in the mobile phase with 5 mM pH 10.0 borate buffer accounting for the remaining percent. Thiourea served again as the unretained marker in order to determine the electroosmotic mobility according to Equation 4.9. All other variables were the same as described for Figure 4.9. Each point on the graph represents the average of 3 runs. Standard deviations were below 1% in all cases (error bars are therefore not shown). The experiments were repeated two more times with different capillaries yielding identical results.

Both plots indicate a parabolic shape with a more pronounced change being seen for MeOH than for ACN, particularly at low percentages of organic solvent. A similar

relation has been reported in the literature for microparticulate stationary phase containing silanol groups albeit the aqueous buffer differed.[47] The observed behavior is therefore governed by the composition of the mobile phase and not by the nature of the moiety in the stationary phase donating the proton, i.e., silanol or sulfonate. The parabolic shape is also in reasonable agreement with data relating the ratio of dielectric constant and viscosity to the percentage organic solvent if pure water accounts for the aqueous component. For both ACN and MeOH, this ratio reaches a minimum at around 50% organic solvent content.[41]

The upper experiments were continued in a reversed fashion as well, i.e., after having increased the organic content from zero to 90 percent in a step-wise fashion, additional values were recorded again with lower percentages. These values also lie on the graph, i.e., hysteresis was not observed indicating that the monolith was not damaged or subjected to irreversible swelling or shrinkage when employing high percentages of either ACN or MeOH. The possibility of employing a mobile phase consisting only of ACN had been investigated in preliminary studies but two hours of reconditioning were required when returning to a mobile phase with an aqueous portion (values above 90% ACN were therefore not included in the upper graph).

Overall, the findings indicate that, for both MeOH and ACN, the electroosmotic mobility reacts to changes in percentage organic solvent in the mobile phase as expected. Since a profound change in electroosmotic mobility takes place at low percentages of MeOH, particular care has to be taken in order to avoid random variations when working in this range (e.g., by evaporation from the mobile phase vials). Otherwise one would easily sacrifice robustness and reproducibility.

The variation of the electroosmotic mobility with pH is yet another point of interest. Sigmoidal profiles were reported for CEC and CE when using individual particles where silanol groups from both the capillary wall *and* the particle surface were the sole contributors to the EOF.[61, 83, 159] Such profiles were also reported for different monoliths containing AMPS.[158] Generally, care must be taken for the pH-profiles not to vary ionic strength and pH simultaneously when changing the type of buffer employed. Also, buffers should be preferred that possess a reasonable buffering capacity at the pH of interest, i.e., they should be operated within their pK_A values ± 1.5.[160] Therefore, the following buffers were selected: acetate for pH 3.9, acetate for pH 5.5, phosphate for pH 7.0, Tris for pH 8.1 and borate for pH 9.2. Measuring the electroosmotic mobility using a phosphate buffer at pH 2.2 was attempted, too, but no flow achieved. A possible explanation could be protonation of the sulfonate residues. All ionic strengths were adjusted to 10 mM by adding the necessary amounts of NaCl, with the calculations carried out utilizing freely accessible software [161] as recommended by other researchers.[162] This software also considers activity coefficients. The pH-dependence of the electroosmotic mobility is expressed in the following figure:

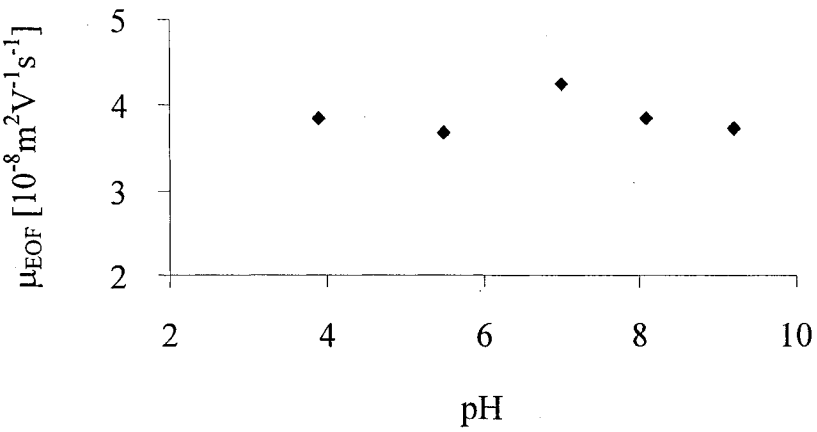

Figure 4.11: Plot of the electroosmotic mobility (μ_{EOF}) versus pH of the aqueous component of the mobile phase (refer to text for details). Total length of the capillary was 37.2 cm with 21 cm length inlet to detector and an applied voltage of 10 KV. All other variables were the same as described for Figure 4.9. Each point on the graph represents the average of 3 runs. Standard deviations were below 1% in all cases (error bars are therefore not shown). The results were confirmed on a second capillary.

Figure 4.11 shows a nearly pH-independent behavior in the pH range of interest and thus varies slightly from the results reported by other groups who also used AMPS in their polymerization mixtures but observed a slight increase in the electroosmotic mobility with increasing pH.[61, 158] They did not reveal their buffer recipes, though, and measured fewer points over a smaller pH range.

A peculiarity of this study is that it originally intended to measure the relation between the activity of hydronium ions (typically equated to pH) in solution and the electroosmotic mobility. Yet it shall be emphasized at this point that the pH scale does not necessarily correlate with the hydronium ion activity to the same extent as in the case of dilute, aqueous buffers. This fact is caused by the addition of ACN to the mobile phase. Due to its inherently different dielectric constant (as compared to water), ACN

induces a variety of changes, e.g., in the liquid junction potential of the pH-electrode or in the pK_A-values of the buffer components.[163] As a result, the findings depicted in Figure 4.11 cannot be extrapolated towards any other solvent systems nor be directly compared to any other pH study that has not been conducted under the same conditions using exactly the same buffer recipes.

The last variable to be investigated is the ionic strength. Recalling Equation 1.3 (p.11) which described an inverse relation between ionic strength and ζ-potential, the electroosmotic mobility should consequently be expected to decrease with increasing ionic strength:

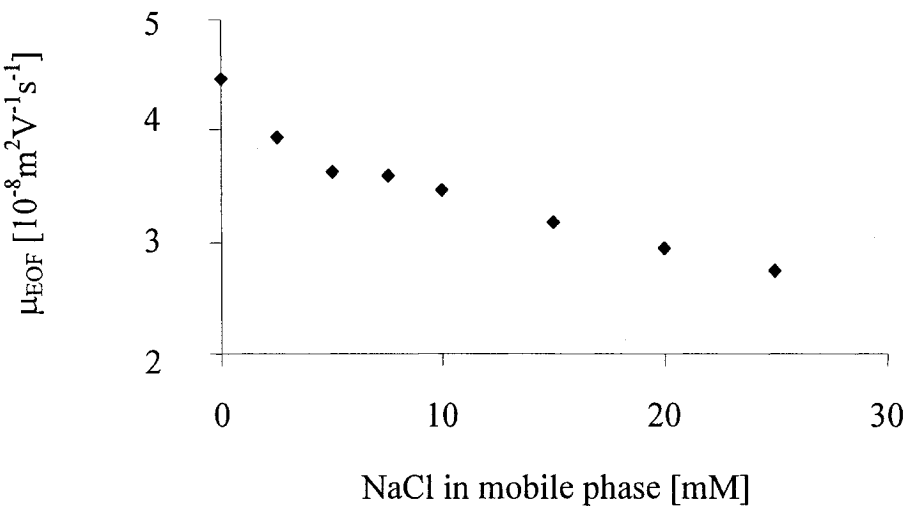

Figure 4.12: Plot of the electroosmotic mobility (μ_{EOF}) versus concentration of NaCl in the mobile phase consisting of 50% ACN / 50% 5 mM pH 9.3 borate buffer (V/V). Total length of the capillary was 37.2 cm with 21 cm length from inlet to detector. The applied voltage was 10 KV. Each point on the graph represents the average from 3 runs. Standard deviations were below 1% in all cases (error bars are therefore not shown). The results were confirmed on a second capillary.

The reciprocal relation between electroosmotic mobility and the ionic strength is manifested in the curve in Figure 4.12. Since Equation 1.3 remains valid only for 1:1 electrolytes, NaCl was selected for this study. For the same reason, the contribution from borate buffer to the ionic strength was not included in the upper graph and the concentration of NaCl was reported, not the overall ionic strength. An alternative motive for selecting NaCl is its use in ion-exchange chromatography.[145] The sulfonate moieties might display potential exchanger sites for cation-exchange chromatography. Elution of the analyte would then be brought about by adding a chaotropic reagent to the mobile phase with NaCl being one possible candidate. Unfortunately, the addition of more than 30 mM of NaCl to the mobile phase was not feasible: the current broke down and bubbles were observed.

To summarize the results from this section it can be stated that the EOF in the section of the capillary containing the monolith is generated by the sulfonate moieties and cannot exceed a maximum value. The validity of Equations 1.2 and 1.3 was verified and the observed measurements were in reasonable agreement with measurements carried out by other groups that employed AMPS in different monoliths.

4.5 The use of UV-transparent capillaries

Polyimide-coated, fused-silica capillaries are the separation vehicle of choice for the vast majority of researchers in both CE and CEC, with a few exceptions reporting the use of polymer capillaries.[164, 165] Chapter 1.7 (p.32) already listed the reasons that motivated the use of Teflon-coated capillaries as an alternative. Most notably is their

inherent advantage that, unlike with polyimide-coated capillaries, the coating does not have to be removed in order to allow photopolymerization and detection through the capillary. This section now mentions some properties of Teflon-coated capillaries encountered during the course of this research. Although their use has been reported for over a decade now,[166, 167] few authors employ them and no characterization in the literature can be found to date except for the one reported by the author of this thesis.[116, 168] A preliminary observation made by others [169] and confirmed by the author is the incompatibility of the capillary with hydrofluorocarbon based cooling liquids used in the commercial CE instrumentation, e.g., in the Beckman P/ACE 2100 system. This was the reason why the in-house built CEC apparatus illustrated earlier in Figure 1.9 (p.34) was used rather than an available CE instrument.

Since UV-transparent capillaries are also sold as waveguides for spectroscopic applications it came as no surprise that a waveguide effect was noticed depending on whether the room lights were turned on or off.

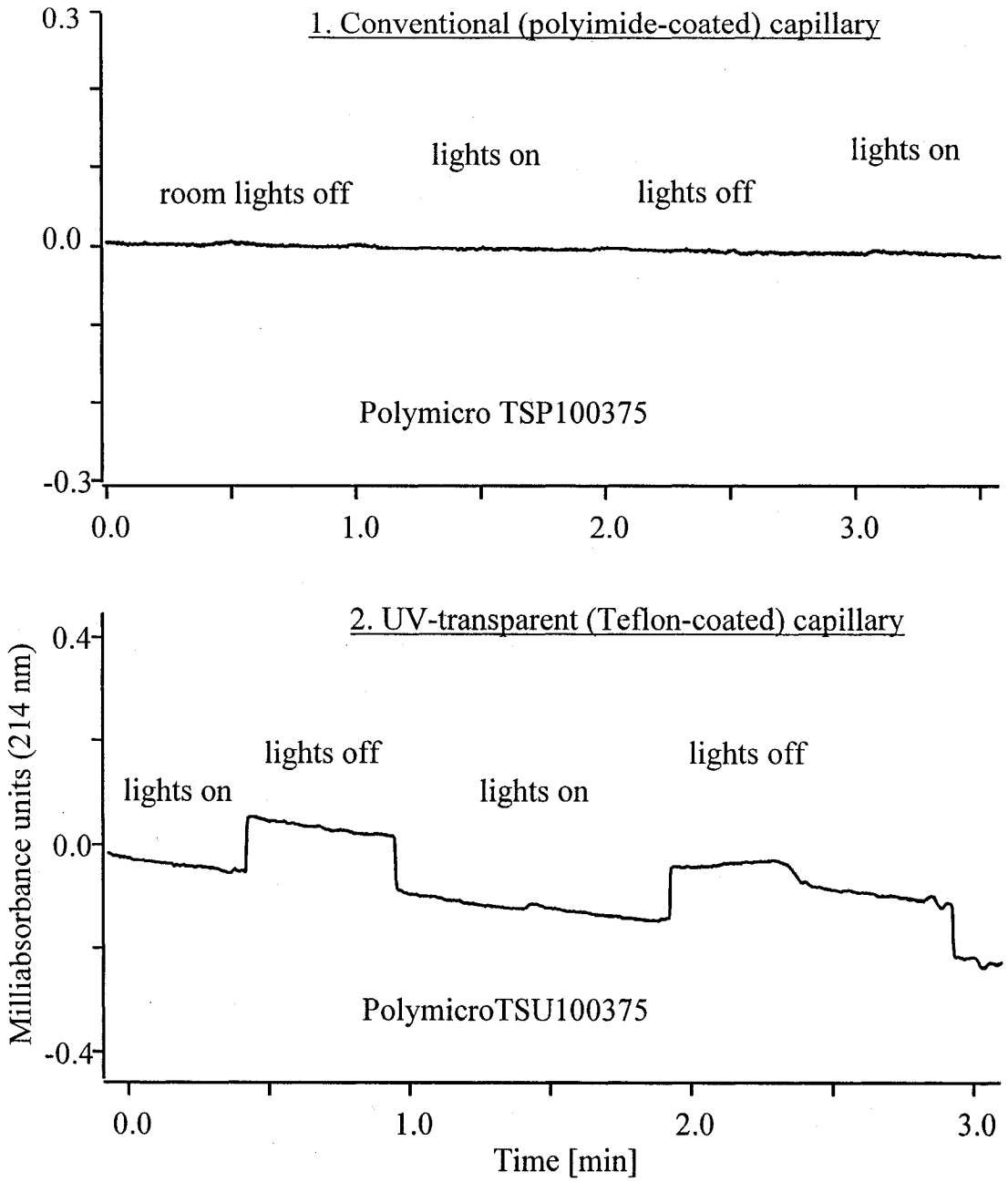

Figure 4.13: Waveguide effect in UV-transparent capillaries. Fluorescent lights illuminated the laboratory. The Unicam 4225 UV detector was operated for this study under the conditions specified in Chapter 2. It should be noted that the monochromator precedes the capillary in this detector. Thus all stray light (from the room lights) will be detected.

The displayed recordings were made in the absence of monolith yet one obtains the same results when the monolith is present in the capillary. Considering the dependence of total internal reflectance on the angle of the incident light,[138] bending of the capillary should prevent the waveguide effect as confirmed by exchanging the type of detector. Measurements using the ISCO CV^4 detector did not respond to any changes in light levels since it required bending of the capillary by roughly 90° over a 10 cm radius for insertion into the detection cell. The simple conclusion gained from these experiments is that light levels should remain constant and be minimized to obtain the maximum signal-to-noise ratio and to avoid baseline fluctuations.

Independent of whether a capillary is intended to be used in either CE or CEC, clean cuts are preferred in order to keep extra-column band broadening or inhomogeneities in the applied electric field as low as possible.[170] [171] Four different cutting "techniques" were therefore investigated and SEM images of four trials for each "technique" were recorded:

1) Scratching the capillary with a conventional cutting stone used for CE and then bending the capillary at the groove until it breaks into two pieces.

2) Same as (1) but pulling the two pieces apart.

3) Same as (1) but "knocking" or "flicking" one piece off using the middle finger.

4) Using the Shortix™ column cutter.[172]

The cleanest results were obtained using either the Shortix™ device or by pulling the two pieces of capillary apart. The following images show an example of a relatively

"clean cut" using the "pulling technique" (2) and one example of a less desirable cut using the "breaking" technique (1):

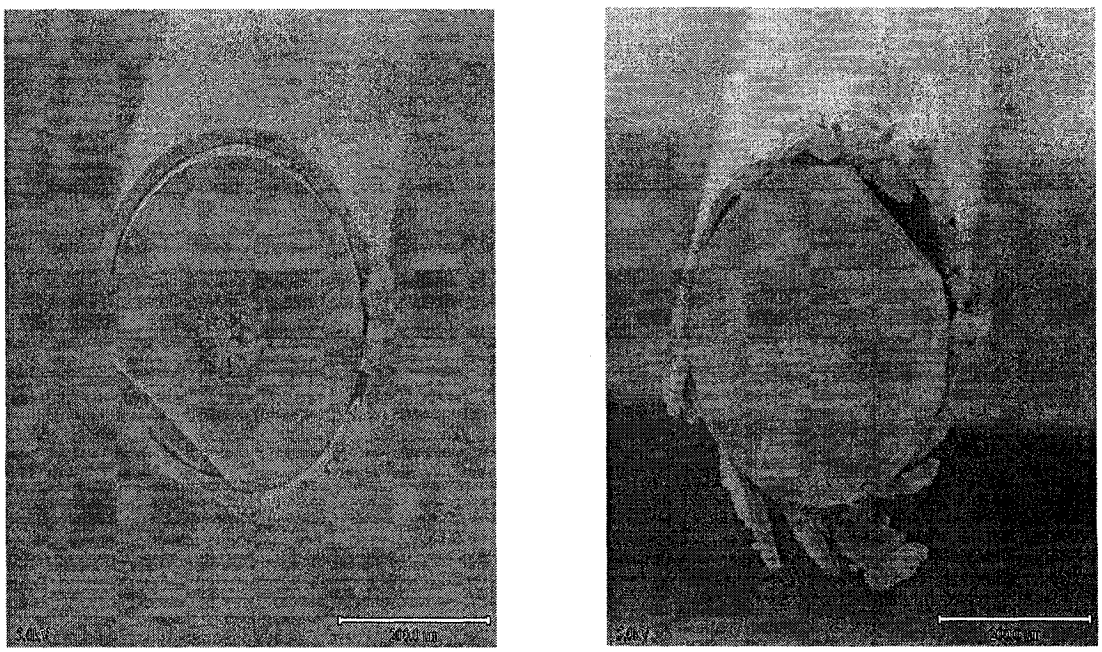

Figure 4.14: SEM images of UV-transparent capillaries after having used two different cutting techniques: "pulling" (left) and "breaking" (right).

One last feature of UV-transparent capillaries to be mentioned here is the porosity of the coating. The following figure compares the Teflon-coating to the polyimide-coating:

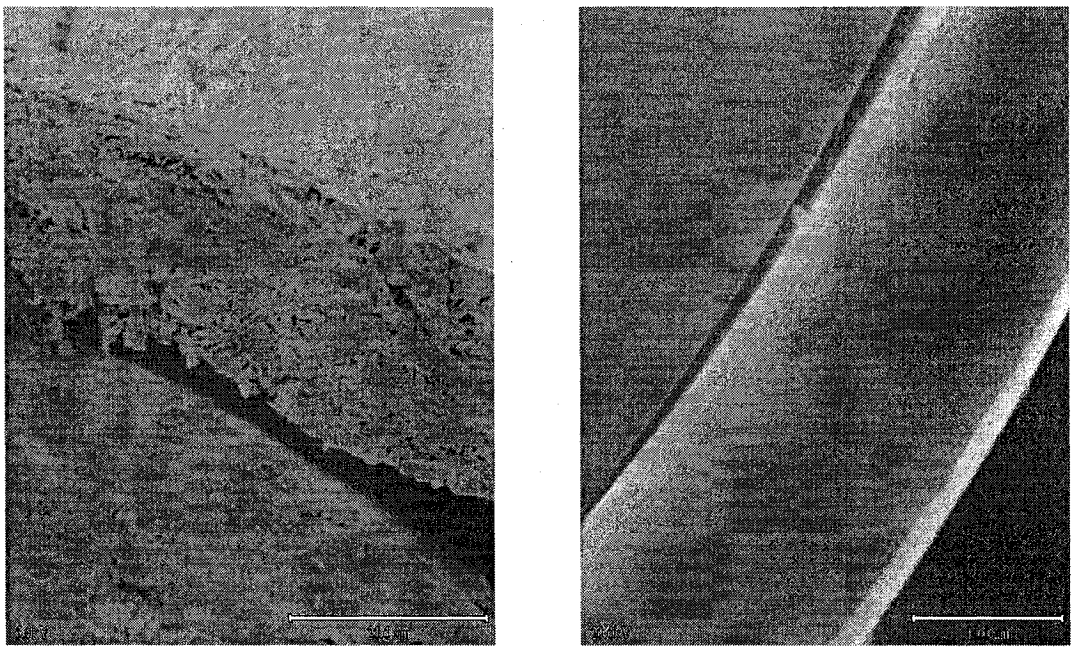

Figure 4.15: SEM images of the coating of a Teflon-coated capillary (left) and polyimide coated capillary (right). Note that magnification was doubled for the polyimide-coated capillary to visualize the occurrence of a small gap between coating and capillary more clearly.

The striking difference in the two images lies in the porosity of the coating: polyimide is virtually non-porous whereas Teflon exhibits a highly porous surface. Of greater concern, though, might be the occurrence of the gap between coating and capillary. It is observed in both cases but significantly more pronounced for the Teflon-coated capillary. This gap might provide nucleation sites for gas-bubbles, the occurrence of which is subject of the next section.

4.6 The occasional occurrence of gas-bubbles

An annoyance many researchers face working in the field of CEC is the occasional occurrence of gas-bubbles somewhere in the capillary. At best, these bubbles result in spikes in the electrochromatogram, at worst they cause the current to break down and render further analysis impossible. According to some researchers, they are formed at the points in the capillary where differences in EOF occur, e.g., at the junction separating the packed from the non-packed section. They are also believed to be caused by excessive Joule-heating in sections containing a particularly high packing density.[92, 124] Their nature has not yet been properly addressed and it is commonly believed that degassing of the mobile phase reservoirs can prevent their generation, something the author of this thesis cannot confirm.

Normally, once bubbles occur the only remedy is connecting the capillary to an HPLC pump and using pressure to flush them out. With respect to CEC in microfluidics, degassing of the mobile phase adds another degree of complexity and connection to an HPLC pump is not very practical for reasons already discussed earlier in Chapter 1.

Bubbles were detected in this work through the breakdown of the current and not by the sudden generation of detector spikes. Upon inspection, they were always clearly visible with the unaided eye. Three remedies were successfully applied to remove bubbles from the capillary:

1) Connection to an HPLC pump using the μ-HPLC setup depicted in Figure 4.3. (p.91).

2) Using hydrodynamic flow induced through a difference in height between inlet and outlet vial.

3) Electrokinetic flushing using pure ACN.

Approach number one is the most reliable way but apart from a lack of innovation and its inherent incompatibility with the microfluidic format it also suffers from the necessity to always have a μ-HPLC setup readily available. However, it is clearly the fastest way to purge out the bubbles although one has to wait afterwards for the applied pressure to decrease until it equals the pressure in the laboratory environment (approximately 1 hour).

The second approach is evidently the most time-consuming one since it takes several days due to the minuscule hydrodynamic flow velocities in the presence of the monolith.

Method number three reveals a way that is compatible with the microfluidic format. Its individuality lies in the impossibility to predict the direction of the flow of the bubbles. This unpredictability seems to be correlated to the size of the bubbles. Smaller bubbles move with the EOF, larger ones against it meaning that the experimenter has to observe in which direction the bubbles migrate after starting to flush the capillary with pure ACN. Aiming to force the bubbles to migrate away from the stationary phase, the applied polarity of the electric field eventually has to be reversed. The following figure displays an electrochromatogram of the separation of three model proteins and thiourea

before a bubble caused the current to break down and *after* the capillary was successfully regenerated by electrokinetic flushing with ACN:

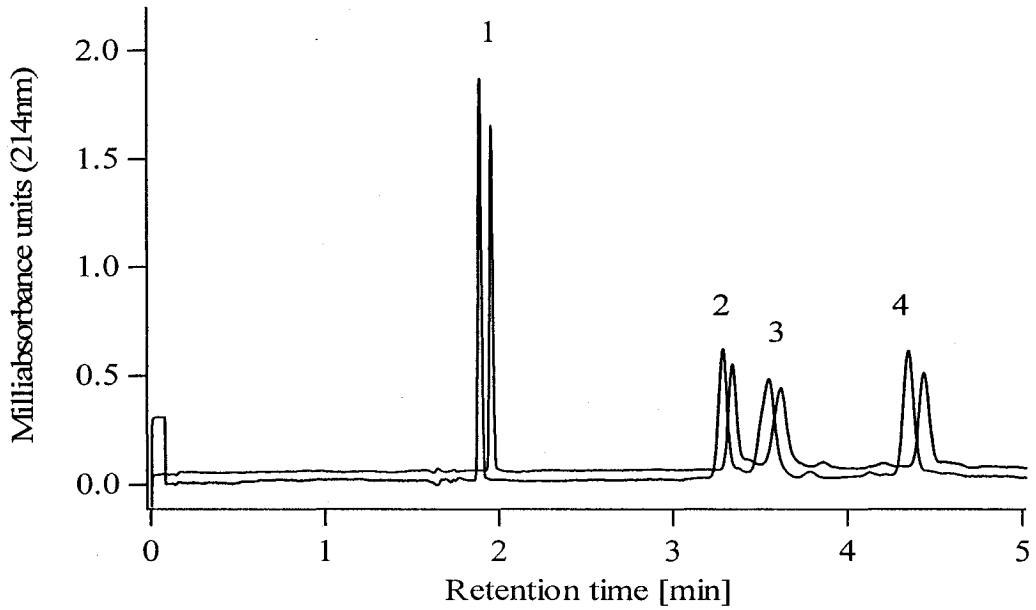

Figure 4.16: Separation of model proteins before (lower trace) the occurrence of bubbles and after (upper trace) successful removing bubbles from the capillary. Order of elution is: thiourea (1), myoglobin (2), transferrin (3) and α-lactalbumin (4). A separation voltage of 10 KV was applied and sample injection performed for 5 s / 2 KV. The mobile phase consisted of 50% ACN / 50% 5 mM pH 10.0 borate buffer. The capillary was flushed with pure ACN after the bubbles had been detected for 30 min and then reconditioned with the same mobile phase but containing 80% ACN and 20% borate buffer for 1 h.

Apart from a small shift in retention times, no significant difference can be seen between the two electrochromatograms. Surprisingly, bubbles appear either at the interface between monolith and the open section of the capillary or they are generated at the capillary outlet and diffuse (or migrate) from there towards the interior of the capillary. They can often be clearly seen inside the capillary with the bare eye and seem to acquire a certain size before they can effectively disrupt the current. Bubbles found at the monolith / open section interface might therefore possibly also have originated at the

capillary outlet. Inspecting the outlet, bubbles are routinely detected on the *exterior* of the capillary. Additionally, one sometimes finds them on the wall of the mobile phase vials. Degassing by inserting a tube connected to a Nitrogen gas tank into both inlet- and outlet vial does not cause the bubbles to move. A possible explanation for their generation might lie in the previously shown gap between the actual capillary and the coating (see Figure 4.15, p.117). This gap might serve as an excellent nucleation site leading to preferred bubble generation at the exterior of the capillary and subsequent migration or diffusion of these bubbles into the interior.

To sum up this section, three different techniques to eliminate bubbles were introduced with the electrokinetic flushing with pure ACN being an innovative and reasonably fast way that does not require any extra equipment. The bubbles appear to be generated at the exterior of the capillary. It shall be pointed out at this point, though, that bubble generation is not an "every day problem" but is only encountered occasionally.

Chapter 5: Towards the Separation of Proteins

For many years, one popular method for the separation of proteins in HPLC has been reversed-phase HPLC exploiting either a C_4- or C_8-functionality.[145] Since the monolith for CEC described in this thesis contains a butyl group, i.e., a C_4-functionality, the separation of proteins appears to be a logical choice for the monolith. Unlike the PAHs used as probes in Chapters 3 and 4, proteins belong to the class of charged analytes at any pH different from their inherent pI-values. For they also contain hydrophobic amino acid residues, their separation should be expected to stem from an interplay between chromatography and electrophoresis. Naturally, extensive preliminary experiments using model proteins need to be carried out first. These studies are summarized in this chapter with emphasis on the question whether it is really a combination of electrophoresis *and* chromatography that drives their separation or if only one of them prevails.

5.1 Separation of model proteins

Figure 5.1 displays a separation of four model proteins in CEC using the monolith:

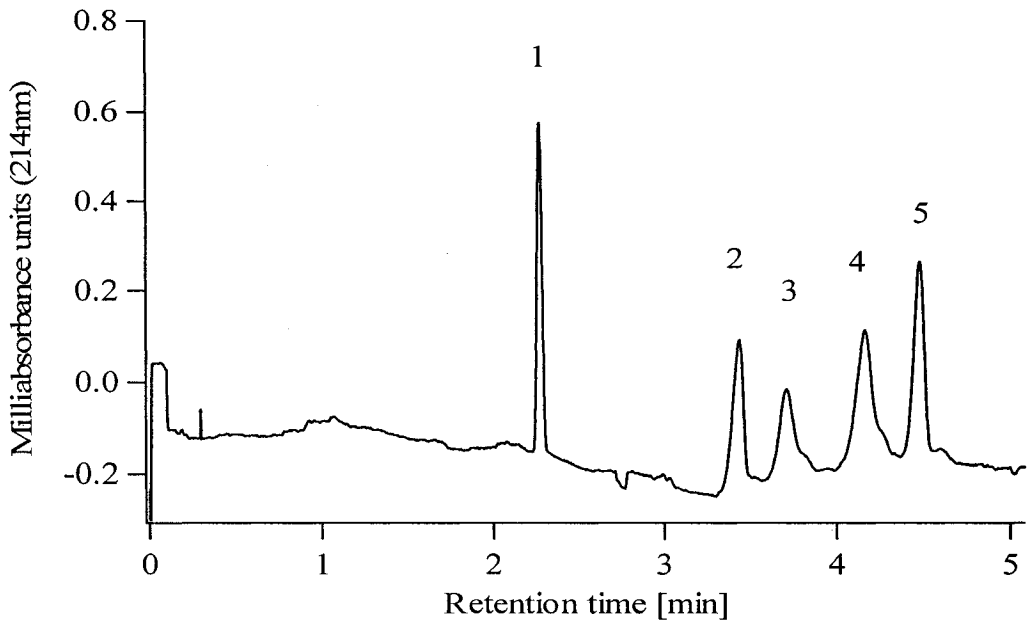

Figure 5.1: Separation of four model proteins by monolithic CEC. Order of elution: thiourea (unretained marker) (1), myoglobin (2), transferrin (3), β-lactoglobulin A (4) and α-lactalbumin (5). Analyte concentrations were: thiourea 63 µg/mL, myoglobin 373 µg/mL, transferrin 363 µg/mL, β-lactoglobulin A 533 µg/mL and α-lactalbumin 360 µg/mL. A separation potential of 10 KV was applied and the sample injection carried out for 5 s / 2 KV. The mobile phase consisted of 50% ACN / 50% 5 mM pH 10.0 borate buffer (V/V). The total length of the capillary was 35.9 cm with 18.9 cm from inlet to detector (containing the monolith). For plate numbers refer to Table 5.5 (p.144).

The proteins were baseline separated within five minutes which falls into the range typically encountered in CEC when comparing these results to published work by other authors.[17, 112] Although of no direct interest in this context, an interesting observation was made upon adding α-chymotrypsin to the mixture, which is illustrated in the next figure:

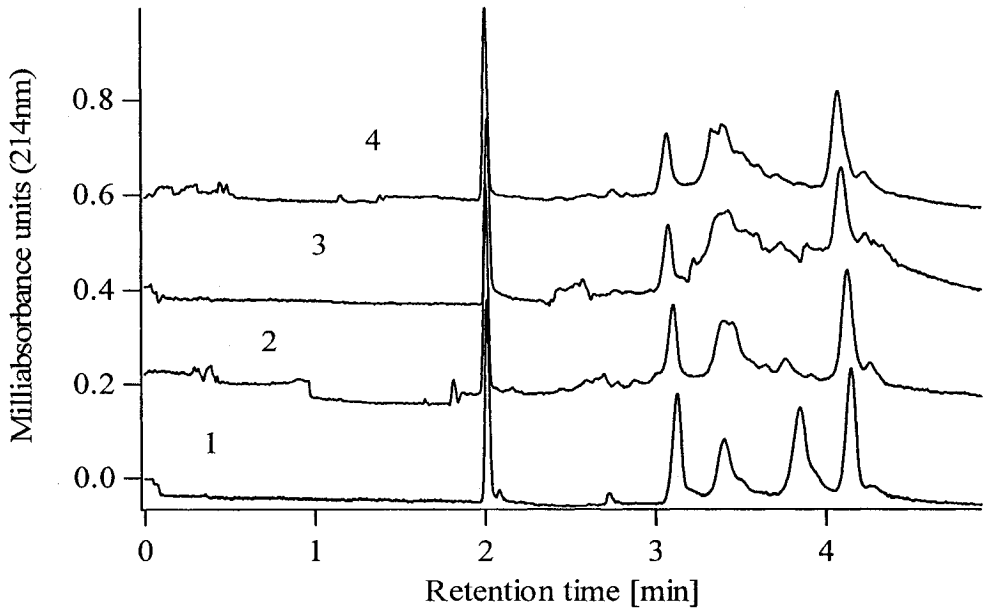

Figure 5.2: Separation of four model proteins before and after addition of α-chymotrypsin to the sample. Trace 1 displays the sample before the addition, Trace 2 immediately after and Trace 3 and 4 five and ten min after the addition, respectively. The order of elution and all parameters and conditions were the same as in Figure 5.1.

The example shows a potential application, i.e., using CEC for monitoring specific protein-protein interactions. Not surprisingly, the quality of the separation clearly deteriorates upon the addition of α-chymotrypsin since the latter one possesses proteolytic qualities.[173] Yet the electrochromatogram testifies further that β-lactoglobulin A seems to be the prime target for digestion by α-chymotrypsin since its peak essentially disappears (with novel peaks appearing next to transferrin). Myoglobin seems to be the second most likely target as seen from its decreasing peak height. α-Lactalbumin does not appear to be largely affected since neither its peak height nor its area decrease. Transferrin is obscured by the peaks developing next to it. The peptide fragments resulting from this enzymatic digestion are assumed to be either too small to be detected or they are the shoulders in the transferring peak seen in the third and fourth run.

The model proteins were primarily chosen according to the following criteria. For one, since extensive studies were required, they should be obtainable in reasonably large quantities at low cost. Some analytes should preferably possess molecular weights close to one another. Their successful separation would indicate size-exclusion *not* to be the dominant underlying separation mechanism. The latter technique is simply a sieving process that could probably more easily achieved using Capillary Gel Electrophoresis whereas the type of CEC described in this thesis strives for a mechanism based on partitioning, as was outlined in Chapter 1. Molecular weights and pI-values of the proteins selected for the experiments shown in Figure 5.1 and 5.2 are listed according to their order of elution in the following table:[174]

Table 5.1: Model proteins involved in this study, their respective monomer molecular weights and pI-values.

Protein	Molecular weight [KDa]	pI-value
Myoglobin	17000	7.4
Transferrin	77000	7.3
β-lactoglobulin A	19000	5.0
α-lactalbumin	16000	4.9
α-chymotrypsin	26000	8.5

From Figures 5.1 and 5.2 it is evident that the separation is not related to the molecular weight and thus to the size of the analyte. Therefore, at first blush, a size-exclusion separation mechanism does not seem to take place but rather the anticipated interplay between chromatography and electrophoresis.

5.2 Inter- and intra-capillary reproducibility

A mixture of three of the previously described model proteins (myoglobin, transferrin, α-lactalbumin plus thiourea as an unretained marker) was selected to serve as a testing mixture for investigating two different types of reproducibility, namely *inter-* and *intra*-capillary reproducibility. Inter-capillary reproducibility, i.e., the reproducibility from capillary to capillary, relates primarily to the reproducibility of the fabrication process. Although the results can be disenchanting, the use of an internal standard often compensates for variations in retention times and secures reliable peak identification. Intra-capillary reproducibility, on the other hand, describes the reproducibility of the separation process in one capillary. Stationary phase- or reagent instabilities, integration errors, flow rate variations (caused, for example, by temperature fluctuations) as well as variations in the amount of analyte injected are common factors to be considered here.[142, 175] For the specific case of protein separations in CE, irreversible adsorption to the capillary wall has been shown to lessen reproducibility.[176-178] In CEC, the possibility of irreversible adsorption to the monolith or capillary wall should also be taken into account. Again, the use of an internal standard for peak area and retention times might assist since it can compensate for injection and flow rate variations. Moreover, it should be assumed that, like in CE, peak areas in CEC can be expected to vary with retention times since molecules do not pass the detector cell with constant velocity. In this case, computing corrected peak areas, i.e., dividing the peak area by the retention time might aid.[177, 178]

Thiourea was used in this study as an internal standard. Since it is commonly used in CEC as an EOF-marker, it should offset EOF-variations. Unlike proteins, thiourea is

neutral and should not interact electrostatically with the stationary phase material or the capillary wall. Hence, it can also compensate for injection variations (problems caused by adsorption could otherwise easily be mistaken as injection errors).

All parameters were identical to those described in Figures 5.1 and 5.2. For the inter-capillary reproducibility, 10 capillaries were manufactured on 10 different days. A standard protein mixture consisting of myoglobin, transferrin and α-lactalbumin was then run on each capillary 5 consecutive times. For each protein, the mean retention time and mean peak area obtained from each of the 10 capillaries was used to quantify the inter-capillary reproducibility. The %RSD of the 5 runs with each capillary was used for the intra-capillary reproducibility. All manufacturing conditions were kept as constant as possible (Chapter 2). The results from both inter- and intra-capillary reproducibility can serve as a quality criterion when testing new capillaries.

Table 5.2 shows the results of the inter-capillary study. When comparing the means of the retention times from each day, a reproducibility of about 15% is observed for the proteins. This value improves significantly when using relative retention times. The same behavior is seen for peak areas (with the exception of α-lactalbumin):

Table 5.2: Inter-capillary reproducibilities of 10 capillaries, with 5 consecutive runs on each capillary. All parameters and conditions were kept identical to the ones described for Figure 5.1.

	Thiourea	Myoglobin	Transferrin	α-lactalbumin
%RSD of absolute means of 5 runs on each capillary				
Retention time	7.7	13.4	14.4	18.4
Area	8.3	7.1	18.9	7.9
%RSD of relative means (using thiourea as internal standard)				
Retention time	N.A.	5.4	6.9	11.6
Area	N.A.	6.6	15.7	9.2

Comparing the intra-capillary reproducibilities on each day (Table 5.3) average %RSD values for the absolute retention times of around 3% can be obtained. An improvement to about 1.5% is seen, again by using the internal standard. The average intra-capillary reproducibility of absolute peak areas is around 9%, it can also be improved to around 7% by using the internal standard. The use of corrected peak areas does not bring any improvement (results not shown):

Table 5.3: Intra-capillary reproducibilities of 10 capillaries, with 5 consecutive runs on each capillary. All parameters and conditions were kept identical to the ones described for Figure 5.1.

	Thiourea	Myoglobin	Transferrin	α-lactalbumin
Average of %RSD of absolute values				
Retention time	2.1	2.5	2.8	3.1
Area	5.6	9.3	10.7	8.5
Average of %RSD of relative values				
Retention time	N.A.	1.4	1.6	1.7
Area	N.A.	6.9	10.0	6.1

Considering the improvement brought by the internal standard it is expected that differences in the EOF-velocity in-between capillaries can be held responsible for the differences in retention times. Since the laboratory-built instrument was not thermostated these variations could be caused, for example, by temperature fluctuations. Slight variations in the length of the monoliths also have to be accounted for. The differences in EOF are much smaller within one capillary and are again improved by the internal standard, temperature fluctuations might have been once more the cause. The relatively low reproducibility of peak areas (both inter- and intra-capillary) could be caused by variations of the amount of sample injected since the use of thiourea as an internal standard does bring improvement here as well. The exact cause for those variations remains the subject for further research. Adsorption of proteins to the wall or the

monolith based on electrostatic interactions might also play a role. More efficient rinsing procedures might alleviate this factor.

5.3 Rinsing procedure

As mentioned above, an adequate rinsing procedure in-between runs to minimize adsorption of the proteins to the capillary wall and monolith should improve the intra-capillary reproducibilities. Several rinsing procedures have been described in the CE literature.[131] Apart from the need for effective cleaning, the rinsing step should damage neither wall nor monolith, should not lead to excessive Joule heating and should not be too time consuming either. Two methods, each involving 16 consecutive runs, are compared here. The first one does not apply a rinsing step at all. The second one rinses for 5 minutes with mobile phase containing 0.05% SDS (w/V), followed by 8 minutes reconditioning with pure mobile phase in order to stabilize the current to its initial value. It can be seen in Table 5.4 that the reproducibility of the relative peak areas can be significantly improved by introducing the rinsing step. The retention time reproducibility remains unaffected (with the exception of α-lactalbumin), indicating that rinsing and reconditioning time are long enough and not obscured by potential adsorption of SDS to the stationary phase:

Table 5.4: Comparison of intra-capillary reproducibilities (n=16) with and without a rinsing step in-between runs. All parameters and conditions were kept identical to Figure 5.1.

	Myoglobin	Transferrin	α-lactalbumin
%RSD of relative retention times			
Rinsing	1.6	1.3	1.5
Non-rinsing	1.4	1.4	1.5
%RSD of relative peak areas			
Rinsing	4.5	3.2	3.2
Non-rinsing	7.9	12.1	5.4

5.4 Relationship between plate height and mobile phase velocity

One point of interest is if the plate heights for the model proteins possess the same independence of velocity that was observed earlier for PAHs (Figure 4.1, p.82). The main difference between model proteins and PAHs is the occurrence of charges on the former. Figure 5.3 shows the plots obtained for thiourea and two model proteins:

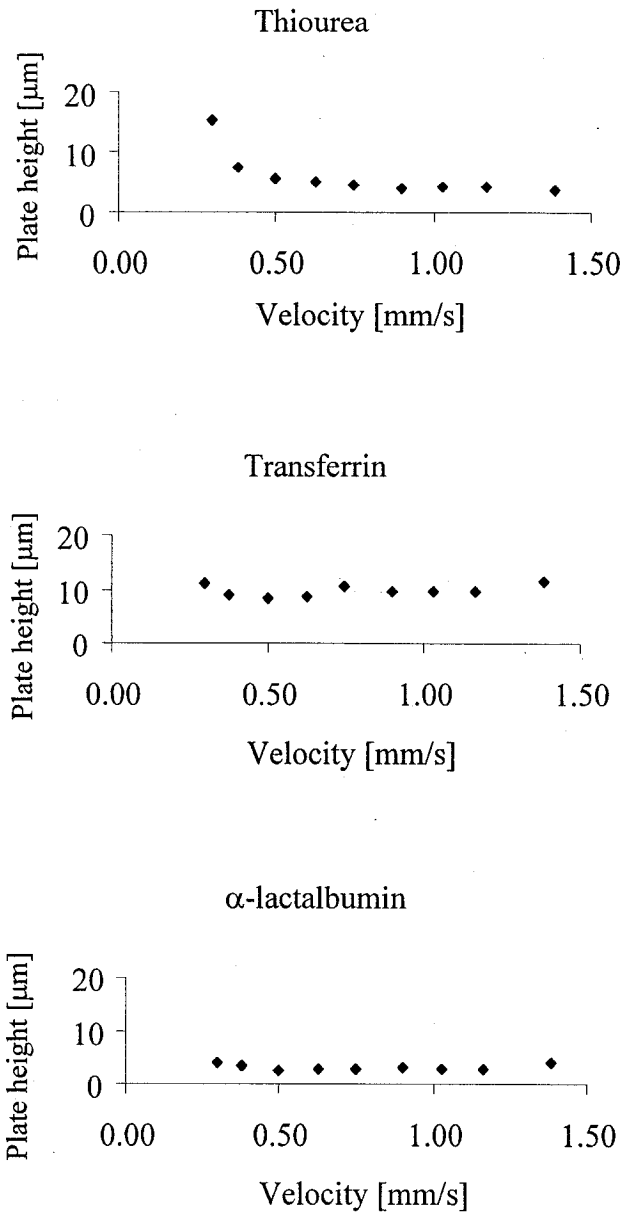

Figure 5.3: Plots of plate height versus mobile phase velocity for two model proteins and thiourea. The mobile phase consisted of 50% ACN / 50% 5 mM pH 10.0 borate buffer (V/V). Injection was carried out for 5 s / 2 KV with the applied voltage ranging from 2 KV to 10 KV. The velocities were determined from the ratio of the elution time of the unretained marker thiourea and the column length from inlet to detector (16.8 cm). Total length of the capillary was 33.1 cm. The peak width at half height corresponds to the variance and was therefore used to determine the plate height according to Equation 1.7 (p.16). All other parameters and conditions were kept identical to the ones described for Figure 5.1 (p.123).

At mobile phase velocities above 0.5 mm/s both protein plots exhibit nearly velocity independent plate heights, therefore high velocities can be used for these proteins as well without sacrificing efficiency, which might again indicate the absence of any stagnant mobile phase. Once more, the upper limit could not be determined due to arcing of the electrodes at higher voltages. A steep descent of the graph for thiourea at lower velocities highlights the influence of the B-term in the van Deemter equation, i.e., longitudinal diffusion (Equation 1.16, p.23). This descent is not seen in the plots for the proteins due to their lower diffusion coefficients.

5.5 Relationship between plate height and injection time

Figure 5.4 illustrates the relationship between peak height and injection time for myoglobin and α-lactalbumin:

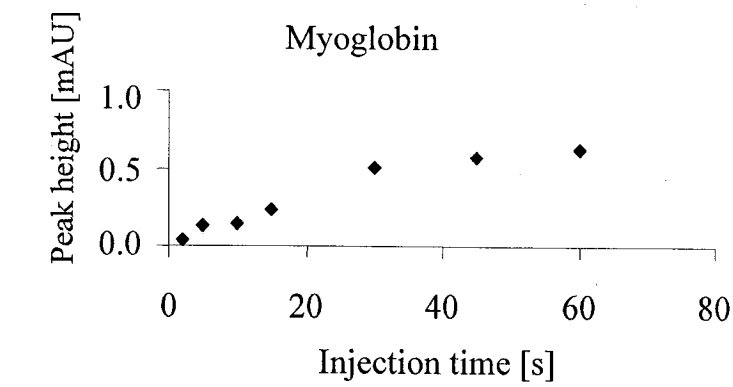

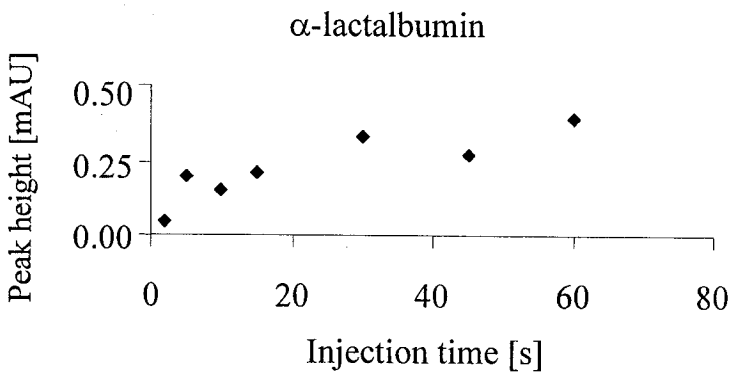

Figure 5.4: Relation between plate height and injection time for myoglobin and α-lactalbumin. All parameters and conditions were kept identical to the ones described for Figure 5.1 (p.123) and confirmed on a second capillary.

The two graphs demonstrate an increase in peak height by prolonging the injection time. A similar behavior has been reported by Quirino et al. [179] for CEC using a sol-gel monolith. Both mobile phase and sample solvent were the same in the work presented here meaning they did not differ in ionic strength or percentage organic solvent. Therefore, one would not expect preconcentration caused by electrokinetic

sample stacking. Neither would one anticipate chromatographic field enhancement caused by differences in hydrophobicity between sample and mobile phase.[180] A more evident explanation is that for short injection times, the injected plug length is small compared to the distance the analyte diffuses over the course of the separation. However, for longer injection times, the plug length becomes wider than the diffusion distance resulting in peak heights that are essentially independent from the injection times. Considering the dependence of detection limits on peak heights,[181] these findings are beneficial when detecting dilute quantities of analyte.

5.6 Loadability of proteins

Purification of minute amounts of proteins for quality monitoring in the biotechnological industry proposes another application involving protein separations. In this context, it is important to know the maximum amount of protein that can be separated without the peaks starting to overlap. The next figure shows that the maximum analyte concentrations in a mixture of three model proteins are around 2 mg/mL for each protein under the given injection conditions before the peaks begin overlapping.

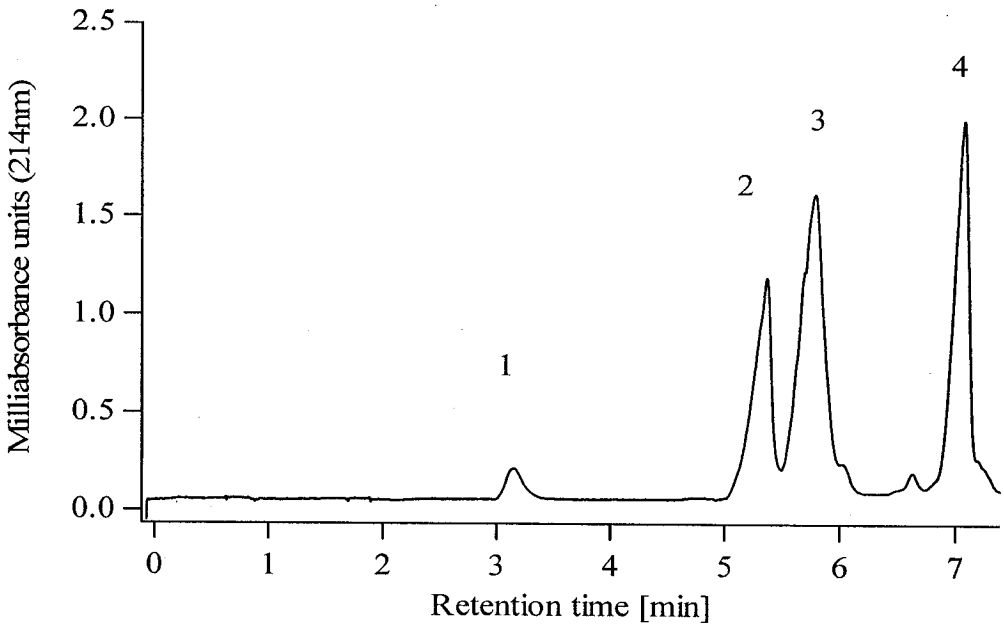

Figure 5.5: Loadability of proteins. Analyte concentrations were thiourea (1) 160 µg/mL, myoglobin (2) 2240 µg/mL, transferrin (3) 2640 µg/mL, α-lactalbumin 1900 µg/mL. All parameters and conditions were kept identical to the ones described for Figure 5.1 (p.123).

5.7 Influence of the percentage acetonitrile on the capacity factors

By increasing the amount of ACN in the mobile phase, the separation of three model proteins shows exactly the opposite behavior as compared to the earlier findings for PAHs (Figure 4.2, p.84):

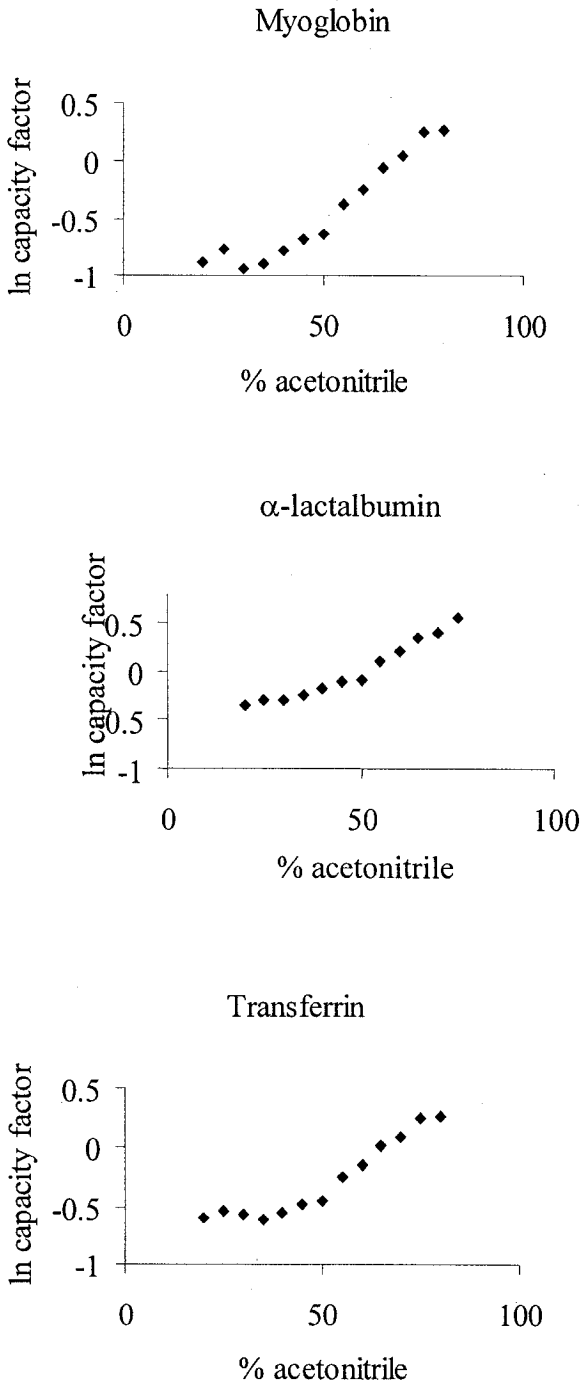

Figure 5.6: Plots of ln capacity factor for three model proteins versus percentage ACN in mobile phase, with 5 mM pH 10.0 borate buffer accounting for the remaining percent (V/V). Thiourea served as unretained marker to determine the EOF and calculate the capacity factors according to Equation 4.1 (p.85). All other parameters and conditions remained identical to the ones reported for Figure 5.1 (p.123).

From chromatographic theory, an increase in capacity factor indicates an increase in analyte – stationary phase interaction. In reversed-phase chromatography, one would expect to reduce the analyte-stationary phase interaction by increasing the percentage of organic solvent.[145] This explains the behavior of the relatively small, neutral PAHs as was illustrated earlier in Figure 4.2 (p.82). PAHs were also added to the protein sample as a control in a separate experiment (not shown here) and the same results obtained as in Figure 4.2. Although EOF changes (as illustrated in Figure 4.10, p.107) could explain the observed behavior for proteins (the EOF decreases below 50% ACN in the mobile phase) this is deemed rather improbable since it should have affected the PAHs as well, i.e. let to an ascent in their plots and not to a descent. In the case of the proteins, combined electrophoretic and chromatographic separation mechanisms are expected to be at work in CEC. Also, it was pointed out in a recent publication by Rathore and Horváth [149] that by using the formula employed to calculate the capacity factors (Equation 4.1, p.85) one obtains a number that, unlike its equivalent in HPLC, does not contain any easily accessible information about thermodynamic or mechanistic aspects. Thus, it could be deemed inappropriate to draw conclusions about the degree of analyte-stationary phase interaction for proteins, which possess electrophoretic mobilities and may be unfolded to varying degrees, from the calculated capacity factor. The capacity factor in CEC more accurately serves as a peak locator useful for the calculation of resolution and selectivity. Still, it can be safely said that in the steep part of the curve small changes in the percentage ACN can have significant impact on the apparent retention of the proteins. This may in turn have profound consequences on the robustness (and reproducibility) of

the CEC method. It also provides a mechanism to tune the selectivity and overall resolution of CEC separations.

5.8 Comparison of CEC to μ-HPLC, aqueous and non-aqueous CE

Despite the complexity of the capacity factor, the results from the previous section might nevertheless call into doubt that chromatography plays a profound role in protein separations by CEC. Rather, the data hint that electrophoresis might actually govern the separation after all. μ-HPLC can be considered to be the method of choice to prove the occurrence of chromatographic interactions. If the model proteins can be separated by μ-HPLC the occurrence of a chromatographic type of interaction would be proven since charge and thus electrophoresis do not contribute to separation in μ-HPLC. Figure 4.3 (p.91) showed the instrumental setup required for μ-HPLC and Figure 4.5 (p.95) depicted the separation of transferrin and thiourea. One limiting factor of this comparison is that μ-HPLC employs the very same capillaries as CEC, i.e., Teflon-coated fused-silica capillaries. Therefore, the occurrence of electrophoresis cannot be excluded completely because, potentially, a streaming potential builds up. The separation of myoglobin, α-lactalbumin and thiourea by μ-HPLC is illustrated in the following picture:

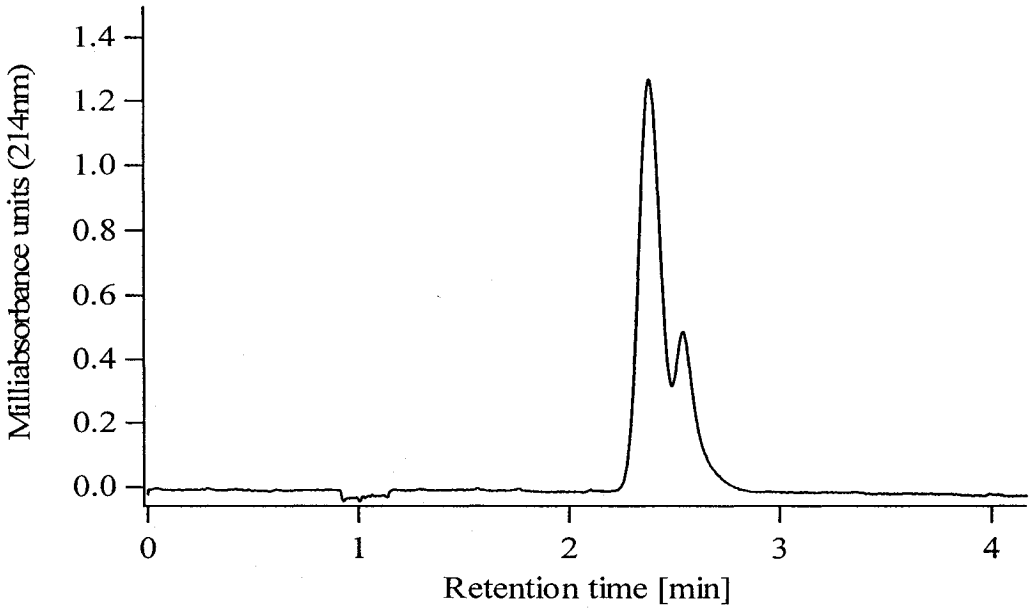

Figure 5.7: Separation of myoglobin, α-lactalbumin and thiourea by μ-HPLC. The injection volume was 20 μL with an instrumental flow rate of 0.5 mL/min. Total length of the capillary was 35 cm with 21 cm length from inlet to detector. Analyte concentrations and separation conditions were identical to the ones described in Figure 5.1 (p.123). The first peak was attributed to myoglobin and α-lactalbumin, the second one to thiourea. Spiking experiments confirmed the peak identities.

Figure 5.7 essentially confirms what Figure 4.5 (p.95) already indicated: the model proteins elute before thiourea. This does not exclude a chromatographic mechanism, though, since it is possible (at least in theory) that the proteins do interact slightly with the stationary phase yet with the restriction that they can only interact where the stationary phase is actually accessible to them. For instance, they might not be capable of interacting with stationary phase located inside micropores only accessible to thiourea provided that such micropores indeed exist (it was mentioned earlier in Chapter 4 that their occurrence has not been verified). If a significant amount of stationary phase is exposed *inside* such micropores and the proteins due to size-restrictions can only interact with stationary phase located *outside* the micropores one might only observe

slight or no resolution at all. All these assumptions could unfortunately not be experimentally verified unlike the following, last hypothesis: it could be that the proteins are not separated because electrostatic repulsions from the sulfonate groups are too strong. Yet the same separation using a monolith prepared without AMPS did not show any separation of the proteins either and therefore rules out this hypothesis (results not shown here). On a side note, since the three proteins are not separated at all, an eventually occurring streaming potential should be negligible, i.e., essentially no electrophoresis takes place in the μ-HPLC mode.

The author did obtain a significantly different elution profile when comparing the CEC results to aqueous CE, though:

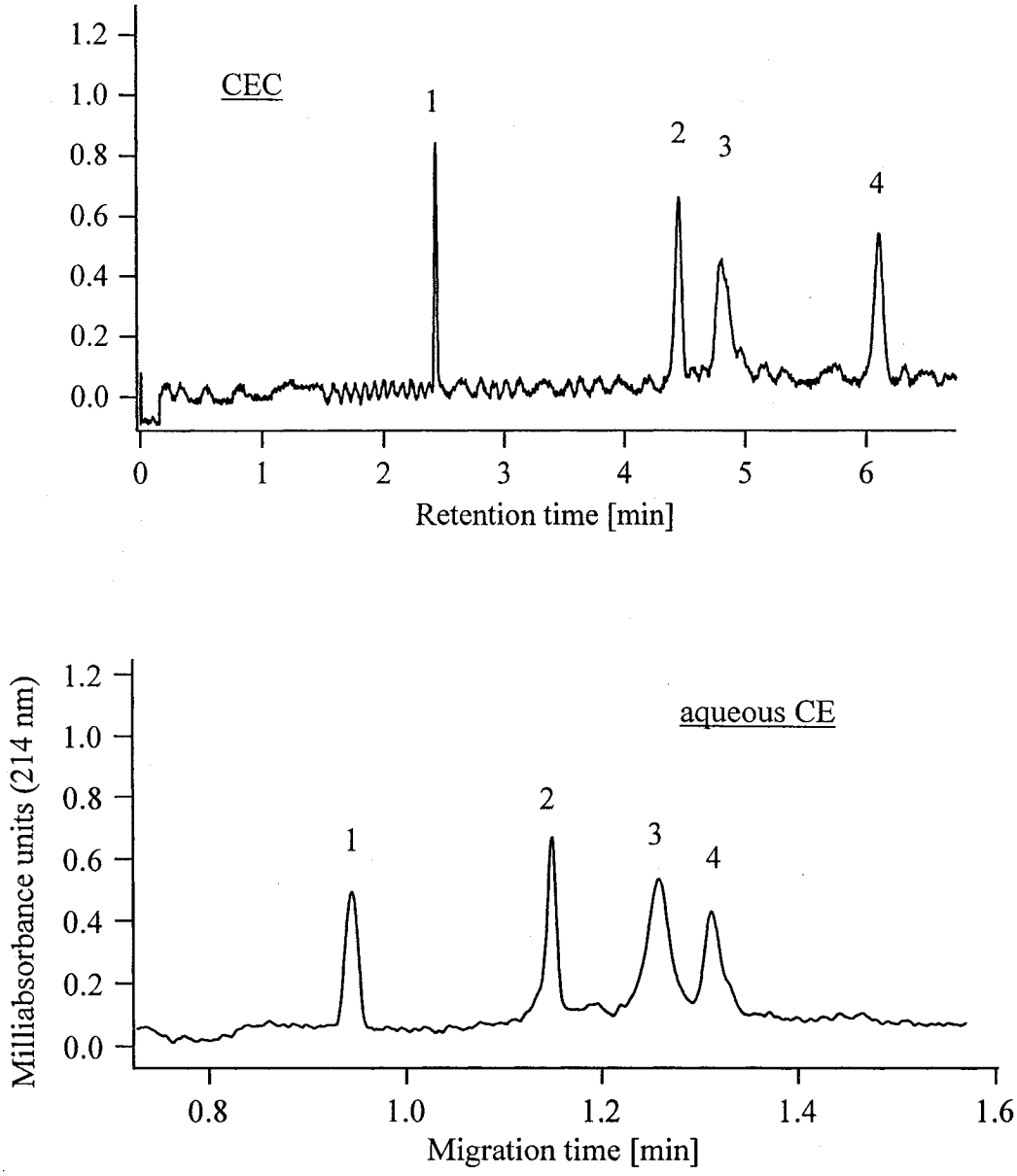

Figure 5.8: CEC (upper trace) and aqueous CE (lower trace) for thiourea and three model proteins. The order of elution was identical in both cases: thiourea (1), myoglobin (2), transferrin (3) and α-lactalbumin (4). Analyte concentrations were identical to the ones described in Figure 5.1. For the CE study a voltage of 17.3 KV was applied and the injection carried out for 5 s / 2.3 KV. The CEC study was carried out by applying a voltage of 15 KV and the injection performed at 5 s / 2 KV. The total length of the capillary was 37.3 cm in both cases and 21.1 cm to detector. The mobile phase in CEC consisted of 50% ACN / 50% 5 mM pH 10.0 borate buffer (V/V) and in aqueous CE only of the aqueous component, i.e., 100% 5 mM pH 10.0 borate buffer. The ISCO CV^4 was employed for both studies. An explanation why different separation voltages were used in the two studies is given in Appendix III (p.188).

The electropherogram differs from the electrochromatogram with respect to the resolution. Although the overall order of elution remains the same, transferrin (3) elutes considerably closer to myoglobin (1) than to α-lactalbumin (2) in the case of non-aqueous CE. The following table compares the two techniques in terms of retention times and separation efficiency (the latter one expressed as number of theoretical plates):

Table 5.5: Comparison in terms of retention times, half widths and number of theoretical plates for three model proteins and thiourea for CEC and aqueous CE. All parameters and conditions were identical to the ones described for Figures 5.1 and 5.8. Plate numbers were obtained using the widths at half heights according to Equations 1.7 (p.16) and 1.17 (p.24).

	Thiourea (N=5)	Myoglobin (N=5)	Transferrin (N=5)	α-lactalbumin (N=5)
Average retention time [s]				
CEC	150	268	291	368
Aqueous CE	57	70	76	79
Average width at half height [s]				
CEC	1.4	3.6	6.4	4.7
Aqueous CE	0.9	0.7	1.4	0.9
Number of theoretical plates per column				
CEC	64,000	29,000	11,000	33,000
Aqueous CE	26,000	66,000	18,000	48,000

Aqueous CE proves to be advantageous with respect to time and efficiency by approximately a factor of two compared to CEC. Nevertheless, due to the distinctively different elution profile, CEC has the potential to provide complementary information. Since the previously mentioned μ-HPLC studies indicated that chromatography most likely does not play a significant role in the overall separation process, an alternative explanation for the differences in elution profiles between aqueous CE and CEC might be the degree of denaturation in the respective mobile phases. CE used aqueous borate buffer whereas CEC employed a binary solvent consisting of borate buffer and ACN. Circular Dichroism (CD) Spectroscopy is a suitable method to investigate the degree of protein denaturation.[138, 182] The following figure depicts a CD spectrum of myoglobin in 5 mM pH 10.0 borate buffer (used for aqueous CE) and in the mobile phase employed for all of the protein studies in CEC, i.e., 50% ACN / 50% 5 mM pH 10.0 borate buffer:

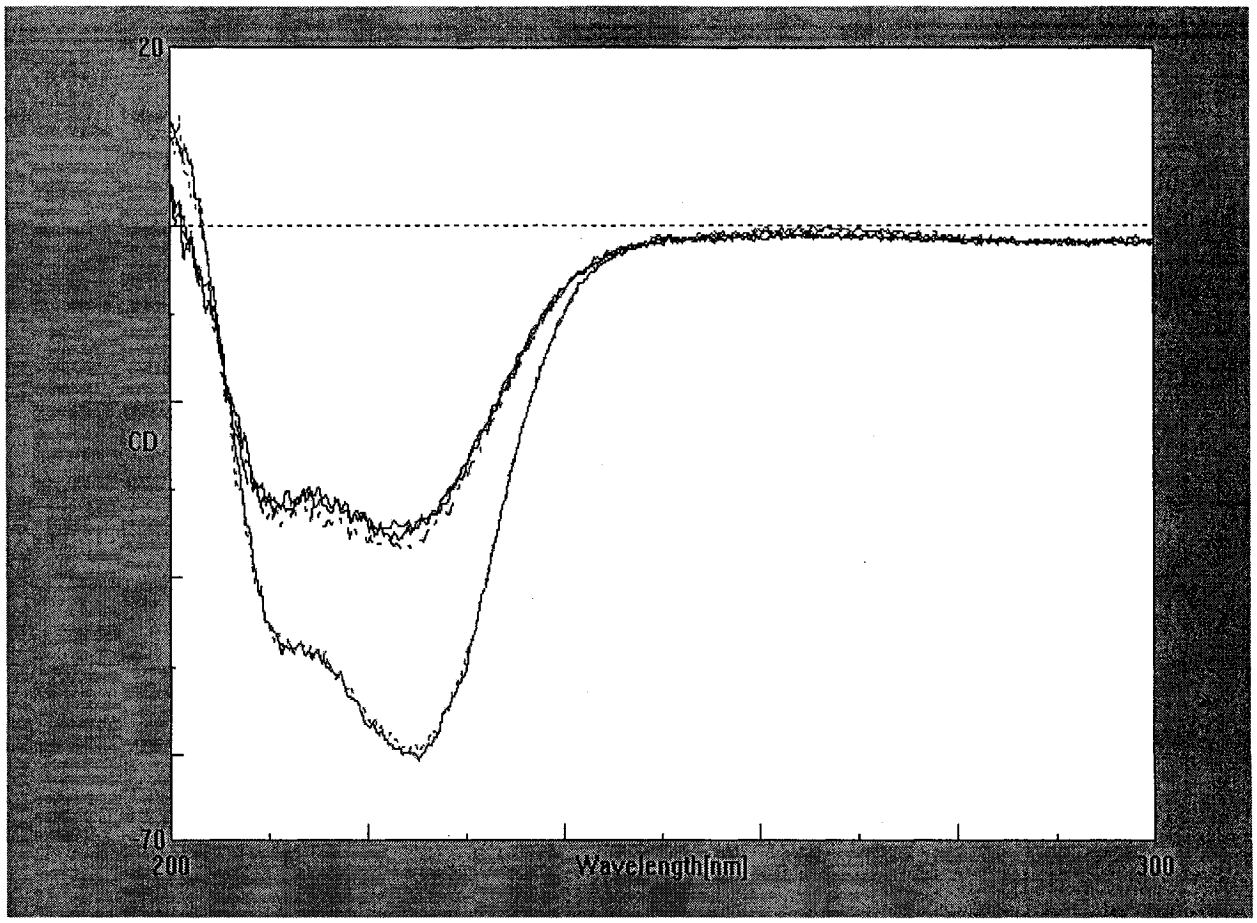

Figure 5.9: CD spectra for myoglobin in 5 mM pH 10.0 borate buffer and 50% ACN / 50% 5 mM pH 10.0 borate buffer (V/V). The lower three traces (which essentially completely overlap) show the spectrum in aqueous buffer, the upper ones the spectrum in mobile phase.

The spectra differ greatly in the two solvent systems. Considering the dependence of electrophoretic mobility on the shape of the analytes (Equation 1.5, p.14), different elution profiles become explainable by assuming divergent shapes in different solvent systems.

Comparisons with non-aqueous CE mark an attempt to support the notion that nevertheless at least a small degree of chromatography occurs. Non-aqueous CE is also a promising reference technique since all conditions are the same except for the presence of

the monolith. If the elution profile remains identical, one can most certainly exclude any chromatography from taking place. Preliminary studies had indicated that the non-aqueous CE results remained unaffected, no matter if the capillary had been pretreated like in CEC (i.e., silanized) or not. Therefore, no silanization was carried out for this study or for any of the other studies involving non-aqueous CE (see Chapter 6). Figure 5.10 shows a typical electropherogram for the separation of the three model proteins and thiourea by non-aqueous CE:

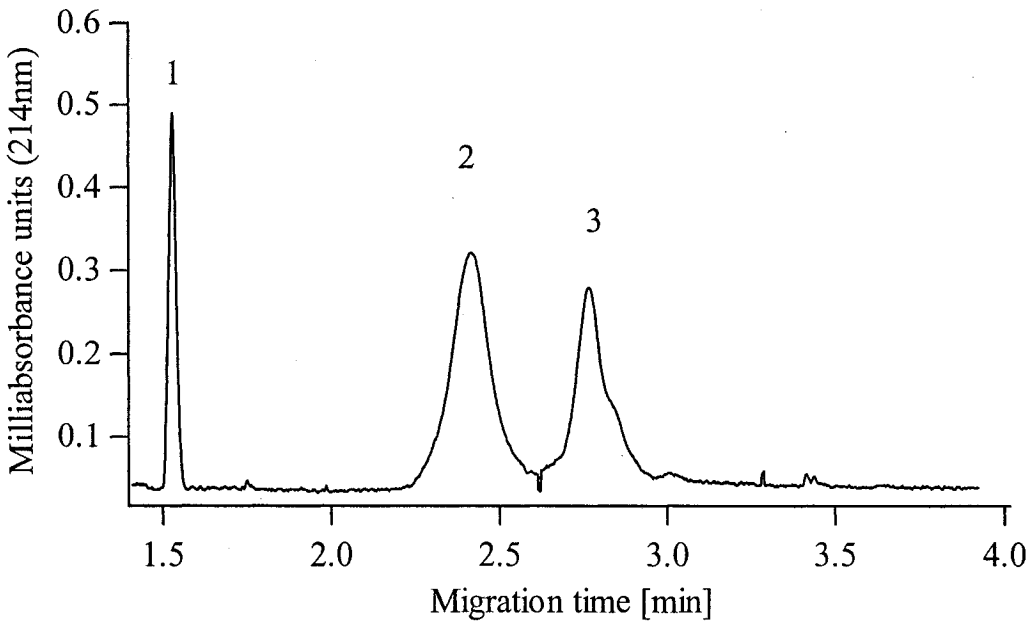

Figure 5.10: Separation of three proteins by non-aqueous CE. Order of elution: thiourea (unretained marker) (1), transferrin (2) and α-lactalbumin (3). A potential of 17.3 KV was applied and the injection carried out for 5 s / 2.3 KV. The mobile phase consisted of 50% ACN / 50% 5 mM pH 10.0 borate buffer (V/V). The total length of the capillary was 35.9 cm with 18.9 cm from inlet to detector. Analyte concentrations were identical to the ones in Figure 5.8 (p.142).

Myoglobin does not elute under these conditions as confirmed by several additional runs on the same and two other capillaries. Irreversible adsorption to the wall might be one explanation. Regrettably, theses findings do not shed any additional light on the question if chromatography really contributes to the separation since the resolution between transferrin and α–lactalbumin does not appreciably differ between CEC and non-aqueous CE. The resolution R can be quantified using the following formula:[8]

$$R = \frac{1.18(t_r y - t_r x)}{w_{1/2}x + w_{1/2}y}$$

Equation 5.1: Resolution R between two adjacent peaks (dimensionless); $t_{,r}y$ represents the migration or retention time of the second peak, $t_{,r}x$ the migration or retention time of the first peak, $w_{1/2}x$ indicates the width at half height of the first peak and $w_{1/2}y$ indicates the width at half height of the second peak (all units in s or min, respectively).

In CEC, one obtains a resolution of 2.0 for transferrin and α–lactalbumin (using the data in Table 5.5, p.144) whereas non-aqueous CE yields 1.8 (with N=5 in both cases). Such a small difference further nurtures the idea that, for theses two analytes, chromatography does not play a major role in their separation. To recapitulate the insights gained in this chapter it shall therefore be said that electrophoresis is most likely the main contributor for the separation of the model proteins presented here. Nevertheless, employing the monolith for protein separations is not in vain as seen from the emergence of a peak for myoglobin in CEC compared to non-aqueous CE. The monolith provides a stable coating that prevents the adsorption of myoglobin to the capillary walls. This coating might also enhance reproducibility when dealing with more

complex matrices (as will be shown by the separation of human serum in the following chapter). CEC has the potential to provide complementary information with respect to aqueous CE. Apart from investigating the role of chromatography, both inter-and intra-capillary reproducibilities were investigated and an effective rinsing procedure established. The relationship between injection time and peak height was evaluated. Furthermore, maximum loadabilities were determined.

Chapter 6: Further Applications

Stimulated through conversations with other members of the department concerning their on-going projects, several potential applications for CEC using this particular monolith emerged during the course of this thesis. They ranged from samples with known and rather simple composition, for example, supposedly pure oligonucleotides, to complex biological fluids, for instance, serum spiked with two different drugs, human amniotic fluid and bovine milk. Five selected applications will be presented in this chapter. The first one deals with monitoring the product of an organic synthesis, which, due to the rare nature of this particular synthesis, is a unique application. The ensuing separation of selected oligonucleotides has never been carried out in CEC either. Separating non-steroidal anti-inflammatory drugs (NSA) both in a simple matrix (mobile phase) and a more complex one (serum) follows. Lastly, two crude separations of bovine milk and human amniotic fluid will be presented.

The goal of this chapter is to hint at potential applications of this particular monolith towards applications of CEC in the "real world" and to underline its versatility. None of the applications presented here describes a "complete story", meaning they offer plenty of room for potential successors to pursue them further and investigate them in greater detail.

6.1 Monitoring the synthesis of anthracene-2,3-dialdehyde

Anthracene-2,3-dialdehyde (ADA) has recently gained attention as a potential derivatizing agent for analytes containing a primary amino function, for example, amino acids.[183-186] Prior to reaction, it is a fluorogenic agent whereas the reaction product becomes fluorescent. Equation 1.18 (p.39) demonstrated the linear relation between detected signal in fluorescence detection and the radiant power of the light source. Consequently, sources with high radiant power allow for the detection of minute amounts of analyte. ADA, in particular, permits relatively inexpensive green Helium-Neon lasers or green solid state lasers to be used thanks to their matching excitation wavelength of 543 nm. Due to its limited commercial availability, the synthesis of ADA was pursued in the author's laboratory by a project student, Mrs. Erin Templeton, based on a previously published procedure (see Appendix II, p.184).[187] Over the course of that particular project CEC emerged as a useful tool for rapid quality control. The following figure illustrates a comparison between CEC, aqueous CE, non-aqueous CE and μ-HPLC evaluating the purity of the synthesis product:

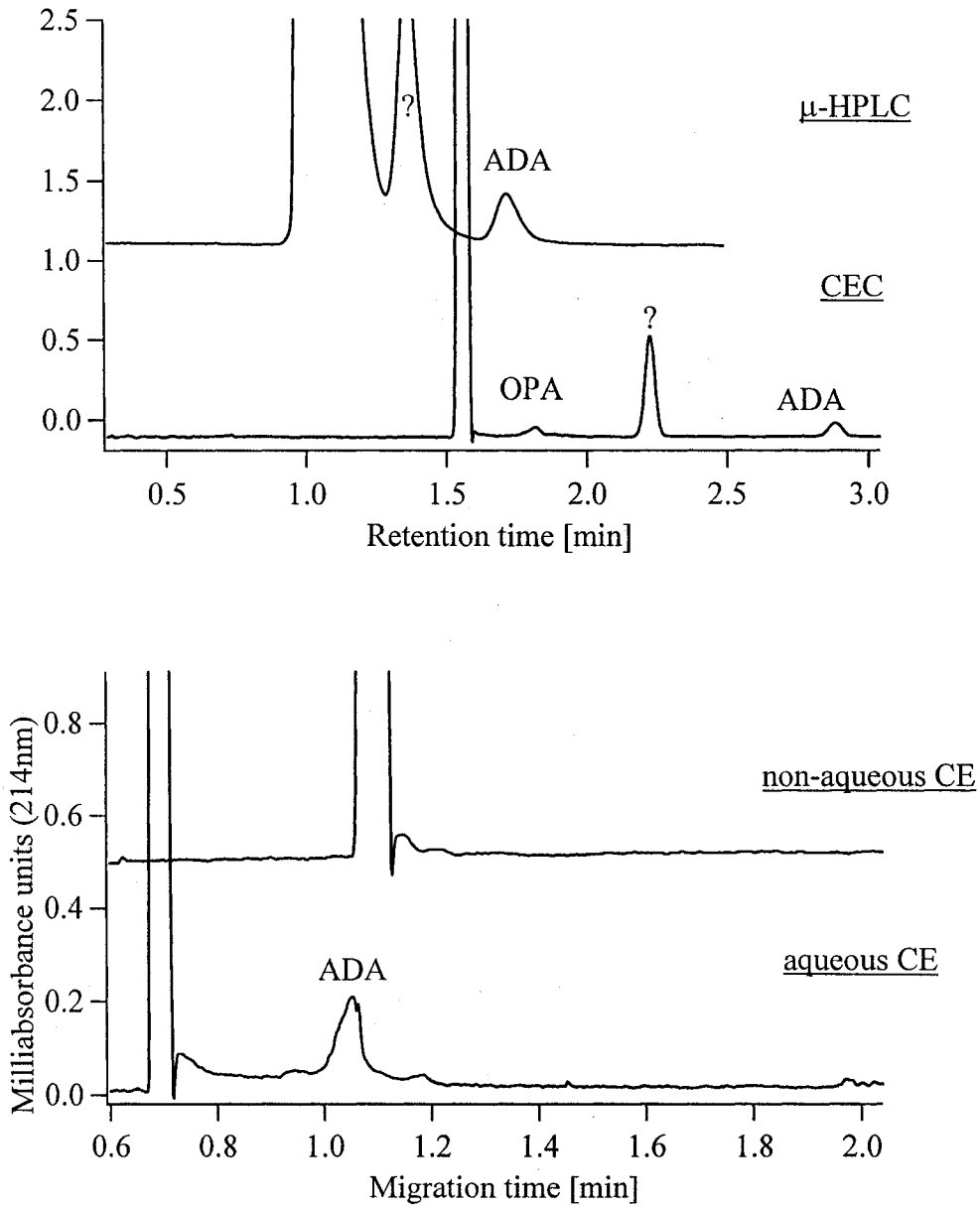

Figure 6.1: Comparison of μ-HPLC, CEC, non-aqueous and aqueous CE for quality control of the synthesis of ADA. Every run was carried out five times with only one trace for each set shown here. Total length of the capillary was 27.9 cm in all cases; the distance from inlet to detector was 15.8 cm (containing the monolith in CEC and μ-HPLC). Mobile phase consisted of 80% ACN / 20% 5 mM pH 10.0 borate buffer (V/V) for all cases except for aqueous CE (100% 5 mM pH 10.0 borate buffer). Injection volume for μ-HPLC was 20 μL and a flow rate of 0.5 mL/min was applied. Injection was carried out for 5 s at 1 KV for CEC and 0.5 KV for 5 s for aqueous and non-aqueous CE; the separation was performed at 10 KV for CEC and 11.5 KV for aqueous and non-aqueous CE. Identity of the peaks labeled OPA and ADA was confirmed by spiking the sample with the respective analytes.

In comparison to the two CE methods, CEC permits baseline resolution of both the product peak and two other peaks. The peak labeled OPA (standing for *o*-phthaldialdehyde) can only be identified using CEC and not by any of the other methods. Since it is one of the reactants its occurrence does not come as a surprise. The identity of the peak assigned a question mark remains unknown. Although slightly slower than the CE methods, a total analysis time of 3 min can still be considered reasonably fast. The μ-HPLC method serves as the final evidence that a chromatographic separation mechanism indeed takes place. Its performance could be optimized further if injection loops delivering smaller sample volumes were available.

6.2 Monitoring the purity of single-stranded oligonucleotide samples

Among numerous applications, single-stranded oligonucleotides are frequently used as primers for the polymerase chain reaction or site-directed mutagenesis. A neighboring laboratory at Concordia University encountered difficulties when attempting to use supposedly identical oligonucleotides purchased from two different manufacturers. Since oligonucleotides essentially always possess the same charge to size ratio (like any other DNA sample), their separation is difficult to achieve by CE (albeit not impossible for short strands) making Capillary Gel Electrophoresis the method of choice for tasks like DNA sequencing.[188, 189] With regard to *in vitro* solid state synthesis of oligonucleotides, reversed-phase HPLC is commonly used to purify oligonucleotides.[190] For this reason, CEC using this particular monolith might offer an interesting alternative here because it can exploit the chromatographic separation mechanism provided by the

C_4-functionality. To the author's best knowledge, CEC has not been applied to the separation of oligonucleotides to date, although the use of monoliths for this purpose in both HPLC and μ-HPLC has been reported [191] as well separations of nucleotides by CEC.[192] The following figure illustrates the separation of the two supposedly identical oligonucleotides samples by CEC:

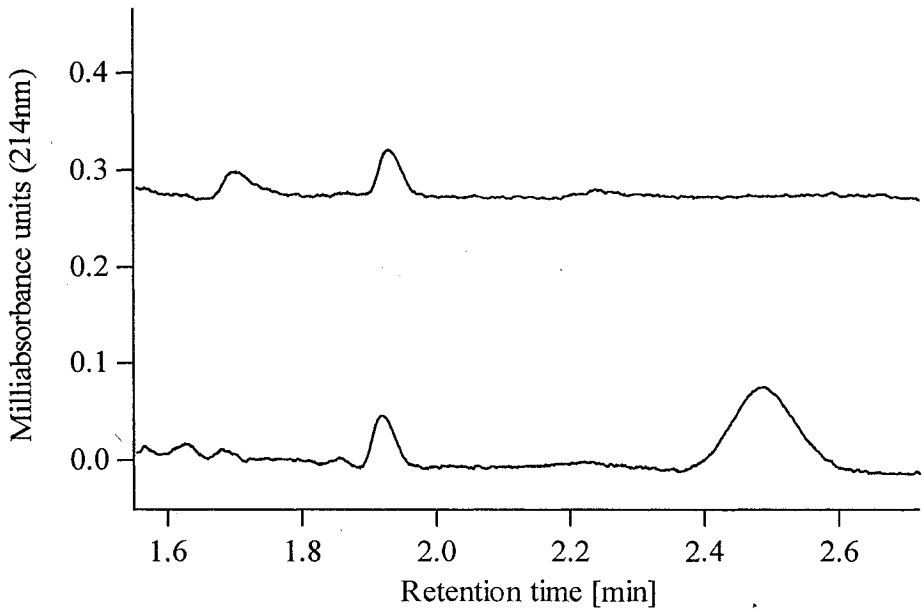

Figure 6.2: Comparison between two supposedly identical oligonucleotides from two different manufacturers by CEC. The upper trace displays PermHisTag1 from Biocorp, the lower one the same oligonucleotide from IDT (see Chapter 2 for details). Theoretically, both oligonucleotides should contain 61 bases. Total length of the capillary was 30.9 cm with 18.1 cm length of the monolith. Mobile phase consisted of 10% ACN / 90% 5 mM pH 10.0 borate buffer (V/V). Injection was carried out for 5 s / 2 KV and a separation voltage of 10 KV was applied. Each run was repeated three times with identical results. Only one trace is shown here.

Although the peaks could not be identified, the electrochromatogram attests the two samples to be non-identical. In order to prove that chromatography governs the

separation of oligonucleotides in CEC, two different oligonucleotides were combined and separated by CEC, aqueous and non-aqueous CE, leading to the following picture:

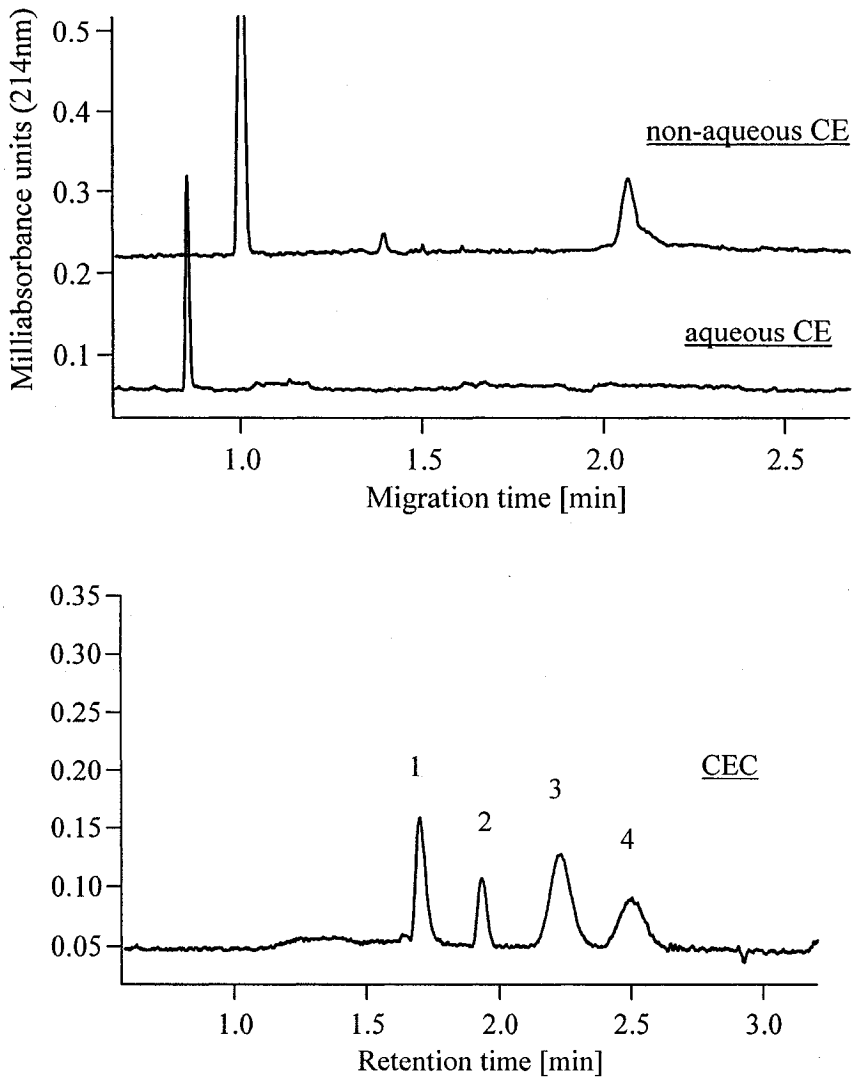

Figure 6.3: Comparison between CEC, aqueous and non-aqueous CE for the separation of two different oligonucleotides: PermHisTag (61 bases) and D246E (45 bases). Every run was carried out three times with only one trace for each set shown here. Total length of the capillary was 30.9 cm in all cases; the distance from inlet to detector was 18.1 cm (containing the monolith in CEC). Mobile phase consisted of 90% ACN / 10% 5 mM pH 10.0 borate buffer (V/V) in CEC and non-aqueous CE and 100% 5 mM pH 10.0 borate buffer for aqueous CE. Injection was carried out for 5 s at 2 KV for all cases. Separation was performed at 10 KV for CEC and 11.5 KV for aqueous and non-aqueous CE. In separate experiments the peaks labeled '1', '2' and '3' were allocated to D246E, the peak labeled '2' was also found in PermHisTag as well as the peak labeled '4'.

Naturally, the ultimate goal of any oligonucleotide separation would be to achieve at least partial resolution between analytes that differ by only one base as it can be accomplished by reversed-phase HPLC.[190] The presented separation is still far away from actually managing this task. However, it does prove the ability of CEC to separate several ingredients of the mixture whereas neither aqueous nor non-aqueous CE can accomplish this goal. Since oligonucleotides are charged analytes at pH 10, this separation underlines that the monolith is principally able to separate not just neutral but also charged molecules based on hydrophobic interaction with the stationary phase, i.e., the butyl function. Unfortunately, none of the peaks could be identified so far but only be assigned to stem from one sample or the other.

6.3 The separation of non-steroidal anti-inflammatory drugs

Numerous "over-the-counter" medications contain one or more NSA, not just to ease inflammation but also to alleviate pain and to decrease fever. In some cases, caffeine is added to these medications, a combination that, for instance, is advantageous in the treatment of migraine.[193, 194] CEC might offer once more an alternative to established technologies in monitoring either the quality of a selected medication, formulation or to measure the NSA concentrations in biofluids like serum for pharmacokinetic studies. Two pieces of data are shown here: the first one shows the separation of caffeine and ibuprofen in serum. The underlying separation is thought to be an interplay of both CEC and non-aqueous CE. The second piece of data illustrates the separation of caffeine and

three NSA (all belonging to the family of 2-arylpropionic acids) dissolved in mobile phase. Similar analyses were carried out by other groups with CEC involving different stationary phases.[195]

Preliminary studies had illustrated that for the separation of serum proteins neither the order of elution nor the actual elution profile differed between CEC and CE. Yet the one significant change that did take place concerned the very low reproducibility of both aqueous and non-aqueous CE compared to CEC. Most certainly, every researcher using CE for protein analysis is familiar with this type of problem typically caused by irreversible adsorption of proteins to the capillary wall. Although reduced, this adsorption still takes place even at pH 10 due to the occurrence of positive charges in the lysine and arginine side-chains (their respective pK_A-values are 10.5 and 12.5, respectively [196]). A large variety of both permanent and non-permanent coatings have been developed over the years to prevent protein adsorption.[176, 197] They often involve tedious recipes and result in expensive capillaries once they become commercially available. This implies that if the monolith can provide decent reproducibilities, it fulfills a purpose even in the absence of any chromatography taking place since its manufacture process is reasonably fast and thereby competes with many established coating technologies. The following figure illustrates three overlaid consecutive separations of thiourea, caffeine and ibuprofen in human serum by both CEC and non-aqueous CE:

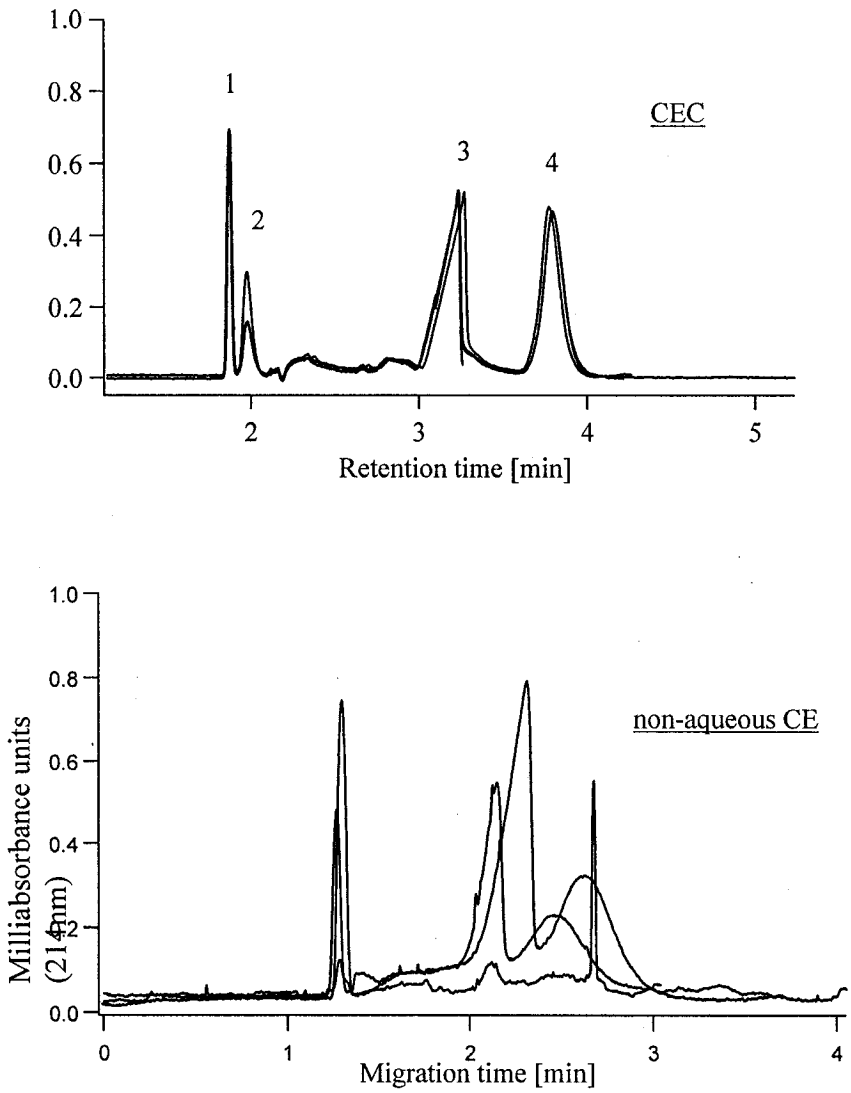

Figure 6.4: Comparison between CEC and non-aqueous CE for the separation of thiourea, caffeine and ibuprofen in human serum. The peaks were identified by consecutive addition of standards as follows: thiourea (1) 95 μg/mL, caffeine (2) 73 μg/mL, ibuprofen (3) 382 μg/mL and albumin (4). The serum was dissolved in mobile phase and accounted for 3.3 % of the total sample volume. Mobile phase consisted of 10% ACN / 90% 5 mM pH 10.0 borate buffer (V/V). The length of the capillary was 30.9 cm in both cases with 18.1 cm distance from inlet to detector (containing the monolith in CEC). The injection lasted 5 s at 2 KV for both CEC and non-aqueous CE and the separation was carried out at 10 KV for CEC and at 11.5 KV for non-aqueous CE. No filtration or centrifugation step was applied to the sample prior to injection. No rinsing steps were carried out in any of the techniques. Number of theoretical plates for CEC were: thiourea (102,000 N/m), caffeine (40,000 N/m), ibuprofen (19,000 N/m) and albumin (24,000 N/m).

With respect to the ibuprofen peak, the skewed peak shapes most likely result from electrodispersion. Although generally undesired, they facilitate peak identification. An improvement could be brought about by using lower concentrations of ibuprofen to minimize differences in conductivity between sample and mobile phase. Overall, the separation clearly highlights the superior separation by CEC as compared to non-aqueous CE where, by a mere qualitative overlay of electropherograms, the lack of reproducibility becomes obvious. A comparison with aqueous CE (not shown here) resulted in similar "non-reproducibilities". The literature certainly shows many recipes to enhance reproducibility not just by coating the capillary walls but also by applying an appropriate rinsing procedure (see Chapter 5). However, they are all accompanied by the side effect of time-consumption. The qualitative results presented here show that a high degree of reproducibility can be reached without applying a rinsing step.[131] Moreover, chromatography does contribute to the overall CEC separation as indicated by the separation of thiourea and caffeine, both of which are neutral compounds at pH 10.0 (unlike ibuprofen which is charged negatively at this pH, see Appendix II, p.184). Consequently, due to the absence of any charges, the separation of thiourea and caffeine cannot be accomplished in either aqueous or non-aqueous CE. The role of chromatography becomes less evident in the case of ibuprofen, though, as can be seen in the following figure showing the relation between capacity factor and ACN content in the mobile phase for ibuprofen:

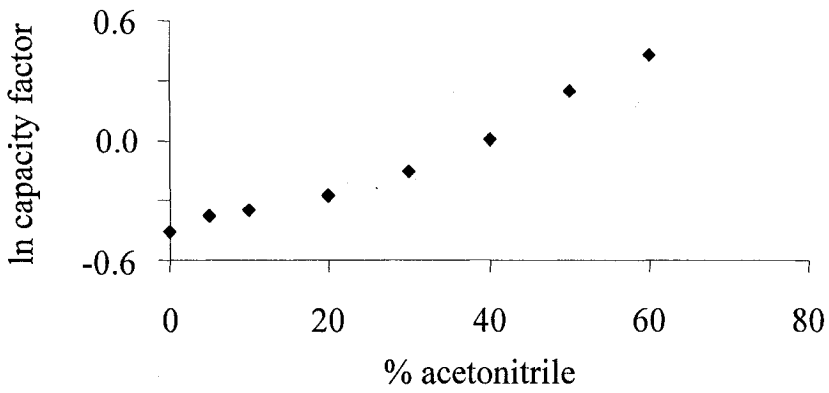

Figure 6.5: Plot of ln capacity factor for ibuprofen versus percentage ACN in mobile phase, with 5 mM pH 10.0 borate buffer accounting for the remaining percent (V/V). Thiourea served as unretained marker to determine the EOF and calculate the capacity factors according to Equation 4.1 (p.82). All other parameters and conditions were kept identical to the ones described for Figure 6.4 (p.158).

Similar to the separation of model proteins it can be stated that the capacity factor serves as a peak locator and does not allow a final conclusion whether electrophoresis or chromatography is the dominant driving force in this separation (although denaturation definitively does not play a role for ibuprofen, thus strengthening the potential dominance of electrophoresis). The plot testifies that the complex behavior observed earlier for the separation of model proteins (see Chapter 5) can also be found for the separation of small analytes provided they are charged. Interestingly, raising the percentage of ACN in the mobile phase reverses the order of elution between ibuprofen and albumin (not shown here). This reversal might not be solely attributed to either chromatography or electrophoresis but again to denaturation of albumin at elevated ACN content. Unfortunately, increasing the percentage organic solvent in the mobile phase is of limited

practical use since precipitation of the proteins takes place at higher percentages of ACN (unless, of course, this is the desired effect).

Naturally, chromatography should be the only contributing separation mechanism if ibuprofen is neutral. The following picture shows the separation of three NSA and caffeine under acidic conditions:

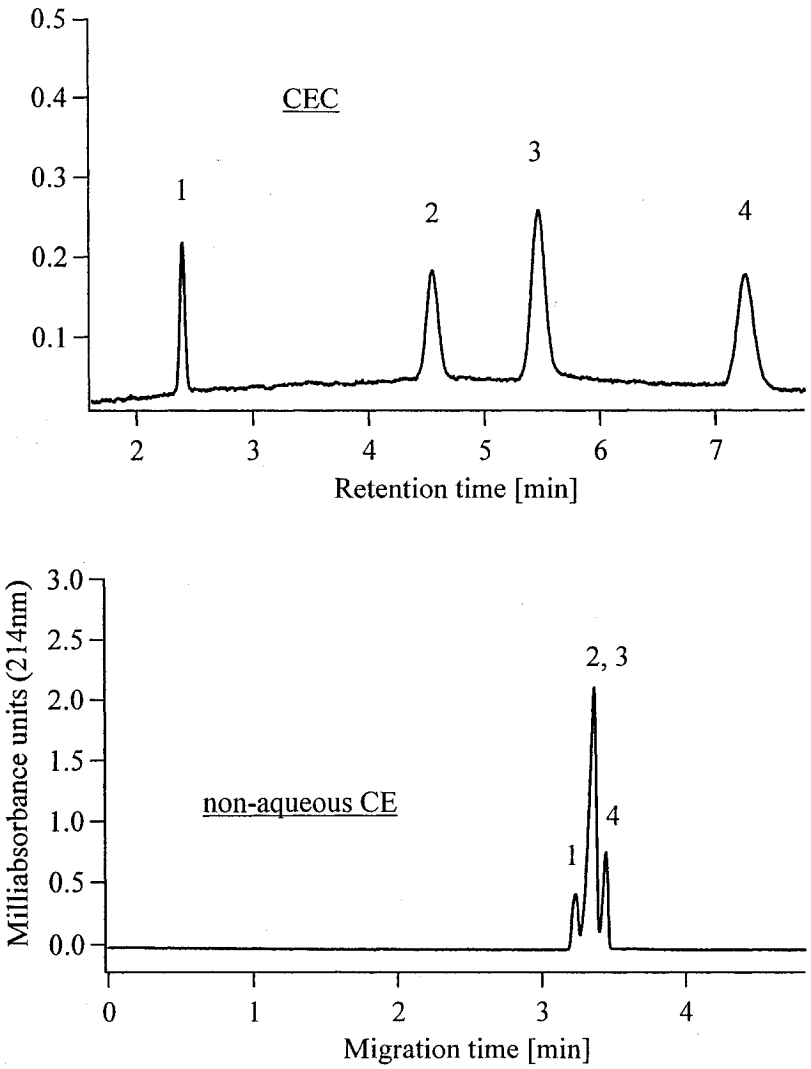

Figure 6.6: Separation of three non-steroidal anti-inflammatory drugs and caffeine by CEC and non-aqueous CE. In CEC the peaks eluted in the following order: caffeine (1) 101 μg/mL, ketoprofen (2) 176 μg/mL, naproxen (3) 87 μg/mL and ibuprofen (4) 245 μg/mL. In non-aqueous CE, the elution order was: caffeine (1), ibuprofen (2), naproxen (3) ketoprofen (4) (same concentrations as in CEC). The mobile phase consisted of 50% ACN / 50% 5 mM pH 3.8 acetate buffer (V/V) in both cases. Separation was carried out at 10 KV for CEC and 11.5 KV for non-aqueous CE, respectively. Sample injection lasted 5 s at 1 KV in both cases. Number of theoretical plates for CEC: caffeine (66,000 N/m), ketoprofen (42,000 N/m), naproxen (39,000 N/m) and ibuprofen (55,000 N/m).

The separation was preformed using acidic conditions in order to prevent deprotonation of the NSA (refer to Appendix II, p.184, for their structures and pK_A-values). The electrochromatogram proves chromatography to be the driving force under acidic conditions since the separation cannot be accomplished by electrophoresis alone.

6.4 Human amniotic fluid and bovine milk

Two additional separations illustrated in this work deal with rather complex biofluids: bovine milk proteins and components of human amniotic fluid. Their separation by CEC is depicted in the last figure of this thesis:

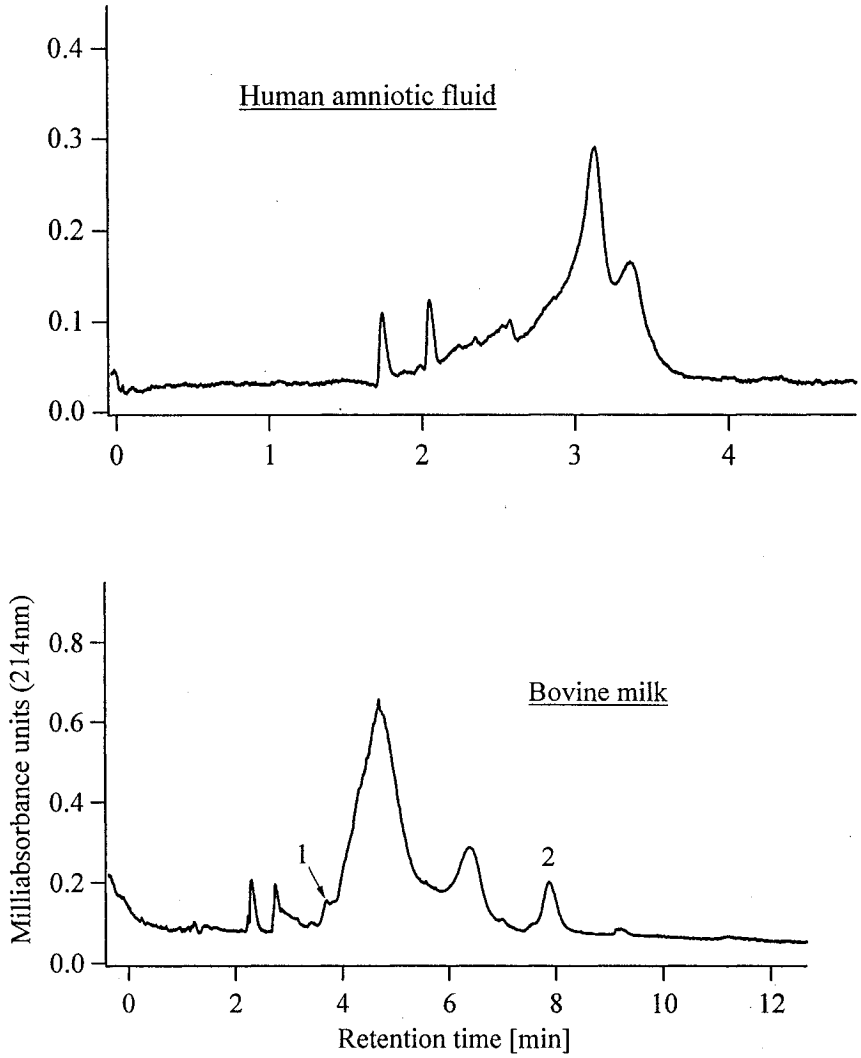

Figure 6.7: Separation of amniotic fluid (upper electrochromatogram), and bovine milk (lower electrochromatogram) by CEC. Peaks in the amniotic fluid sample have yet to be identified. Peaks in the milk sample were identified through spiking by Mrs. Marie-Eve Beaudoin as follows: β-casein (1) and α-lactalbumin (2).The mobile phase consisted of 10% ACN / 90% 5 mM pH 10.0 borate buffer (V/V) in the case of amniotic fluid and of 50% ACN / 50% 5 mM pH 10.0 borate buffer (V/V) for the milk. Separations were carried out at 10 KV with the injection performed for 10 s at 2 KV for the amniotic fluid and 5 s at 2 KV for the milk. The monolith length was 18.1 cm in both cases; total length was 30.9 cm for the amniotic fluid and 38.0 cm for the milk. Prior to injection, the amniotic fluid was diluted 1:1 in the respective mobile phase. The milk was diluted 1:10, also in mobile phase. No further pretreatment, i.e., centrifugation or filtration, was carried out.

Independent from their preliminary nature, the two separations demonstrate the potential for rapid analysis of complex biofluids by CEC. Naturally, further method development has to ensue in order to achieve better resolution between the analytes, especially in the case of milk where established HPLC-based separations achieve baseline separation of all six major bovine milk proteins, albeit within 40 min.[199] Work done by another CHEM450 student, Mrs. Marie-Eve Beaudoin, who was co-supervised by the author of this thesis, showed the milk separations usually to be highly reproducible for up to four runs when using raw milk ("fresh from the cow").[200] This is impressive considering that no filtration or centrifugation step was carried out prior to injection. Here, the first few millimeters of the monolith most probably act as a physical filter. The most recent (and so far only) CE-based method for amniotic fluid accomplishes separation of eight analytes within approximately eight minutes.[201] The CEC separation shown here has not reached the same quality yet but should allow for improved compatibility for MS detection due to the lower ionic strength of the mobile phase. Thus, interfacing CEC to a MS will be an indispensable part of future work as well due to its unique potential to provide both structural and quantitative information which is of particular importance for a case like amniotic fluid where many components have yet to be identified.

Summarizing the insights gained in this chapter it can be stated that there are numerous possible applications for this particular monolith in CEC that cannot be conducted using either aqueous or non-aqueous CE. This fulfills a more general demand requested from every separation technique which is the need to be applicable for various, highly diverse separation problems.

Chapter 7: Conclusions and Outlook

Discouraged by the technical difficulties when using microparticulate stationary phase and polymer frits for both the capillary and the chip format the presented work described generation, characterization and various applications of an alternative, i.e., a photopolymerized monolithic stationary phase. Its successful incorporation in both the capillary- and the chip format was accomplished. Applications in the chip format were limited due to low UV-transparency and high costs of the glass chips. Due to the relatively low number of fluorescent analytes and in order to avoid derivatization chemistry, future work in this respect should aim on the use of quartz chips which are UV-transparent. The use of UV-lasers (e.g., A KrF-laser to detect aromatic moieties at around 248 nm [138]) should compensate for the short optical pathlengths encountered. An alternative detection method would be MS.

The monolith was characterized through the separation of PAHs confirming its ability to separate neutral compounds based on chromatography and independent from the field strength applied. The latter factor indicates high mass transfer rates typically found in monoliths, possibly due to the absence of stagnant mobile phase. Electrical and hydrodynamic measurements (i.e., conductivity and resistance to flow) to obtain information on pore size and tortuosity followed. The porosity lies below the values reported for other monoliths. Changing the composition of the polymerization mixture might help to increase the porosity and enhance mass transfer further. A comparison between SEM and AFM imaging showed the latter one being more suitable for visualizing mesopores abundant in the polymer. AFM studies that image the monolith in

its "natural" environment, i.e., the respective mobile phase, should complement this line of research.[198] Intensive characterization of the EOF dependence on a variety of variables was conducted permitting a certain degree of predictability for future separations that vary these variables. UV-transparent capillaries were investigated in terms of waveguide effect and cutting techniques. Additional experiments will have to compare these capillaries to polyimide-coated ones regarding heat-transfer characteristics and stability in different solvents. Recipes were presented for removal of sporadically occurring gas bubbles without having to resort to high pressure flushing, findings that will be of profound importance for CEC in the chip format.

Based on its C_4-moiety, the separation power of the polymer was characterized using model proteins. The methodology was compared to aqueous- and non-aqueous CE as well as μ-HPLC. The contribution of a chromatographic mechanism to the separations of these model proteins remains debatable since μ-HPLC could not separate the selected analytes. Reasons for the different elution profile when compared to aqueous CE might rather be caused by denaturation stemming from differences in mobile phase composition, as was confirmed by CD spectroscopy. Inter- and intra-capillary reproducibilities indicated a reproducible manufacturing process as well as reproducible separations that were improved by introducing a rinsing procedure. Future work should attempt to shed more light on the interplay between chromatography and electrophoresis by testing additional model analytes. The chromatographic contribution could also be enhanced if a potentially more suitable monolithic stationary phase was created by incorporating other functionalities, e.g., diol groups or longer alkyl chains. If interaction between model proteins and stationary phase is diminished due to size restrictions, then

changing the porosity of the polymer might be an option to enhance chromatography. The potential of separating proteins based on ion-exchange chromatography through use of the sulfonate moiety could be exploited as well.

Lastly, several potential applications of the monolith were shown ranging from monitoring synthesis products and oligonucleotides to the separation of smaller molecules in media of varying complexity. In all applications, CEC proved to be advantageous in comparison to both aqueous and non-aqueous CE. Also, since oligonucleotides are charged analytes, their separation proves that the monolith is principally capable of separating charged analytes and not only neutral ones. Even in the absence of a chromatographic contribution to the separation of some analytes, a better reproducibility in a complex matrix like serum could be accomplished by CEC, probably caused by diminished adsorption of proteins to the stationary phase. Attempting to transfer some of these applications into the chip format is one potential future project. Comparison of CEC with alternative modes of CE, e.g., Micellar Electrokinetic Chromatography or CE using coated capillaries, is another aspect of future work. CEC regarding "real" samples in more complex matrices appears promising as demonstrated by the separations of human amniotic fluid and bovine milk.

References

(1) Pretorius, V.; Hopkins, B. J.; Schieke, J. D. *Journal of Chromatography* **1974**, *99*, 23-30.

(2) Jorgenson, J. W.; DeArman Lukacs, K. *Journal of Chromatography* **1981**, *218*, 209-216.

(3) Knox, J. H.; Grant, I. H. *Chromatographia* **1987**, *24*, 135-143.

(4) Knox, J. H.; Grant, I. H. *Chromatographia* **1991**, *32*, 317-328.

(5) Mistry, K.; Krull, I. S.; Grinberg, N. *Journal of Separation Science* **2002**, *25*, 935-958.

(6) Zhang, S.; Huang, X.; Zhang, J.; Horváth, C. *Journal of Chromatography A* **2000**, *887*, 465-477.

(7) Liu, Z.; Otsuka, K.; Terabe, S. *Journal of Chromatography A* **2002**, *965*, 241-253.

(8) Harris, D. C. *Quantitative Chemical Analysis*, Fifth ed.; W.H. Freeman and Company: New York, 1999.

(9) Legido-Quigley, C.; Marlin, N. D.; Melin, V.; Manz, A.; Smith, N. W. *Electrophoresis* **2003**, *24*, 917-944.

(10) Landers, J. P. *Handbook of Capillary Electrophoresis*, Second ed.; CRC Press: Boca Raton, 1997.

(11) Colón, L. A.; Maloney, T. D.; Fermier, A. M. *Journal of Chromatography A* **2000**, *887*, 43-53.

(12) Effenhauser, C. S.; Bruin, G. J. M.; Paulus, A. *Electrophoresis* **1997**, *18*, 2203-2213.

(13) Bowser, M. T.; Bebault, G. M.; Peng, X.; Chen, D. D. Y. *Electrophoresis* **1997**, *18*, 2928-2934.

(14) Basak, S. K.; Velayudhan, A.; Kohlmann, K.; Ladisch, M. R. *Journal of Chromatography A* **1995**, *707*, 69-76.

(15) Ocvirk, G.; Verpoorte, E.; Manz, A.; Grasserbauer, M.; Widmer, H. M. *Analytical Methods and Instrumentation* **1995**, *2*, 74-82.

(16) He, B.; Tait, N.; Regnier, F. *Analytical Chemistry* **1998**, *70*, 3790-3797.

(17) Ericson, C.; Hjertén, S. *Analytical Chemistry* **1999**, *71*, 1621-1627.

(18) Oleschuk, R. D.; Shultz-Lockyear, L. L.; Ning, Y.; Harrison, D. J. *Analytical Chemistry* **2000**, *72*, 585-590.

(19) Ceriotti, L.; Verpoorte, E.; de Rooji, N. F. in *Micro Total Analysis Systems 2000;* J.M. Ramsey, A. van den Berg, Eds.; Kluwer Academic Publishers: Dordrecht, The Netherlands 2000.

(20) Morishima, K.; Dulay, M. T.; Benett, B. D.; Wheeler, A. R.; Quirino, J. P.; Zare, R. N. in *Micro Total Analysis Systems 2001;* J.M. Ramsey, A. van den Berg, Eds.; Kluwer Academic Publishers: Dordrecht, The Netherlands 2001.

(21) Penner, N. A.; Slentz, B. E.; Regnier, F. in *Micro Total Analysis Systems 2001;* J.M. Ramsey, A. van den Berg, Eds.; Kluwer Academic Publishers: Dordrecht, The Netherlands 2001.

(22) Harrison, D. J.; Fan, Z. H.; Seiler, K.; Manz, A.; Widmer, H. M. *Analytica Chimica Acta* **1993**, *283*, 361-366.

(23) McDonald, J. C.; Duffy, D. C.; Anderson, J. R.; Chiu, D. T.; Wu, H.; Schueller, O. J. A.; Whitesides, G. M. *Electrophoresis* **2000**, *21*, 27-40.

(24) Corman, T.; Enoksson, P.; Stemme, G. *Journal of Micromechanical Microengineering* **1998**, *8*, 84-87.

(25) Harrison, J. D.; Fluri, K.; Seiler, K.; Fan, Z.; Effenhauser, C. S.; Manz, A. *Science* **1993**, *261*, 895-897.

(26) Haswell, S. J. *Analyst* **1997**, *122*, 1R-10R.

(27) Freemantle, M. *Chemical and Engineering News* **1999**, 27-36.

(28) Jeong, Y.; Kim, S.; Chun, K.; Chang, J.; Chung, D. S. *Lab on a Chip* **2001**, *1*, 143-147.

(29) Svec, F.; Peters, E. C.; Sýkora, D.; Yu, C.; Fréchet, J. M. J. *Journal of High Resolution Chromatography* **2000**, *23*, 3-18.

(30) Jacobson, S. C.; Hergenröder, R.; Moore, A. W.; Ramsey, J. M. *Analytical Chemistry* **1994**, *66*, 4127-4132.

(31) Pesek, J. J.; Matyska, M. T.; Mauskar, L. *Journal of Chromatography A* **1997**, *763*, 307-314.

(32) Kutter, J. P.; Jacobson, S. C.; Matsubara, N.; Ramsey, J. M. *Analytical Chemistry* **1998**, *70*, 3291-3297.

(33) Pesek, J. J.; Matyska, M. T.; Swedberg, S.; Udivar, S. *Electrophoresis* **1999**, *20*, 2343-2348.

(34) Huang, X.; Zhang, J.; Horváth, C. *Journal of Chromatography A* **1999**, *858*, 91-101.

(35) Whitehead, R.; Rice, C. L. *Journal of Physical Chemistry* **1965**, *69*, 4017-4024.

(36) Harrison, D. J.; Fluri, K.; Seiler, K.; Fan, Z. H.; Effenhauser, C. S.; Manz, A. *Science* **1993**, *261*, 895-897.

(37) Atkins, P. W. *Physical Chemistry*, Fifth ed.; W.F. Freeman and Company: New York, 1994.

(38) Foret, F.; Křivánková, L.; Boček, P. In *Electrophoresis Library*; Radola, B. J., Ed.; VCH Verlagsgesellschaft: Weinheim, 1993.

(39) Laidler, K. J.; Meiser, J. H. *Physical Chemistry*, Second ed.; Houghton Mifflin Company: Boston, 1995.

(40) Dukhin, A. S.; Goetz, P. J. *Ultrasound for Characterizing Colloids*; Elsevier: Amsterdam, 2002.

(41) Schwer, C.; Kenndler, E. *Analytical Chemistry* **1991**, *63*, 1801-1807.

(42) Whitaker, K. W.; Sepaniak, M. J. *Electrophoresis* **1994**, *15*, 1341-1345.

(43) Wright, P. B.; Lister, A. S.; Dorsey, J. G. *Analytical Chemistry* **1997**, *69*, 3251-3259.

(44) Riekkola, M. L. *Electrophoresis* **2002**, *23*, 3865-3883.

(45) Grob, M.; Steiner, F. *Electrophoresis* **2002**, *23*, 1853-1861.

(46) Fujimoto, C.; Fujise, Y.; Matsuzawa, E. *Analytical Chemistry* **1996**, *68*, 2753-2757.

(47) Dittmann, M. M.; Rozing, G. P. *Journal of Microcolumn Separations* **1997**, *9*, 399-408.

(48) Wan, Q. H. *Journal of Chromatography A* **1997**, *782*, 181-189.

(49) Wan, Q. H. *Analytical Chemistry* **1997**, *69*, 361-363.

(50) Patankar, N. A.; Hu, H. H. *Analytical Chemistry* **1998**, *70*, 1870-1881.

(51) Rathore, A. S.; Wen, E.; Horváth, C. *Analytical Chemistry* **1999**, *71*, 2633-2641.

(52) Cunnings, E. B.; Griffiths, S. K.; Nilson, R. H.; Paul, P. H. *Analytical Chemistry* **2000**, *72*, 2526-2532.

(53) Tallarek, U.; Rapp, E.; Scheenen, T.; Bayer, E.; Van As, H. *Analytical Chemistry* **2000**, *72*, 2292-2301.

(54) Bartle, K. D.; Myers, P. *Journal of Chromatography A*- **2001**, *916*, 3-23.

(55) Gusev, I.; Horváth, C. *Journal of Chromatography A* **2002**, *948*, 203-223.

(56) Breadmore, M. C.; Shrinivasan, S.; Wolfe, K. A.; Power, M. E.; Ferrance, J. P.; Hosticka, B.; Norris, P. M.; Landers, J. P. *Electrophoresis* **2002**, *23*, 3487-3495.

(57) Liao, J. L.; Chen, N.; Ericson, C.; Hjertén, S. *Analytical Chemistry* **1996**, *68*, 3468-3472.

(58) Huang, X.; Zhang, J.; Horváth, C. *Journal of Chromatography A* **1999**, *1999*, 91-101.

(59) Yu, C.; Xu, M.; Svec, F.; Fréchet, J. M. J. *Journal of Polymer Science: Part A: Polymer Chemistry* **2002**, *40*, 755-769.

(60) Wu, R.; Zou, H.; Fu, H.; Jin, W.; Ye, M. *Electrophoresis* **2002**, *23*, 1239-1245.

(61) Yan, W. Y.; Zhang, Z. C.; Gao, R. Y.; Yan, C.; Qin-Sun, W. *Journal of Liquid Chromatography and Related Technologies* **2002**, *25*, 2965-2976.

(62) Gusev, I.; Huang, X.; Horváth, C. *Journal of Chromatography A* **1999**, *855*, 273-290.

(63) Karger, B. L.; Snyder, L. R.; Horváth, C. *An Introduction to Separation Science*; John Wiley & Sons: New York, 1973.

(64) Xiang, R.; Horváth, C. *Analytical Chemistry* **2002**, *74*, 762-770.

(65) Smith, N. W.; Evans, M. B. *Chromatographia* **1995**, *41*, 197-203.

(66) Svec, F.; Peters, E. C.; Sýkora, D.; Fréchet, J. M. J. *Journal of Chromatography A* **2000**, *887*, 3-29.

(67) Colón, L. A.; Guo, Y.; Fermier, A. *Analytical Chemistry News & Features* **1997**, 461A-467A.

(68) Poppe, H.; Stol, R.; Kok, W. T. *Journal of Chromatography A* **2002**, *965*, 75-82.

(69) Grimes, B. A.; Lüdtke, S.; Unger, K. K.; Liapis, A. I. *Journal of Chromatography A* **2002**, *979*, 447-466.

(70) Petersen, N. J.; Mogensen, K. B.; Kutter, J. P. *Electrophoresis* **2002**, *23*, 3528-3536.

(71) Horváth, C.; Lin, H. J. *Journal of Chromatography* **1976**, *126*, 401-406.

(72) Horváth, C.; Lin, H. J. *Journal of Chromatography* **1978**, *149*, 43-48.

(73) Dittmann, M. M.; Wienand, K.; Bek, F.; Rozing, G. P. *LC-GC* **1995**, *13*, 802-814.

(74) Dittmann, M. M.; Rozing, G. P. *Journal of Chromatography A* **1996**, *744*, 63-74.

(75) Giddings, I. C. *The Dynamics of Chromatography*; Marcel Dekker, New York 1965.

(76) Dadoo, R.; Yan, C.; Zare, R. N.; Anex, D. S.; Rakestraw, D. J.; Hux, G. A. *LCGC* **1997**, *15*, 630-635.

(77) Angus, P. D. A.; Demarest, C. W.; Catalano, T.; Stobaugh, J. F. *Electrophoresis* **1999**, *20*, 2349-2359.

(78) Wen, E.; Asiaie, C.; Horváth, C. *Journal of Chromatography A* **1999**, *855*, 349-366.

(79) Josic, D.; Buchacher, A.; Jungbauer, A. *Journal of Chromatography B* **2001**, *752*, 191-205.

(80) Sternberg, J. C. *Advances in Chromatography* **1966**, *2*, 65.

(81) Pyell, U.; Rebscher, H.; Banholczer, A. *Journal of Chromatography A* **1997**, *779*, 155-163.

(82) Dadoo, R.; Zare, R. N.; Yan, C.; Anex, D. S. *Analytical Chemistry* **1998**, *70*, 4787-4792.

(83) Kitagawa, S.; Tsuda, T. *Journal of Microcolumn Separations* **1994**, *6*, 91-96.

(84) Boughtflower, R. J.; Underwood, T.; Paterson, C. J. *Chromatographia* **1995**, *40*, 329-335.

(85) van den Bosch, S. E.; Heemstra, S.; Kraak, J. C.; Poppe, H. *Journal of Chromatography A* **1996**, *755*, 165-177.

(86) Miyawa, J. H.; Alasandro, M. S. *LC-GC* **1998**, *16*, 36-41.

(87) Colón, L. A.; Reynolds, K. J.; Alicea-Maldonado, R.; Fermier, A. M. *Electrophoresis* **1997**, *18*, 2162-2174.

(88) Yan, C.; US Pat. 5 453 163 (26 September 1995).

(89) Fermier, A. M.; Colón, L. A. *Journal of Microcolumn Separations* **1998**, *10*, 439-444.

(90) Stol, R.; Mazereeuw, M.; Tjaden, U. R.; van der Greef, J. *Journal of Chromatography A* **2000**, *873*, 293-298.

(91) Altria, K. D.; Grant, I. *LCGC* **1998**, *16*, 560-564.

(92) Carney, R. A.; Robson, M. M.; Bartle, K. D.; Myers, P. *Journal of High Resolution Chromatography* **1999**, *22*, 29-32.

(93) Bogaert, M.; Chem 419 Report, Department of Chemistry and Biochemistry, Concordia University: Montreal, 2000.

(94) Chen, J.-R.; Dulay, M. T.; Zare, R. N.; Svec, F.; Peters, E. *Analytical Chemistry* **2000**, *72*, 1224-1227.

(95) Wang, Q. C.; Svec, F.; Fréchet, J. M. J. *Analytical Chemistry* **1993**, *65*, 2243-2248.

(96) Fujimoto, C.; Kino, J.; Sawada, H. *Journal of Chromatography A* **1995**, *716*, 107-113.

(97) Svec, F.; Fréchet, J. M. J. *Journal of Molecular Recognition* **1996**, *9*, 326-334.

(98) Palm, A.; Novotny, M. V. *Analytical Chemistry* **1997**, *69*, 4499-4507.

(99) Xie, S.; Allington, R. W.; Svec, F.; Fréchet, J. M. J. *Journal of Chromatography A* **1999**, *865*, 169-174.

(100) Chirica, G. S.; Remcho, V. T. *Analytical Chemistry* **2000**, *72*, 3605-3610.

(101) Buchmeiser, M. R. *Journal of Chromatography A* **2001**, *918*, 233-266.

(102) Hoegger, D.; Freitag, R. *Journal of Chromatography A* **2001**, *914*, 211-222.

(103) Sun, X.; Chai, Z. *Journal of Chromatography A* **2002**, *943*, 209-218.

(104) Kato, M.; Sakai-Kato, K.; Matsumoto, N.; Toyo'oka, T. *Analytical Chemistry* **2002**, *74*, 1915-1921.

(105) Kornyšova, O.; Šurna, R.; Snitka, V.; Pyell, U.; Maruška, A. *Journal of Chromatography* **2002**, *971*, 225-235.

(106) Unger, K. K.; Bidlingmaier, B.; du Fresne von Hohenesche, C.; Lubda, D. in *Characterization of porous solids VI*; F. Rodriguez-Reinoso, B. M., J. Rouquerol, K.K. Unger, Eds.; Elsevier: Amsterdam, 2002; Vol. 144, pp 155-122.

(107) Lee, D. P. *Journal of Chromatography* **1988**, *443*, 143-153.

(108) Hjertén, S.; Li, Y. M.; Liao, J. L.; Mohammad, J.; Nakazato, K.; Petterson, G. *Nature* **1992**, *356*, 810-811.

(109) Tanaka, N.; Nagayama, H.; Kobayashi, H.; Ikegami, T.; Hosoya, K.; Ishizuka, N.; Minakuchi, H.; Nakanishi, K.; Cabrera, K.; Lubda, D. *Journal of High Resolution Chromatography* **2000**, *23*, 111-116.

(110) Viklund, C.; Pontén, E.; Glad, B.; Irgum, K.; Hörstedt, P.; Svec, F. *Chemistry of Materials* **1997**, *9*, 463-471.

(111) Ngola, S. M.; Fintschenko, Y.; Choi, W. Y.; Shepodd, T. J. *Analytical Chemistry* **2001**, *73*, 849-856.

(112) Zhang, S.; Zhang, J.; Horváth, C. *Journal of Chromatography A* **2001**, *914*, 189-200.

(113) Cabral, J. L.; personal communication with Polymicro Technologies, 2003.

(114) Fouassier, J. P. *Photoinitiation, Photopolymerization and Photocuring*; Carl Hanser Verlag: New York, Vienna, Munich, 1995.

(115) Yu, C.; Svec, F.; Fréchet, J. M. J. *Electrophoresis* **2000**, *21*, 120-127.

(116) Bandilla, D.; Skinner, C. D. *Journal of Chromatography A* **2003**, *1004*, 167-179.

(117) Carson, R.; Chem 450 Report, Department of Chemistry and Biochemistry, Concordia University: Montreal, 2001.

(118) Bandilla, D.; Skinner, C. D., Poster presentation at 84th CSC Conference, Montreal, May 26th-30th, 2001.

(119) Heine, H. G. *Tetrahedron Letters* **1972**, *47*, 4755.

(120) Hinckley, J. O. N. *Journal of Chromatography* **1975**, *109*, 209-217.

(121) Grushka, E.; McCormick, R. M.; Kirkland, J. J. *Analytical Chemistry* **1989**, *61*, 241-246.

(122) McAdams, W. H. *Heat transmission*, Third ed.; McGraw-Hill Book Company: New York, 1954.

(123) Bello, M. S.; Righetti, P. G. *Journal of Chromatography* **1992**, *606*, 95-102.

(124) Chen, L.; Chen, L.; Yan, X.; Wan, Q. H. *Journal of Chromatography A* **2003**, *986*, 297-302.

(125) Majors, R. E. *LCGC* **1998**, *16*, 96-106.

(126) Rapp, T. L.; Morris, M. D. *Analytical Chemistry* **1996**, *68*, 4446-4450.

(127) Fan, Z. H.; Harrison, D. J. *Analytical Chemistry* **1994**, *66*, 177-184.

(128) Effenhauser, C. S.; Manz, A.; Widmer, H. M. *Analytical Chemistry* **1993**, *65*, 2637-2642.

(129) Biondi, S. A.; Wolk, J. A.; Kopf-Sill, A. R. in *Micro Total Analysis Systems 2001;* J.M. Ramsey, A. van den Berg, Eds.; Kluwer Academic Publishers: Dordrecht, The Netherlands 2001.

(130) Nilsson, S.; Santesson, S.; Degerman, E.; Johansson, T.; Laurell, T.; Nilsson, J.; Johansson, J. in *Micro Total Analysis Systems 2000;* J.M. Ramsey, A. van den Berg, Eds.; Kluwer Academic Publishers: Dordrecht, The Netherlands 2000.

(131) Kunkel, A.; Wätzig, H. *Electrophoresis* **1999**, 2379-2389.

(132) Terry, S. C. Dissertation, Stanford University, 1975.

(133) Ericson, C.; Holm, J.; Ericson, T.; Hjertén, S. *Analytical Chemistry* **2000**, *72*, 81-87.

(134) Finot, M.; Jemere, A. B.; Oleschuk, R. D.; Takahashi, L.; Harrison, D. J. in *Micro Total Analysis Systems 2001;* J.M. Ramsey, A. van den Berg, Eds.; Kluwer Academic Publishers: Dordrecht, The Netherlands 2001.

(135) Singh, A. K.; Throckmorton, D. J.; Shepodd, T. J. in *Micro Total Analysis Systems 2001;* J.M. Ramsey, A. van den Berg, Eds.; Kluwer Academic Publishers: Dordrecht, The Netherlands 2001.

(136) Ceriotti, L.; de Rooij, N. F.; Verpoorte, E. *Analytical Chemistry* **2002**, *74*, 639-647.

(137) Végvári, A.; Hjertén, S. *Electrophoresis* **2002**, *23*, 3479-3486.

(138) Ingle, J. D.; Crouch, S. R. *Spectrochemical Analysis*; Prentice-Hall: Upper Saddle River, New Jersey, 1988.

(139) Que, A. H.; Mechref, Y.; Huang, Y.; Taraszka, J. A.; Clemmer, D. E.; Novotny, M. V. *Analytical Chemistry* **2003**, *75*, 1684-1690.

(140) Bings, N. H.; Wang, C.; Skinner, C. D.; Colyer, C. L.; Thibault, P.; Harrison, D. J. *Analytical Chemistry* **1999**, *71*, 3292-3296.

(141) Kelly, M. A.; Altria, K. D.; Clark, B. J. *Journal of Chromatography A* **1997**, *768*, 73-80.

(142) Wätzig, H.; Dette, C. *Journal of Chromatography* **1993**, *636*, 31-38.

(143) Morrison, R. D.; Dolan, J. W. *LCGC* **2000**, *18,* 936-939.

(144) Fessenden, F. *Organic Chemistry*; Wadsworth: Belmont, California, 1986.

(145) Mant, C. T.; Hodges, R. S. *High-Performance Liquid Chromatography of Peptides and Proteins: Separation, Analysis and Conformation*; CRC Press: Boca Raton, Florida, 1991.

(146) Lister, A. S.; Dorsey, J. G.; Burton, D. E. *Journal of High Resolution Chromatography* **1997**, *20*, 523-528.

(147) http://scooter.cyto.purdue.edu/pucl_cd/flow/vol4/1_email/05951195/0335.htm.

(148) Bablekis, V.; Chem419 Report, Department of Chemistry and Biochemistry, Concordia University: Montreal, 2001.

(149) Rathore, A. S.; Horváth, C. *Electrophoresis* **2002**, *23*, 1211-1216.

(150) Cantwell, F.; Chem421 Manuscript, University of Alberta: Edmonton, Canada, 1996.

(151) Chen, L.; Chen, L.; Yan, X.; Want, Q. H. *Analytical Chemistry* **2002**, *74*, 5157-5159.

(152) Al-Bokari, M.; Cherrak, D.; Guiochon, G. *Journal of Chromatography A* **2002**, *975*, 275-284.

(153) Vander Heyden, Y.; Popovici, S. T.; Schoenmakers, P. J. *Journal of Chromatography A* **2002**, *957*, 127-137.

(154) Hansma, P. K.; Elings, V. B.; Marti, O.; Bracker, C. E. *Science* **1988**, *242*, 209-216.

(155) Pullen, P. E.; Pesek, J. J.; Matyska, M. T.; Frommer, J. *Analytical Chemistry* **2000**, *72*, 2751-2757.

(156) Knaupp, S.; Wätzig, H. *Journal of Chromatography A* **1997**, *781*, 55-65.

(157) Cifuentes, A.; Díez-Masa, J. C.; Fritz, J.; Anselmetti, D.; Bruno, A. E. *Analytical Chemistry* **1998**, *70*, 3458-3462.

(158) Bedair, M.; El Rassi, Z. *Electrophoresis* **2002**, *23*, 2938-2948.

(159) Seifar, R. M.; Heemstra, S.; Kok, W. T.; Kraak, J. C.; Poppe, H. *Journal of Microcolumn Separations* **1998**, *10*, 41-49.

(160) Tindall, G. W. *LCGC* **2002**, *20*, 1114-1118.

(161) http://www.bi.umist.ac.uk/users/mjfrbn/buffers/Makebuf.asp.

(162) Tindall, G. W. *LCGC* **2003**, *21*, 28-32.

(163) Tindall, G. W. *LCGC* **2002**, *20*, 1028-1032.

(164) Schneider, P. J.; Engelhardt, H. *Journal of Chromatography A* **1998**, *802*, 17-22.

(165) Schneider, P. J.; Engelhardt, H. *CLB Chemie in Labor und Biotechnik* **1998**, *49*, 347-350.

(166) Wang, T.; Bruin, G. J.; Kraak, J. C.; Poppe, H. *Analytical Chemistry* **1991**.

(167) Wang, T.; Hartwick, R. A. *Analytical Chemistry* **1992**, *64*, 1745-1747.

(168) Bandilla, D.; Cabral, J. L.; Skinner, C. D. *Electrophoresis* **2004** *submitted.*

(169) Jiang, W.; Awasum, J. N.; Irgum, K. *Analytical Chemistry* **2003**, *75*, 2768-2774.

(170) Guttman, A.; Schwartz, H. E. *Analytical Chemistry* **1995**, *67*, 2279-2283.

(171) Rozing, G. P. *American Laboratory* **1998**, *30*, 33.

(172) Geijels, V. L. J. *American Laboratory* **2002**, *34*, 9-10.

(173) White, A.; Handler, P.; Smith, E. L.; Hill, R. L.; Lehman, I. R. *Principles of Biochemistry*, Sixth ed.; McGraw-Hill: New York, 1978.

(174) http://xa.expasy.org.

(175) Bristow, A. W. T.; Bumfrey, T. J. *Chromatographia* **2002**, *55*, 321-325.

(176) Córdova, E.; Gao, J.; Whitesides, G. M. *Analytical Chemistry* **1997**, *69*, 1370-1379.

(177) Wätzig, H.; Degenhardt, M.; Kunkel, A. *Electrophoresis* **1998**, *19*, 2695-2572.

(178) Altria, K. D.; Fabre, H. *Chromatographia* **1995**, *40*, 313-319.

(179) Quirino, J. P.; Dulay, M. T.; Bennett, B. D.; Zare, R. N. *Analytical Chemistry* **2001**, *73*, 5539-5543.

(180) Zhang, Y.; Zhu, J.; Zhang, L.; Zhang, W. *Analytical Chemistry* **2000**, *72*, 5744-5747.

(181) Wätzig, H. *Journal of Chromatography A* **1995**, *700*, 1-7.

(182) Scopes, R. K. *Analytical Biochemistry* **1974**, *59*, 277-282.

(183) Kwakman, P. J. M.; Koelewijn, H.; Kool, I.; Brinkman, U. A. T.; De Jong, G. J. *Journal of Chromatography* **1990**, *511*, 155-166.

(184) Collins, G. E.; Rose-Pehrsson, S. L. *Analyst* **1994**, *119*, 1907-1913.

(185) Aminuddin, M.; Miller, J. N. *Talanta* **1995**, *42*, 775-778.

(186) Papachristou, Z.; Bandilla, D.; Banks, P. R.; Skinner, C. D. *Electrophoresis* **2004**, *submitted.*

(187) Mallouli, A.; Lepage, Y. *Synthesis* **1980**, *9*, 689.

(188) Swerdlow, H.; Wu, S. L.; Harke, H.; Dovichi, N. J. *Journal of Chromatography* **1990**, *516*, 61-67.

(189) Carrilho, E.; Ruiz-Martinez, M. C.; Berka, J.; Smirnov, I.; Goetzinger, W.; Miller, A. W.; Brady, D.; Karger, B. L. *Analytical Chemistry* **1996**, *68*, 3305-3313.

(190) Gilar, M. *Analytical Biochemistry* **2001**, *298*, 196-206.

(191) Sýkora, D.; Svec, F.; Fréchet, J. M. J. *Journal of Chromatography A* **1999**, *852*, 297-304.

(192) Zhang, M.; Yang, C.; El Rassi, Z. *Analytical Chemistry* **1999**, *71*, 3277-3282.

(193) Gensthaler, B. M. *Pharmazeutische Zeitung* **2002**, *51*.

(194) Wenzel, R. G.; Sarvis, C. A.; Krause, M. L. *Pharmacotherapy* **2003**, *23*, 494-505.

(195) De Rossi, A.; Desiderio., C. *Journal of Chromatography A* **2003**, *984*, 283-290.

(196) Lehninger, A. L.; Nelson, D. L.; Cox, M. M. *Principles of Biochemistry*, Second ed.; Worth Publishers: New York, 1993.

(197) Melanson, J. E.; Baryla, N. E.; Lucy, C. A. *Analytical Chemistry* **2000**, *72*, 4110-4114.

(198) Cabral, J. L.; Bandilla, D.; Skinner, C. D. *Analytical Chemistry* (**2003**) *submitted.*

(199) Bobe, G.; Beitz, D. C.; Freeman, A. E.; Lindberg, G. L. *Journal of Agriculture and Food Science* **1998**, *46*, 458-463.

(200) Beaudoin, M. E.; Chem 450 Report, Department of Chemistry and Biochemistry, Concordia University: Montreal, 2003.

(201) Stewart, C. J.; Iles, R. K.; Perrett, D. *Electrophoresis* **2001**, *22*, 1136-1142.

Appendix I: Design of the Confocal Microscope Used for Detection of Fluorescent Analytes in a Microfluidic Device

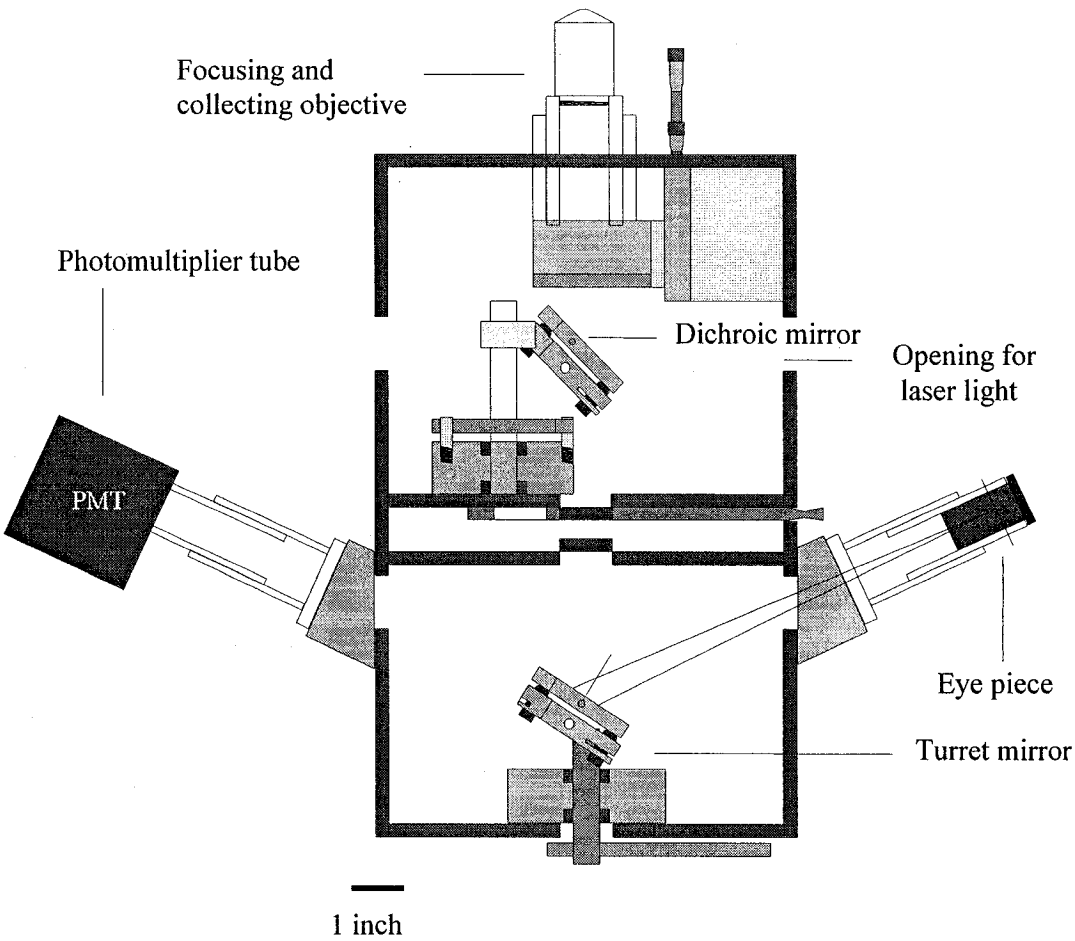

Figure AI.1: Design of the confocal microscope employed for the detection of fluorescent analytes in microfluidic devices.

The confocal microscope was designed by Dr. C. Skinner. Laser light is projected onto the dichroic mirror through the upper right opening and projected upwards on a microfluidic device on top of the objective (not shown here). Fluorescent light is collected at 180° angle, transmitted backwards through the dichroic mirror and onto the turret mirror where it is reflected either onto the PMT or onto the eyepiece.

Appendix II: Molecular Structures

A) Polyaromatic hydrocarbons

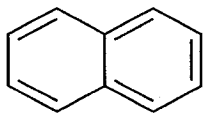

Naphthalene Mr 128.18

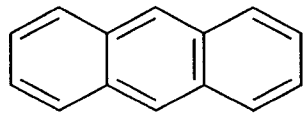

Anthracene Mr 178.24

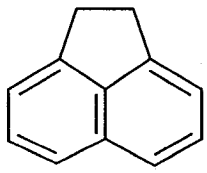

Acenaphthene Mr 154.21

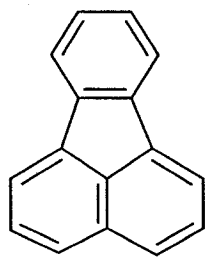

Fluoranthene Mr 202.26

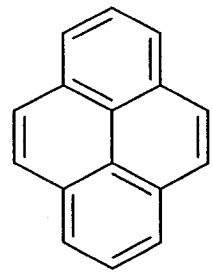

Pyrene Mr 202.26

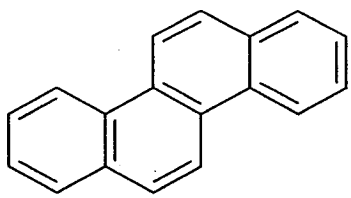

Chrysene Mr 228.29

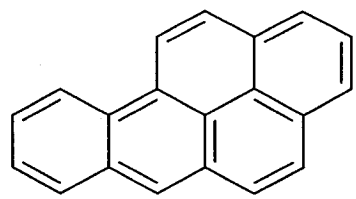

Benzo[a]pyrene Mr 252.32

2) Synthesis of anthracene-2,3-dialdehyde

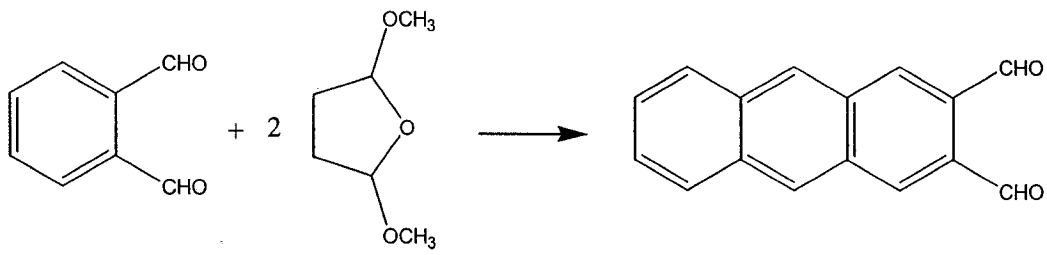

Benzene-1,2-dialdehyde 2,5-Dimethoxytetrahydrofuran Anthracene-2,3-dialdehyde (ADA)

The synthesis was carried by out Mrs. Erin Templeton according to the procedure published by Mallouli and Lepage.[187] Briefly, the reactants are dissolved and heated in acetic acid in the presence of pyridine under reflux for 24 h, resulting in orange crystals of ADA.

3) Sequences of oligonucleotides

PermHisTag1:

5' CCC CC ATG GGC CAC CAC CAC CAC CAC CAC GCT ATC CTC TCC AGT ATG TTC AAT CCT TCA CC 3'

D246E:

5' CGG CTG CAT CGT ATT TCT GCA GTC GAG CAC GAG CAG AAT ATG GCG 3'

4) Non-steroidal anti-inflammatory drugs

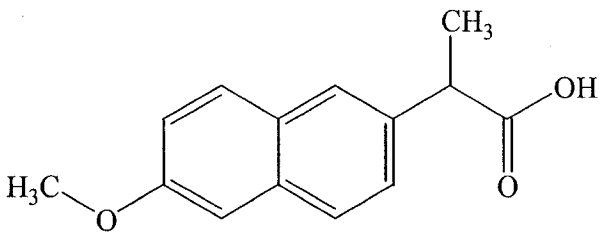

Naproxen $pK_A = 4.5$

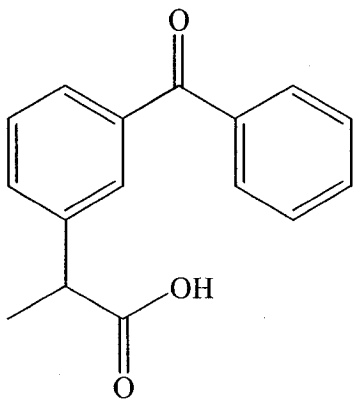

Ketoprofen $pK_A = 6.0$

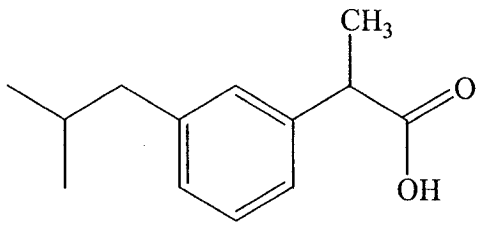

Ibuprofen $pK_A = 4.4$

5) Other reagents

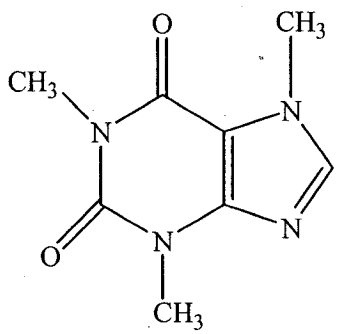

Caffeine

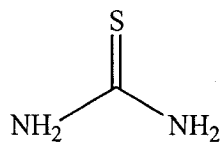

Thiourea

Appendix III: Comparison between CEC and CE: How to Choose the Appropriate Separation Voltage

In CEC, incorporation of a monolith results in non-uniform resistance across the capillary. The segment from the inlet end to the detector (containing the monolith) will naturally possess a higher resistance than the segment stretching from the detector to the outlet end. In order to permit a useful comparison with CE, where a uniform resistance occurs throughout the whole column, the electric field strength inside the monolith in CEC has to be known and approximately the same field strength applied to CE.

The field strength inside the monolith can be obtained by conceptualizing the capillary as two resistors in series (monolith and open section). By measuring the current of the whole capillary and then removing the non-packed section before recording the current again at the same voltage, both the resistance of the packed and the non-packed (open) section of the capillary are obtained. The voltage drop across the monolith is calculated by taking the difference between input and output voltage with the latter one being obtained from the following formula:

$$V_{out} = V_{in}\left(\frac{R_{open}}{R_{open} + R_{monolith}}\right)$$

Equation AIII.1: Voltage drop V_{out} across a monolith in V; V_{in} denotes the input voltage (i.e., applied voltage) in V, R_{open} stands for the resistance of the open section of the capillary in Ohm and $R_{monolith}$ for the resistance of the monolith in Ohm.

This voltage drop divided by the length of the monolith then yields the electric field strength throughout the monolith. Typically, the voltage ratio between packed and open section is about 2:1.

A comparison between CE and CEC is only useful if both techniques employ the same mobile phase, i.e., the results can only be compared to non-aqueous CE. Otherwise, changes in conductivity take place that cannot be accounted for. Due to the lack of alternatives, though, the same electric field strength was applied for both aqueous- and non-aqueous CE.

Appendix IV: Original Publications Resulting from this Thesis

This section lists all journal publications (printed, accepted or submitted) and conference presentations that resulted from this thesis until the date of the thesis defense on March 26th, 2004. Since large parts of the thesis have not been published in journals so far, further publications are planned for the near future.

Journal Publications (all peer-reviewed):

"Review: capillary electrochromatography of peptides and proteins"
D. Bandilla, C. Skinner, accepted, *Journal of Chromatography A*

"Characterization of UV-transparent, Teflon-coated capillaries for capillary electrochromatography and capillary electrophoresis"
D. Bandilla, J.L. Cabral, C. Skinner, submitted to *Electrophoresis*

"Derivatization of amino acids with anthracene-2,3-dialdehyde and their separation by micellar electrokinetic chromatography"
Z. Papachristou, Z., **D. Bandilla,** P. Banks, C. Skinner, submitted to *Electrophoresis*

"Pore size characterization of a monolith for capillary electrochromatography via atomic force microscopy in air- and liquid phase"
J.L. Cabral, **D. Bandilla,** C. Skinner, submitted to *Analytical Chemistry*

"Protein separation by monolithic capillary electrochromatography"
D. Bandilla, C. Skinner, *Journal of Chromatography A*, 2003, 1004(1-2), 167-179, and *Proteomic Select – The Virtual Journal of Proteomics*, 22 July 2003, 15

Conference presentations:

"Protein capillary electrochromatography on tunable monolithic stationary phases"
J.L. Cabral, **D. Bandilla**, C. Skinner, accepted for Poster presentation, 87th CSC Conference, May 29th-June 1st, 2004, London, Ontario

"Capillary electrochromatography of milk proteins"
M.-E. Beaudoin, **D. Bandilla**, C. Skinner, Poster presentation, 14th Annual Frederick Conference on Capillary Electrophoresis, November 3rd-4th, 2002, National Cancer Institute, Frederick, Maryland

"Electrochromatography as a novel separation technique for protein analysis"
J.L. Cabral, **D. Bandilla**, C. Skinner, Poster presentation, 86th CSC Conference, August 10^{th}-15^{th}, 2003, Ottawa, Ontario

"Protein separation by capillary electrochromatography"
J.L. Cabral, **D. Bandilla**, C. Skinner, Poster presentation, HPLC 2003 Conference, June 15^{th}-19^{th}, 2003, Nice, France

"Capillary electrochromatography of biomolecules: from model separations to real life applications"
D. Bandilla, C. Skinner, Poster presentation, 13th Annual Frederick Conference on Capillary Electrophoresis, October 21^{st}-22^{nd}, 2002, National Cancer Institute, Frederick, Maryland

"Capillary electrochromatography: an alternative to slab-gel electrophoresis for protein separations?"
D. Bandilla, C. Skinner, Poster presentation, Fifth Annual Graduate Student Research Conference, September 20^{th}-21^{st}, 2002, Concordia University, Montréal, Québec

"Capillary electrochromatography of proteins and biofluids"
D. Bandilla, C. Skinner, Oral presentation, 85th CSC Conference, June 2^{nd}-6^{th}, 2002, Vancouver, British Columbia

"Analysis of biofluids by capillary electrochromatography"
D. Bandilla, C. Skinner, Poster presentation, Analytica Conference, April 23^{rd}-26^{th}, 2002, Munich, Germany

"Towards electrochromatography in microfluidic devices"
D. Bandilla, C. Skinner, Oral presentation, Fourth Annual Graduate Student Research Conference, September 21^{st}, 2001, Concordia University, Montréal, Québec

"Electrochromatography in microfluidic devices: a comparative study"
D. Bandilla, C. Skinner, Poster presentation, 84th CSC Conference, May 26^{th}-30^{th}, 2001, Montréal, Québec

Appendix V: Suggested Reading

This thesis is based on original research papers and review articles in respected scientific journals. Although not considered by the author, three textbooks on CEC have been published over the last three years which are listed in the following:

(1) Krull, I. S.; Stevenson, R. L.; Mistry, K.; Swartz M. E. *Capillary Electrochromatography and Pressurized Flow Capillary Electrochromatography: An Introduction;* HNB Publishing: New York, 2000.

(2) Bartle, K. D.; Myers, P. *Capillary Electrochromatography;* Royal Society of Chemistry: Cambridge, 2001.

(3) Deyl, Z.; Svec, F. *Capillary Electrochromatography;* Elsevier: Amsterdam, 2001.